Geometric frustration: the case of triangular antiferromagnets

Pierre-Éric Melchy

UNIVERSITÉ DE GRENOBLE

THÈSE

Pour obtenir le titre de
de docteur de l'université de Grenoble
Spécialité : physique (matière condensée)

Arrêté ministériel : 7 août 2006

Présentée et soutenue publiquement par

Melchy Pierre-Éric

le **8 octobre 2010**

Frustration géométrique: le cas des antiferromagnétiques triangulaires

Thèse dirigée par **Mineev Vladimir** et codirigée par **Zhitomirsky Mike**

JURY

M. Holdsworth Peter	École Normale Supérieure de Lyon	Rapporteur
M. Honecker Andreas	Université de Göttingen	Rapporteur
Mme Lacroix Claudine	Institut Néel, CNRS	Présidente
M. Zhitomirsky Mike	INAC, CEA	

Abstract

This doctoral dissertation presents a thorough determination of the phase diagrams of classical Heisenberg triangular antiferromagnet (HTAF) and its anisotropic variants based on theoretical and numerical analysis (Monte Carlo). At finite-field HTAF exhibits a non-trivial interplay of discrete $\mathbb{Z}_3$ symmetry and continuous S^1 symmetry. They are successively broken (discrete then continuous) with distinct features at low and high fields: in the latter case the ordering is along transverse direction; in the former case an intermediate collinear phase is stabilised before 120-degree structure is. Due to zero-field behaviour, transition lines close at $(T, h) = (0, 0)$.

Single-ion anisotropy is here considered. Easy-axis HTAF for moderate anisotropy strength $0 < d \leqslant 1.5$ possesses $\mathbb{Z}_6 \otimes S^1$ symmetry at zero-field which induces triple BKT-like transitions. At finite field the symmetry is the same as for HTAF: both thus share the same symmetry-breaking pattern. Yet specificities can be observed in the easy-axis system: splitting of zero-temperature transition at one-third magnetisation plateau, reduction of the saturation field.

Easy-plane HTAF belongs to the class of universality of XY triangular antiferromagnet: it thus interesting to start with this system. Zero-field behaviour results from the breaking of $\mathbb{Z}_2 \otimes S^1$ symmetry, where the discrete component is an emerging chiral symmetry. An intermediate magnetically chiral ordered phase exists which extends to finite-field where the symmetry is $\mathbb{Z}_2 \otimes \mathbb{Z}_3$. The upper limit of this intermediate phase along field axis is a multicritical point at which transition lines are inverted. Above, the intermediate phase is a collinear phase. At high field the compound symmetry is broken as a whole $\mathbb{Z}_6$.

Résumé

Cette thèse de doctorat présente la détermination théorique et numérique (Monte Carlo) du diagramme de phase du système classique antiferromagnétique de Heisenberg sur réseau triangulaire (HAFT) et de ses variantes anisotropes. Sous champ HAFT présente une intrication non triviale des symétries discrète Z3 et continue S1. Elles sont successivement brisées (discrète puis continue) selon des modalités différentes à champ fort et modéré : dans ce cas-là l'ordre a lieu selon la direction transverse ; dans ce cas-ci une phase colinéaire intermédiaire est stabilisée avant la phase à 120 degrés. Du fait du comportement à champ nul les lignes de transitions se terminent à $(T, h) = (0, 0)$.

L'anisotropie mono-ionique est ici considérée. HAFT avec anisotropie d'axe facile pour une anisotropie modérée, $0 < d \leqslant 1.5$, possède une symétrie $\mathbb{Z}_6 \otimes S^1$ à champ nul, qui induit une triple transition BKT. Sous champ, la symétrie est identique à HAFT : les deux partagent donc le même scénario de brisure de symétries. Le système anisotrope présente toutefois des spécificités ; séparation de la transition à température nulle au champ de tiers d'aimantation, réduction du champ de saturation.

HAFT avec anisotropie de plan facile appartient à la classe d'universalité de XY AFT il est donc intéressant de commencer par ce système-ci. Le comportement à champ nul résulte de la symétrie $\mathbb{Z}_2 \otimes S^1$ où la composante discrète est une symétrie chirale émergente. Une phase intermédiaire chirale magnétiquement désordonnée est stabilisée ; elle se prolonge sous champ, où la symétrie est réduite à $\mathbb{Z}_2 \otimes \mathbb{Z}_3$, jusqu'à un point multicritique auquel les transitions s'inversent. Au-dessus de celui-ci la phase intermédiaire est colinéaire. Sous champ fort la symétrie composite se brise comme une symétrie $\mathbb{Z}_6$ unique.

Acknowledgement

Arnaud, Philippe, Jean-Paul, Arnaud, and François-Xavier. Their joyful warmth, their supportive presence, their challenging pieces of advice, their simple sharing the ups and downs are parts of what has helped me up. Persons I am profoundly grateful to and lovingly thankful to for their countless efforts to foster my development, for their being infinitely open-minded regarding my choices, wills and desires, for their never lacking support whatever the dire situation they, I, or we may be facing are my parents and my brother.

Last I'd like to thank these inspiring figures that enlighten my sky, all these great persons who make me proud of being called a human-being, whether they may be scientists, philosophers, artists or other great achievers, famous or not, of what can be called the best part of our humanity. Out of my personal sky I could name quite a few of these stars that lead my course. However I limit myself to the one who stood by my side throughout the writing of this dissertation and represents a model for any writer for his avoiding any superfluous note: Johann Sebastian Bach.

Contents

Chapter 1

Introduction

Condensed matter physics deals with matter in its condensed form: what does this tautology state? In this context *condensed* can be defined as *held together thanks to internal interactions*. It means that this branch of physics doesn't investigate elementary entities but the collective behaviour of interacting particles. Its name was coined rather recently (1967) by P. W. Anderson and V. Heine when they renamed their *Solid-state Theory* laboratory at Cambridge, UK, *Theory of Condensed Matter*. From a perspective in terms of macroscopic physical properties, they made the focus evolve towards the underpinning phenomenon, the grounding effect of which extends beyond the sole solid state, namely many-body interactions and the induced collective phenomena measurable either at a microscopic or macroscopic level. One of the most striking feature of collective phenomena is phase transition. Phase transitions are a commonly experienced fact — anybody cycling in winter does know that water in its solid form, also known as glaze when covering the ground, has quite distinct properties. Yet their understanding and their description is far less straightforward and has been fostering the development of theories and experiments by physicists for generations. They arise whenever there are competitive processes governing the equilibrium of a system: varying external parameters such as temperature, pressure, magnetic field, it is then possible to change the equilibrium configuration. The trouble in condensed matter physics stems from the hardship to analytically describe systems with more than two interacting particles: yet any realistic system such as this very sheet of paper consists of several billions of billions of atoms — this is no reason to conclude that this thesis is intractable: another important characteristic of condensed matter physics is to look at systems at the relevant scale and I doubt the atomistic one is the right choice for this piece of work! To overcome this hardship it has been necessary to develop ways of treating systems with a huge number of particles in a tractable way: this is what statistical mechanics can do. It makes use of the observation that physical properties of a given system can be correctly described by probabilistic distributions. Boltzmann can

without hesitation be named the father of this revolutionary approach.[1] Thanks to this revolutionary viewpoint it has been possible to describe macroscopic properties of matter from microscopic underpinning phenomena. The formalism of statistical mechanics, however originally devised in a classical language, could fully be extended to quantum context with a straightforward correspondence. With this toolbox in hand physicists could further develop the understanding of collective phenomena, among which critical phenomena that occur at phase transitions.

In a way or another various modern descriptions of critical phenomena are built upon the observation criticality is characterised by a loss of scale hierarchy: about phase transition the system look the same at different scales — this auto-similarity is coined as fractal. In other words details don't matter. An early understanding of this statement took the form of mean field as enunciated by Weiss in 1907 [128]: this approach consists in considering for each particle the interactions with its neighbours and the environment at the level of mean values. However simplistic such a treatment may seem it has revealed not only fruitful to orientate intuitions but also exact in certain limits (roughly speaking in high dimensions for short-ranged interactions). Another development of this idea was proposed by Landau with his phenomenological description of second-order phase transitions[2] based on a symmetry analysis of the system. Landau's discussion is in fact two-fold. On the one hand he explicited symmetry rules governing a second-order phase transition: at a continuous transition there must be a group-subgroup relation between the symmetry groups of each phase on both sides of the transition. This leads to a classification of possible continuous phase transitions given a model with a specific symmetry group. On the other hand he proposed an hydrodynamic-like development of the free energy functional in terms of successive powers of the order parameter and its gradient (which is possible at a continuous transition as the order parameter goes to zero[3]). Both sides of this reasoning work together as the development of the free energy functional introduces terms that must respect the symmetry of the model. This fruitful theory elegantly circumvents a major difficulty of statistical mechanics, namely the explicit calculation of partition function given a specific Hamiltonian. A later development fully pushing this idea of scale-invariance and discarding irrelevant details was the development during the 1960's of renormalisation group by Kadanoff [41] and Wilson [129, 130]. The underlying idea is to describe the model at larger and larger

---

[1]Boltzmann's epitaph reads: $S = k \log W$.

[2]After Ehrenfest's first classification of phase transitions according to continuity properties of the derivatives of free energy (in that classification an n-th order transition is a transition at which first discontinuity occurs for the n-th derivative), modern classification distinguishes first-order transitions characterised by the existence of non-zero latent heat from second-order ones that are continuous (without any latent heat) and associated with a diverging correlation length at the transition. Infinite-order transitions exist as well such as Berezinskii-Kosterlitz-Thouless transition that is dealt with in this dissertation.

[3]Extensions of Landau's formalism to certain first-order transitions can be done as presented for example in [119].

scales using a coarse-graining approach: during this transformation, that is called a flow, coupling constants of the model undergo changes that constitute a semi-group (hence the name that mathematically speaking is not exact) with certain constants flowing to zero, which means they don't play any role for the criticality of the system. With this viewpoint it was then possible to introduce classes of universality: such a class groups various systems sharing common *relevant* interactions and consequently common symmetries. Each class can then be defined by a set of critical exponents that describe how quantities of interest such as specific heat behave in the vicinity of the transition. Most of physicists' efforts in the analysis of phase transitions has thus been the determination of the class of universality which the model they investigate belongs to and in another direction the attempt to describe all possible classes of universality.

The latter effort has undergone a dramatic change with conformal field theory. This theory is based on the fact that critical theories are not only invariant under changes of scale as previously introduced with the renormalisation group but also under the action of conformal transformations[4]. If conformal invariance doesn't bring anything new in dimensions $d \geqslant 3$, for $d = 2$ it does bring new constraints that should enable to catalogue bidimensional critical phenomena. This statement singles out the specificity of dimension 2. $2d$ is in many regards specific as it offers a wealth of models with exotic critical behaviours that cannot be found in other dimensions; some of them even evade treatment with methods such as mean-field approximation, renormalisation group, and other methods perfectly working at higher dimensions. A way to grasp this specificity of bidimensional models is to think of their topological properties: as can readily be observed continuous deformations that are the pictorial way to glimpse at topology are far more restricted in $2d$ than in higher dimensions where it is often possible to circumvent a singularity using the extra dimensions. On the other side most methods used in $1d$ systems are specific to this dimension with the extreme constraint of the dimensionality that induces specific collective excitations.

Beside these theoretical achievements, numerical physics has grown in importance and played quite crucial a role in the understanding of critical phenomena. As previously shortly alluded to one major hindrance in statistical mechanics is the actual handling of partition function. Numerical methods can precisely help overcoming it even without any explicit calculation of the partition function at stake — in the end the interesting elements are physical observables rather than mathematical devices used to built up theories. One major player in the field of numerical statistical physics is Monte Carlo procedure in its various variants. Undoubtedly the algorithm proposed by Metropolis and coworkers [78] fostered the emergence of the field, which has been further boosted by the exponential growth of computing facilities pushing further away the balking limitations of numerical simulations. In a word the idea behind these methods

---

[4]The group of conformal transformation is the subgroup of coordinate transformations that leave the metric invariant up to a scale factor, ie that preserve the angle between two vectors.

is to astutely explore the phase space to catch a faithful glimpse of the system under scrutiny: this is achieved through a Markov chain[5]. Numerics has thus grown as the third pillar on which modern statistical physics stands.

With this well equipped toolbox in hand it becomes possible to deal with physical models among which magnetic systems constitute one of the most appreciated playground thanks to the variety of models that can be both theoretically devised and experimentally studied. An incomparable advantage of magnetic systems is indeed that many experimental techniques are available to both probe macroscopic and microscopic properties: from bulk thermodynamical measurements (specific heat, susceptibility, etc.) to local probing (atomic force microscopy, muon spin resonance), with such fine structural investigation tools as neutron scattering experiments (elastic and inelastic scattering, polarised or unpolarised neutrons, spin echo, etc.). Furthermore it is most of the time possible to write models accurately describing these spin systems or in the reverse way certain models initially theoretically devised and studied have proven relevant for the description of real compounds. For sure magnetic materials are less clean and less tunable than artificial magnetic crystals obtained in quantum optics. The latter are however still out of the energy range of interest and therefore remain promising experimental toys not yet at their full maturity [14].

As said condensed matter deals with collective phenomena and consequently cooperative behaviours. In quite a few circumstances cooperation can lead to an extreme case which is frustration. Roughly speaking (more precise a definition is proposed in the following) frustration occurs whenever it is impossible for all interacting entities to simultaneously reach an optimum. In spin systems the concept was formally introduced in the 1970's. With the rough picture above proposed it can readily be understood that this concept is relevant to a huge variety of problems in statistical mechanics, and even far beyond, as such fields as econophysics or sociophysics flourish. As previously pointed out magnetic systems provide an actual playground to deal with abstract concepts and frustration is no exception: various compounds indeed embody frustration and make it possible to confront models with experiments and reversely to seek inspiration in reality. Frustrated magnets offer quite an interesting playground to test various exciting concepts beside the release (or not) of frustration such as spin liquids, exotic phase transitions, quantum criticality, etc.

With this background in mind it is now possible to proceed to a more precise introduction of grounding concepts and questions supporting this dissertation. Symmetries in $2d$ is the topic of Sec. 1.1. Then a thorough introduction to frustration is proposed in Sec. 1.2. Last an historical perspective on the family that models studied in the following chapters of this dissertation belongs to, namely antiferromagnetic spin sytems on a triangular lattice, is proposed in Sec. 1.3.

---

[5]A Markov chain is a random process such that next step only depends on the current state: it is memoryless, which makes it perfectly suited for numerical simulations.

1.1   Symmetry breaking in $2d$

When dealing with phase transitions in general the question of symmetry breaking naturally comes out. In $2d$ this issue acquires a dramatic specificity. In 1966 Mermin and Wagner demonstrated that the breaking of a continuous symmetry in bidimensional systems is impossible at any finite temperature. As a consequence second-order phase transition in spin systems with continuous rotational symmetry, as is the case of isotropic models of spins with more than one component in zero field, is excluded. This statement doesn't end the story. Berezinskii on the one hand [10, 11], Kosterlitz and Thouless on the other hand [61] argued that despite its continuous symmetry XY model on the square lattice does undergo a finite-temperature transition. No symmetry-breaking is associated with this transition but a dramatic change in the behaviour of stable topological defects. Such a transition is an example of an infinite-order transition; this one is referred to as a BKT transition. The discussion of phase transition in terms of topological defects was formalised by different physicists [82, 76, 75, 79] in the late 1970's. It is based on homotopy groups: these groups concentrate the sufficient information to describe topological properties of objects. The simplest one, the fundamental group, π_1, describes how closed loops in a topological object evolve under a continuous deformation. For example any closed loop on the sphere S^2 can be shrunk to a point, hence the fundamental group of the sphere is the trivial group: $\pi_1(S^2) = 0$. On a circle the situation is less simplistic: some closed loops can twine around the circle without being shrinkable to a single point; moreover these can twine several time, which means an integer can be associated to loops which is its winding number (zero in case of a shrinkable loop). This makes it understandable that the fundamental group of a circle is the group of integers: $\pi_1(S^1) = \mathbb{Z}$. This theory enables the handling of topological defects which exist in physical systems. These topological defects can induce phase transitions, which means it is possible to describe phase transition calculating the homotopy group of the symmetry group of the Hamiltonian. XY model exemplifies this approach: the symmetry group of the Hamiltonian is S^1; as seen above $\pi_1(S^1) = \mathbb{Z}$. As a consequence XY system admits stable point defects that are integer vortices. The observation put forward by Berezinskii, Kosterlitz, and Thouless is that vortices are bound into pairs of vortex-antivortex at low temperature and are free at high temperature, which means a transition occurs in between: this binding-unbinding transition is BKT transition. As a consequence of above mentioned Mermin-Wagner theorem the order settling below the transition is not a long-range order but rather a quasi-long-range order. This low-temperature phase is hence a soft massless phase with power-law decaying correlation functions and continuously varying critical exponents in contrast to what happens in Ising model with its massive low-temperature phase.

An interesting question is then the evolution from one model to the other. A way to study it consists in investigating discrete Abelian models with $\mathbb{Z}_p$ symmetry. Beside this theoretical motivation, the study of such models is motivated by the melting of

bidimensional crystals that are governed by discrete rotational symmetry ($p = 2, 3, 4, 6$ are of experimental relevance). If an XY model perturbed by $\mathbb{Z}_p$ terms was studied by José and coworkers in their seminal 1977's work, first specific studies of pure $\mathbb{Z}_p$ systems came slightly later [28, 17, 27]. These works showed that there is a critical value p_c such that for $p \leqslant p_c$ two massive phases exist as in Ising model whereas for $p \geqslant p_c$ between these two massive phases an intermediate critical massless phase (or quasiliquid) emerges the lower limit of which tends to zero as p goes to infinity in agreement with Mermin-Wagner prescription. An even more striking result has been obtained on p-state clock model, aka $\mathbb{Z}_p$ models: the existence of an extended universality [65]. Above a certain temperature T_{eu} for $p > 4$, thermodynamical properties are proved identical to those of the continuous model $p = \infty$. In particular for $p \geqslant 8$ this collapse starts in the intermediate quasiliquid phase, which implies that the upper transition is a real BKT transition. It constitutes an example of an emergent symmetry.

Another example of an emergent symmetry in bidimensional systems is the one of an extra discrete degeneracy in certain bidimensional systems with a continuous symmetry [122]. This phenomenon revealed by Villain arises as a consequence of multi-q structure. Let's introduce a spin structure $\mathbf{S}_i = \mathbf{u} \cos \mathbf{q} \cdot \mathbf{r}_i + \mathbf{v} \sin \mathbf{q} \cdot \mathbf{r}_i$ where $\mathbf{u}$ and $\mathbf{v}$ are orthogonal unit vectors and $\mathbf{q}$ is an ordering vector[6]. In case this structure describes all ground states, which is the case with spins of dimension $n = 2$ or 3 (unless the ordering vector $\mathbf{q}$ lies at special positions within Brillouin zone in this latter case), this formula shows that an extra discrete degeneracy exists for spins of dimensionality $n = 2$ as soon as the star[7] of $\mathbf{q}$ consists in more than one vector and for $n \geqslant 3$ if the star is not reduced to $\{\mathbf{q}, -\mathbf{q}\}$. Let's explicit this assertion in the former case: changing $\mathbf{q}$ into $-\mathbf{q}$ changes sine into its opposite. As the vectors are bidimensional there is no direct continuous transformation to change $\mathbf{q}$ structure into $-\mathbf{q}$ structure. The existence of this extra degeneracy makes it possible for the system to order at finite temperature despite its original continuous symmetry. A widely discussed example is the case of XY model on the triangular lattice with its emergent chiral order that is presented in Chap. 4.

1.2   Frustration

Frustration is a concept that was formally introduced in the context of spin glasses [121, 123] even though earlier studies dealing with frustrated magnets exist [125, 114, 44, 2]. A characteristic property of frustrated systems, namely their extensive entropy at zero temperature, was discussed as early as 1935 by Pauling [96] in water ice. Frustration can be defined as the impossibility to minimise all individual interaction terms

---

[6]$\mathbf{q}$ is obtained as a vector minimising with respect to $\mathbf{k}$ the Fourier transform $\sum_j J_{ij} \cos \mathbf{k} \cdot (\mathbf{r}_i - \mathbf{r}_j)$ where (J_{ij}) is the set of bilinear exchange constants defining the Hamiltonian $\mathcal{H} = \sum_{\langle ij \rangle} \mathbf{S}_i \cdot \mathbf{S}_j$.

[7]The star of a vector $\mathbf{k}$ is the set of inequivalent vectors generated by the action of the lattice symmetry group on the vector $\mathbf{k}$.

at the same time, may it be due to randomness, to geometric constraints, or to competing interactions. After the formal introduction of the term frustration, frustrated magnets without randomness were studied for a while for their connection with spin glass. Yet it soon became obvious that these magnetic systems that had been studied for some of them before the hype about spin glass could bring more. Thanks to the diversity of experimental methods available to study magnetic systems, this field of research has experienced a continual and vivid cross-fertilisation between theoreticians and experimentalists. Investigations on frustrated magnetic materials have had implications far beyond magnetism itself. Indeed their highly degenerate ground state manifold, their possibly non-collinear or incommensurate order, the assumptive spin liquid, and their possibly novel phase transitions offer a playground to investigate challenging and exciting fundamental questions both in classical and quantum systems. Regarding quantum systems such questions as the link between cuprates supraconductors and $2d$ quantum frustrated antiferromagnets [3] or as deconfined quantum critical point, which is a new paradigm to describe phase transitions beyond Landau-Ginzburg-Wilson paradigm encompassing transitions between phases with no symmetry relation [104, 105], have renewed the vivacity of research on this topic. Interestingly various analytical, numerical and experimental techniques have been used to study frustrated magnetic systems: analytical developments à la Onsager, Landau-Ginzburg treatment and more generally analysis of symmetry and topological properties, mean-field techniques, renormalisation group apparatus, high- and low-T series expansions, Monte Carlo simulations, experimental investigations. In certain cases some of these different approaches may be at odds such as exemplified by the opposition between certain renormalisation group methods ($\varepsilon = d - 2$ development of a non-linear σ model) on the one hand and Monte Carlo simulations and topological discussions on the other hand to describe classical frustrated Heisenberg spin systems [4, 49]. Renormalisation group approaches, Monte Carlo simulations and experimental measurement do not yield a consistent picture of such systems, which is the illustration how non-trivial the critical behaviour of frustrated magnets is. It also points out the necessity to carefully understand the limitations of the techniques that are used in order to identify the origin of such mismatches; hence a better insight into these techniques can be gained. Frustrated magnetism has been at the heart of much highlighted research of the past thirty years as is the case with cuprates high-T_c supraconductors, Josephson junction arrays, multiferroics, etc. The most recent topic creating a real hype in this field was the description of pseudo magnetic monopoles in spin ice systems [18]. Frustration can be studied in insulating crystals as well as in metals or in disordered systems. Hereafter we consider only the case of insulating crystals.

In insulating crystals the relevant picture to understand magnetism is the one of isolated spins located at vertices of a lattice. From the Hubbard model one can derive localised-spin interaction Hamiltonians: depending on spin dimensionality, they are Ising (1d spin space), XY (2d) or Heisenberg (3d) models. The simplest cases consist

in bilinear interaction terms. In such cases the competition of interactions inducing magnetic frustration can stem either from a competition between different interaction paths (typically between nearest-neighbours and next-nearest neighbours) or from the topology of the lattice. Widely studied examples of the former case are $J_1 - J_2$ model on the square lattice, spin ladders, among others [21, 81]. In the latter case the frustration is said to be geometric. Geometrically frustrated magnets build up a major and diverse group of magnets. Geometrically frustrated systems can typically be built with triangular elementary plaquettes that can arrange either on a corner sharing pattern (kagome lattice) or on an edge sharing one (triangular lattice), in $2d$ or $3d$ as well. Another common building block is tetrahedron (corner sharing tetrahedra can form the so-called pyrochlore lattice). Common frustrated lattices comprise the $2d$ triangular lattice, kagome lattice, fcc, and pyrochlore among other ones. Numerous materials in this class exist [36]: anhydrous alum, jarosites, pyrochlores, spinels, magnetoplumbites, garnets,etc. Geometrically frustrated spin systems enable us to study frustration in very simply formulated models and to deal with non-trivial topology questions. Indeed an important characteristic of these systems is the nature of the order parameter which can be such an object as a matrix of $SO(3)$, or a complex vector with $S^1 \otimes Z_3$ symmetry group. Homotopy theory then yields non-trivial topological excitations, which may lead to exotic phase transitions. The identification of a new class of universality is however a tricky issue due to the non-trivial critical behaviour of frustrated spin systems and the complicated order parameter symmetry group. A famous example of such a difficulty is provided by the twenty-year-long controversy about the nature of the phase transition in Heisenberg antiferromagnet in stacked triangular crystals. Early claims of a new universality class based on two-loop renormalisation group analysis and Monte Carlo simulations appeared [47, 48]. Various simulations and theoretical analysis were then published. Using a non-linear σ model Azaria and coworkers [5] claimed the transition should pertain to $O(4)$ universality class if it were not first-order or mean-field tricritical. Tissier and coworkers published an extensive non-perturbative renormalisation group study of frustrated spin systems in dimension between two and three: a consequence of their study is that the transition of Heisenberg stacked triangular antiferromagnet is first-order; they further argue that the reason why numerical simulations stalled around the transition and identified it as second-order with new critical exponent is the existence of a region in the flow diagram where the flow is slow, inducing a very weak first-order character [116, 118]. Last Ngo and Diep published a careful Monte Carlo simulation using both advanced techniques and very large clusters to support the first-order character of the transition [88]. Similarly in this work we present results that firmly stand against a new universality class for the breaking of $S^1 \otimes Z_2$, which agree with the detailed analysis presented on fully frustrated XY spin systems [37].

An important characteristic of frustrated magnets is the extensive degeneracy of low-energy modes, which induces extensive entropy at zero temperature. Such a highly

degenerate ground state manifold can induce some long sought states such as spin liquids or spin glasses without any randomness, which is another reason why so much effort has flowed into research on frustrated spin systems. Spin liquids can be defined as gapped spin systems with a finite correlation length at zero temperature [80]. One good example of this is kagome antiferromagnet; yet its experimental realisation is still lacking: the grail of a perfect spin-1/2 kagome system still seems far away. A dramatic consequence of such a degeneracy is the possible appearance of extra soft modes, at least at $T = 0$ as is the case for XY classical spins on the triangular lattice or for Heisenberg spins on the triangular lattice. This is however a fragile feature that is quite sensitive to various perturbations and makes it even harder to observe, all the harder as an order by disorder phenomenon [124], for example induced by thermal fluctuations, can occur. It is by no way a systematic phenomenon in geometrically frustrated systems as Heisenberg pyrochlore and four-component spin system on kagome lattice show: both remain disordered at low temperature [86].

Yet ways to remove this accidental continuous degeneracy exist. First, thermal fluctuations are expected to induce an order by disorder phenomenon as pointed out by Villain and collaborators at the very beginning of 1980's [124]; however such an ordering may occur in certain cases only at higher order than the second one as discussed by Sheng and Henley [106]. Quantum fluctuations are another way to reduce degeneracy and induce order that will not be developed in this work. Last anisotropy changes symmetry, which may induce ordering: this point is the object of a large part of the work here presented.

1.3 Triangular antiferromagnet: historical perspective

When considering geometric frustration the simpler system to come to the mind is an antiferromagnetic model on the triangular lattice. With their stunning simplicity triangular antiferromagnets have been occupying physicists for several decades. As this dissertation deals with classical systems the historical perspective here proposed leans towards classical systems even though their quantum counterparts do present several interesting features. Reviewing what has been done on triangular antiferromagnets clearly shows various research on these systems have gone different paths. After the historical exact solution of Ising models [125, 126] completed by the demonstration this model belongs to Ising universality class with a $\mathbb{Z}_6$ symmetry-breaking term [1] with an upper transition at $T = 0$ and further refinements in the discussion of $\mathbb{Z}_6$ symmetry-breaking as reinforced by the introduction of next-nearest-neighbour couplings [63, 33], much effort has been devoted either to quantum Ising models with and without field (in the latter case, a transverse field enables to have a glimpse at other interesting models: the dual model is a $\mathbb{Z}_2$ gauge model that is equivalent to quantum kagome antiferro-

magnet, system expected to exhibit a spin-liquid phase) or to stacked triangular Ising antiferromagnet. The investigation of stacked triangular antiferromagnets in case of XY and Heisenberg models has also gathered much attention, probably thanks to experimental realisations of these models [23, 49]. Most investigated layered compounds diverge from $2d$ models as they are in fact chains weakly coupled in a triangular lattice, and thus exhibit $3d$ ordering properties of quasi-$1d$ objects. A large class of compounds pertains to ABX_3 family where A stands for Cs or Rb, B for a magnetic ion, either Mn, Cu, Ni, or Co, and X for one of the halogens, Cl, Br, or I. Depending on the kind of anisotropy in the compound relevant model changes. For those with a strong easy-axis anisotropy Ising model is adapted: this is the case of $CsNiCl_3$, $CsNiBr_3$, and $CsMnI_3$. Easy-plane anisotropy as present in $CsMnBr_3$ and $CsVBr_3$ leads to a description with XY model. As for systems with a very weak anisotropy, such as $CsVBr_3$ and $RbNiCl_3$, they let Heisenberg model correctly describe them. Another reason why stacked systems have been so widely studied is their amenability to mean-field analysis [97, 99, 101, 100]. As already discussed a twenty-year-long controversy opposed proponents of a continuous transition from the paramagnetic to the ordered phase in XY and in Heisenberg stacked triangular antiferromagnet to opponents claiming these transitions were first-order. After the non-perturbative renormalisation group approach by Tissier and coworkers [116, 118, 117], and various numerical treatment, Ngo and Diep proposed clear numerical evidence of a first-order transition thanks to Wang-Landau flat histogram algorithm implemented on quite large clusters [89, 88] (and references therein for previous numerical works).

At the other end research on $2d$ models and quasi-$2d$ compounds has generated fewer publications, many extensively discussing zero-field behaviour. The work by Miyashita and Shiba on the one hand [85] and by Lee and coworkers on the other hand [66, 67] really started the investigations on $2d$ XY model which were complemented by Kawamura's spin-wave calculations [46] and Korshunov's extensive analysis of symmetry and topological excitations [57, 56, 60, 59]. The interest rose due to the emergent chiral transition as already forecast by Villain [122]. As a consequence two symmetry-breaking occur, which at zero-field induces two distinct transitions that some authors failed to distinguish [66, 67] as opposed to others [85, 68, 134, 69, 91]. Yet finite-field behaviour has lacked thorough careful investigations despite the quite fine discussion proposed by Korshunov [57], which was a motivation to undertake such investigations. As far as Heisenberg triangular antiferromagnet is concerned if its quantum version has been rather popular the classical model has been only quite partially studied. Zero-field behaviour, after the pioneering and inspiring topological analysis proposed by Kawamura and Miyashita [51, 50], did attract some interest [5, 6, 109, 133, 132, 53]. As this model has a continuous symmetry in zero-field, after Mermin-Wagner theorem it is expected no finite-temperature transition can occur. Kawamura and Miyashita challenged this view putting forward the existence of two regimes with distinct properties of the stable point topological defects, namely $\mathbb{Z}_2$ vortices. Further numerical achievements [53] and

an experimental realisation of an Heisenberg triangular antiferromagnet [87] propose convincing support for this transition. Finite-field behaviour contrastingly has been at best overlooked [52]. With so little theoretical work on it and with new experimental results on quasi-$2d$ compounds ($Rb_4Mn(MoO_4)_3$, Nakatsuji *et al.*, private communication) did require a correct study.

In this context the work presented in this dissertation intends to propose a clear picture on the whole phase diagram of classical Heisenberg model (Chap. 2) and its anisotropic variants, namely easy-axis (Chap. 3) and easy-plane anisotropic models (Chap. 4) based on a blend of numerical simulations and symmetry analysis without any heavy technical apparatus. If studies were published presenting elements of a phase diagram for anisotropic models [84, 83], the anisotropy was exchange anisotropy. From an experimental point of view single-ion anisotropy as used here seems more relevant. Furthermore from a theoretical point of view its perturbing impact is much more dramatic. As easy-plane anisotropic Heisenberg triangular antiferromagnet is presented and since a precise phase diagram was still absent, XY triangular antiferromagnet has been studied as well and results are presented in Chap. 4.

Chapter 2

Heisenberg Triangular Antiferromagnet

In this chapter we deal with the isotropic version of Heisenberg triangular antiferromagnet (HTAF); in a way this is the original version that is referred to when speaking of Heisenberg antiferromagnetic model on the triangular lattice. In the first section the model is briefly introduced and key properties of its Hamiltonian are exposed. Then results on zero-field behaviour are reviewed and critically compared. Sec. 2.3 and 2.4 are devoted to finite-field behaviour: first we discuss symmetries of HTAF in an external field, then our numerical calculations for this system are presented and the phase diagram of HTAF proposed. Considering existing results on zero-field behaviour of HTAF, a new study has seemed worthless; yet to support this viewpoint and to draw a complete picture of the phase diagram of HTAF as here intended, a critical review of literature on this topic is included.

2.1 Model

To deal with electronic crystalline systems it is necessary to take into account two competing energies describing the behaviour of electrons: Coulomb repulsion and kinetic energy (hopping). If the incompletely filled orbitals ($3d$ in iron-group elements and $4f$ in rare-earth elements) are decribed by localised orbitals, this is encompassed in so-called Hubbard model:

$$\mathcal{H} = \sum_{n,n',s} b_{n'-n} a^{\dagger}_{n',s} a_{n,s} + U \sum_{n} a^{\dagger}_{n,\uparrow} a_{n,\uparrow} a^{\dagger}_{n,\downarrow} a_{n,\downarrow} \tag{2.1}$$

where n indexes sites and s is a spin index, $a^{\dagger}_{n',s}$ a fermionic creation operator creating an electron at site n with spin s and $a_{n,s}$ the associated annihilation operator.

This Hamiltonian can be written in another form when developing it in the low-energy sector:

$$\mathcal{H} = J \sum_{\langle i,j \rangle} \mathbf{S}_i \cdot \mathbf{S}_j \tag{2.2}$$

where I have assumed for simplicity symmetry in the $b_{n'-n}$ terms and then a single exchange energy (J can indeed be written in terms of an exchange integral). This Hamiltonian is called Heisenberg Hamiltonian [136]. When considering systems with large spins it is quite appropriate to describe spins as classical vectors which makes Heisenberg model more tractable. In systems for which this work is relevant such an approximation is correct (most of them are rare-earth compounds) and from now on only classical models are used unless otherwise stated. For simplicity classical spins are normalised to one.

Hereafter we consider HTAF with an applied field:

$$\mathcal{H} = \sum_{\langle i,j \rangle} \mathbf{S}_i \cdot \mathbf{S}_j - \mathbf{h} \cdot \sum_i \mathbf{S}_i \tag{2.3}$$

written in the units of the exchange constant J. Even though we did not specifically work on zero-field behaviour a glimpse on what happens without any field will be given for the phase diagram to be entirely discussed.

Let's discuss the ground states of (2.3) first at zero field then at finite field. A preliminary observation is the following transformation of (2.3):

$$\mathcal{H} = \frac{1}{2} \sum_\Delta \left(\mathbf{S}_{\Delta,1} \cdot \mathbf{S}_{\Delta,2} + \mathbf{S}_{\Delta,2} \cdot \mathbf{S}_{\Delta,3} + \mathbf{S}_{\Delta,3} \cdot \mathbf{S}_{\Delta,1} \right) + \frac{\mathbf{h}}{6} \sum_{\Delta,i} \mathbf{S}_{\Delta,i} \tag{2.4}$$

$$= \frac{1}{4} \sum_\Delta \left(\mathbf{S}_{\Delta,1} + \mathbf{S}_{\Delta,2} + \mathbf{S}_{\Delta,3} - \frac{\mathbf{h}}{3} \right)^2 + const. \tag{2.5}$$

where summation runs over triangular plaquettes Δ.

This transformation makes it plain that to minimise the Hamiltonian a sufficient condition is to equate each square in the sum to zero, which is possible: it even makes it obvious that imposing a specific structure on a given triangle imposes the configuration on the whole lattice. Let's indeed consider a given triangle Δ: let's pick up one configuration satisfying $\mathbf{S}_{\Delta,1} + \mathbf{S}_{\Delta,2} + \mathbf{S}_{\Delta,3} = 0$ (infinity of solutions, among which those with spins pointing at 120 degrees from one another equally share frustration on the three bonds); then on a neighbouring triangle Δ' there is a unique solution to $\mathbf{S}_{\Delta',1} + \mathbf{S}_{\Delta',2} + \mathbf{S}_{\Delta',3} = 0$ as the two spins pertaining to both Δ and Δ' are already fixed, qed. As a consequence ground states respect a three-sublattice pattern, the so-called $\sqrt{3} \times \sqrt{3}$ pattern that is associated with ordering wave vector $\mathbf{q}_0 = (4\pi/3, 0)$. Obviously the condition is a necessary one as well: if one of the squares in the sum were non-zero then the energy of the considered configuration would be strictly larger than the one of configurations with all squares equal to zero – these configurations exist as already

demonstrated – and hence would not be a ground state, qed. Such a constraint however lets a continuous degeneracy appear in the system. There are indeed six degrees of freedom corresponding to the three unit-length vectors (spins) constrained by three equations: three free parameters remain. A closer look at this extra degeneracy shows that it corresponds to the degrees of freedom of the three-spin structure on a triangular plaquette, thence the corresponding order parameter space $SO(3)$.

As previously discussed the ordering respects a three-sublattice pattern: it is thus natural to describe the spin structure as:

$$\langle \mathbf{S}_i \rangle = \mathbf{l}_1 \cos(\mathbf{q}_0 \cdot \mathbf{r}_i) + \mathbf{l}_2 \sin(\mathbf{q}_0 \cdot \mathbf{r}_i) + \mathbf{m} \tag{2.6}$$

where $\mathbf{m}$ is static magnetisation, which is zero at zero field, and $\mathbf{l}_1$ and $\mathbf{l}_2$ are antiferromagnetic ordering vectors. In this language, 120-degree structure corresponds to a pair of orthogonal vectors $\mathbf{l}_1 \perp \mathbf{l}_2$, $|\mathbf{l}_1| = |\mathbf{l}_2|$ and $\mathbf{m} = 0$. In case of a distorted 120-degree structure (either due to field or easy-axis anisotropy) $\mathbf{m} \neq 0$. Let's present two other configurations of importance as well (an overall view of low-field planar configurations can be found in Fig. 3.1). Collinear fully-ordered configuration, so-called up-up-down configuration, is characterised by $\mathbf{l}_2 = 0$ and $\mathbf{l}_1$ and $\mathbf{m}$ collinear. High-field planar V-shape configuration is defined by $\mathbf{l}_2 = 0$, $\mathbf{l}_1$ having components both along the field and transverse to it, and $\mathbf{m}$ along the applied field direction.

2.2 Brief review of zero-field behaviour

At zero field this extra continuous degeneracy of ground state manifold coincides with order parameter space which is $SO(3)$ the group of rotations in 3 dimensions, or in a more pictorial language the rigid body of three spins in a given triangle. Let's discuss possible phase transitions in such an order parameter space. First, an important remark should be put forward: in this two-dimensional system there cannot be any finite-temperature phase transition associated with the breaking of a continuous symmetry, after Mermin-Wagner theorem [77]. With this viewpoint there shouldn't be any finite-temperature transition in HTAF. However the conclusion becomes less obvious when the question is dealt with from a topological viewpoint: indeed stable topological defects exist in HTAF, which may induce a phase transition in a similar way to what happens in XY antiferromagnet as described by Berezinskii [10, 11] on the one hand and by Kosterlitz and Thouless [61] on the other hand (see Sec. 1.1 and 4.1) with the so-called BKT transition. Such a claim was made by Kawamura and Miyashita [51, 50]. Topologically stable defects are given by homotopy groups [82, 76, 75, 79]: line defects by zeroth homotopy group, point defects by first homotopy group and instanton by second homotopy groups. In this case the single non-trivial homotopy group is the first one: $\pi_1(SO(3)) = \mathbb{Z}_2$, which implies the system admits stable $\mathbb{Z}_2$ vortices. How can both viewpoints be reconciled? If later studies based on renormalisation group applied to a

relevant non-linear σ model [5, 6] predict a zero-temperature phase transition pertaining to $O(4)$ universality class, further investigations either based on harmonic expansion and analytical predictions [133] or on Monte Carlo techniques [109, 132, 53] indicate two regimes exist: a low-temperature one, $T < T^*$, which is consistent with renormalisation group predictions, and a high-temperature one, $T > T^*$ in which the influence of free vortices has to be taken into account, which is not done in renormalisation group analysis. Wintel *et al.* and Southern and Young thus point out a crossover between two regimes at $T = T^*$, $T^* \approx 0.28$ (Kawamura *et al.* [53] find $T^* = 0.285 \pm 0.005$): in low-temperature regime spin correlation length and antiferromagnetic susceptibility are well described by renormalisation group; in high-temperature regime a fit to BKT behaviour is much more accurate. The latter indicates a certain similarity with BKT transition. Their conclusion relies on the study of spin correlation length ξ, susceptibility $\chi(\mathbf{q}_0)$ and spin stiffness. ξ is estimated with Orstein-Zernicke relation:

$$
\begin{aligned}
\chi(\mathbf{q}) &= \frac{1}{L^2} \sum_{i,j} \frac{\langle \mathbf{S}_i \cdot \mathbf{S}_j \rangle}{T} e^{i\mathbf{q}(\mathbf{R}_i - \mathbf{R}_j)} \\
&= \frac{\chi(\mathbf{q}_0)}{1 + \xi^2(\mathbf{q} - \mathbf{q}_0)^2}
\end{aligned}
\tag{2.7}
$$

The temperature T^* of this sharp crossover is compatible with Miyashita's and Kawamura's results who found with quite a simple Monte Carlo approach $T \approx 0.3$ as a transition temperature. Contrary to above cited authors who consider it merely as a sharp crossover, Kawamura supports the idea of a peculiar transition. The original argument by Kawamura and Miyashita [50] is based on a thorough discussion of vortices in HTAF. As said these are $\mathbb{Z}_2$ vortices and not $\mathbb{Z}$ vortices as is the case in XY systems that exhibit BKT transition. To track the behaviour of vortices they introduce a vorticity function that is defined on the dual lattice links: 120-degree structure now stands at a vextex of the dual lattice; on the oriented links in the dual lattice the rotation of 120-degree structures from one end of the link to the other is a well-defined object that can be represented by an $SU(2)$ matrix U. Vorticity V is the function defined on closed loops C as follows:

$$
V(C) = \frac{1}{2} tr \left(\prod_{i \in C} U_i \right)
\tag{2.8}
$$

They showed that vorticity undergoes a transition between a perimeter-law asymptotic behaviour at low-temperature ($T < T^*$) and an area-law asymptotic behaviour at high temperature ($T > T^*$), which is similar to the behaviour of Wilson's loops [131, 55]:

$$
V_R = \langle V(C_R) \rangle \xrightarrow[R \to \infty]{} \begin{cases} \exp(-\alpha A) & T > T^* \\ \exp(-\beta R) & T < T^* \end{cases}
\tag{2.9}
$$

where C_R is a loop of length R, A is the enclosed area. In fact this point emphasises the role played by free vortices to drive the system from low-temperature phase to

high-temperature phase. On this particular point all groups do agree. On the nature of the change at T^* there is a disagreement. Kawamura and coworkers further support their viewpoint [53] pointing out the existence of two different length scales. Indeed as already discussed in their early paper [51, 50], the transition cannot be a BKT one. It is then hardly surprising that they disagree with other groups like Wintel and his coworkers who are specifically looking for a BKT transition. Let's further develop the argument. Vorticity exhibits a sharp drop from low-temperature regime to high-temperature regime, similarly to what happens in a usual BKT transition. There is however an important difference: in HTAF spin stiffness doesn't undergo any such sharp drop whereas in usual BKT transition both spin stiffness and vorticity behave the same way with a jump at the same temperature. Here comes the main difference between a BKT transition and what occurs in HTAF: the existence of two different length scales, namely the one of spinwaves and the one of vortices [53]. The former doesn't diverge at the transition contrary to the latter. In other terms the system is characterised by two different stiffnesses. Spin correlation function $C(r_{ij}) = \langle \mathbf{S}_i \cdot \mathbf{S}_j \rangle$ can be factorised into a spinwave contribution and a vortex contribution, the same way it is done for BKT transitions: $C(r_{ij}) = C_{sw}(r_{ij})C_v(r_{ij})$ [40]. Assuming the normal exponential form for correlation functions, correlation length then reads:

$$\xi = \frac{\xi_{sw}\xi_v}{\xi_{sw} + \xi_v} \tag{2.10}$$

Consequently in the vicinity of the transition where $\xi_v \gg \xi_{sw}$ correlation length exhibits a weak essential singularity:

$$\xi \sim \xi_{sw}\left(1 - \frac{\xi_{sw}}{\xi_v}\right) \tag{2.11}$$

Spin correlation length remains finite at low temperature: spin correlation decays exponentially *both* above and below the transition. This exponential decay was expected due to Mermin-Wagner theorem; a more sophisticated argument based on topological considerations consists in the following: symmetries involved in a phase transition can be found and analysed through the space associated with low-temperature phase removing its topological defects, here vortices, and retaining all other parameters equal. In topological language this means calculating the universal covering of the order parameter space. Here the universal covering of $SO(3)$ is S^3, the three-dimensional sphere. S^3 is the order parameter space of Heisenberg ferromagnetic four-component spin system as well: in two dimensions, spin correlations in this system decay exponentially, which indicates the same occurs in HTAF at zero field. Low-temperature phase is not an ordered state in the traditional way but is topologically ordered as the single accessible sector is the one without any free vortex. The nature of low-temperature phase is thus rather uncommon: Kawamura and coworkers proposed to call such a state that is neither a liquid nor an ordered AF state a spin gel [53].

2.3   Finite-field behaviour: symmetry discussion

As discussed in the preceding section, zero-field behaviour excludes finite-temperature transition to a long-range ordered phase with a gapped spectrum, ie a massive phase. It was consequently quite surprising to realise so far published phase diagrams depict transition lines going to a finite-temperature multicritical point at zero-field [52], which disregards an essential feature of HTAF, namely that zero-field configurations are massless. Indeed the existence of such a multicritical point would imply an infinitesimally small field makes the system massive: this is quite questionable a statement! For this reason it was necessary to examine anew finite-field behaviour in Heisenberg triangular antiferromagnet. A more natural viewpoint is indeed that finite-field transition lines close at $(T, h) = (0, 0)$.

Looking back at the antiferromagnetic order parameter in Eq. (2.6) symmetries at finite field can be discussed. If we consider a simple translation $\hat{T}_a$ with a lattice vector $\mathbf{a}$ ($\mathbf{r}_i \rightarrow \mathbf{r}_i + \mathbf{a}$) the order parameter is transformed as

$$\hat{T}_a[\mathbf{l_1} + i\mathbf{l_2}] = (\mathbf{l_1} + i\mathbf{l_2})e^{-i\mathbf{q_0}\cdot\mathbf{a}} \tag{2.12}$$

with the phase factor $\mathbf{q_0} \cdot \mathbf{a} \in \{0, \pm 2\pi/3\}$, which means that an inherent discrete $\mathbb{Z}_3$ symmetry exists besides the continuous S^1 symmetry associated with free rotations about the direction of the applied field $\hat{\mathbf{z}}$. Hence the system is governed by a compound symmetry $S^1 \otimes \mathbb{Z}_3$. Yet as seen with (2.5) a continuous degeneracy still exists: it doesn't match any symmetry in the Hamiltonian. In such a case it is legitimate to wonder whether this degeneracy of ground state manifold is robust against fluctuations. For a degeneracy not associated with any symmetry of the Hamiltonian, no Goldstone mode exists [34], which implies there is no entropy gain for such states. In our case relevant fluctuations are thermal ones. As shown by Sheng and Henley [106], thermal fluctuations must be calculated at higher order than the second one for degeneracy to be removed; a selection does occur reducing degeneracy to $S^1 \otimes \mathbb{Z}_3$. This reduction of degeneracy is an example of an 'order by disorder' scheme [124].

At low temperature and low field the expected stable configuration is the so-called 120-degree configuration which is a natural solution of (2.5). A simple calculation shows that 120-degree configuration is not stable above $h = 3$. Since ground state configurations are defined by the configuration on any triangle, let's write (2.3) using a three-sublattice pattern:

$$\begin{aligned}
\mathcal{H} &= \frac{N}{3} \times \frac{1}{2} \times 6 \left(\mathbf{m_1} \cdot \mathbf{m_2} + \mathbf{m_2} \cdot \mathbf{m_3} + \mathbf{m_3} \cdot \mathbf{m_1}\right) - \frac{N}{3}\mathbf{h}\left(\mathbf{m_1} + \mathbf{m_2} + \mathbf{m_3}\right) \\
&= N\varepsilon
\end{aligned}$$

where $\mathbf{m}_i = \langle \mathbf{S}_i \rangle$ is thermal averaged value of the spins of $i-$th sublattice, N is the number of spins, and ε the average energy per spin:

$$\varepsilon = \mathbf{m_1} \cdot \mathbf{m_2} + \mathbf{m_2} \cdot \mathbf{m_3} + \mathbf{m_3} \cdot \mathbf{m_1} - \frac{\mathbf{h}}{3}\left(\mathbf{m_1} + \mathbf{m_2} + \mathbf{m_3}\right) \tag{2.13}$$
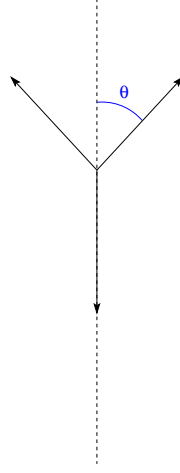
Figure 2.1: Distorted 120-degree structure with the definition of the angle θ. The structure is rotationally symmetric about the dashed axis that stands for the external field direction or the anisotropy axis (as discussed in Sec. 3.1). The three arrows stand for the three spins of a triangular plaquette.

The energy of a deformed 120-degree structure (see Fig. 2.1) then reads:

$$\varepsilon = \cos 2\theta - 2\cos\theta + \frac{h}{3}(1 - 2\cos\theta) \qquad (2.14)$$

The minimisation of (2.14) with respect to θ yields:

$$\cos\theta = \frac{1}{2}\left(1 + \frac{h}{3}\right) \qquad (2.15)$$

which shows such a configuration exists if and only if $h \leqslant 3$.

At $T = 0$ a transition must therefore occur between low-field ($h < 3$) and high-field ($h > 3$) regimes. In fact an intermediate phase separates the low-field low-temperature and quasi long-range ordered 120-degree phase from high-field configuration [35]. The intermediate phase corresponds to one-third magnetisation plateau: it is an up-up-down collinear configuration. Consequently spin-flop transition doesn't exist: instead double continuous transitions occur. At $T = 0$, this intermediate collinear phase is confined to the point $h = 3$ that hence is a critical point that can be studied in quantum limit as an interesting quantum critical point. At finite temperature, thermal fluctuations are strong enough to stabilise this collinear phase in a larger domain of temperature-field plane in low field region (high fields obviously suppress up-up-down structure). At high field thermal fluctuations select a planar configuration instead of umbrella structure [106]: in this configuration two sublattices develop the same magnetisation [22] and non-zero transverse magnetisation exists as illustrated in Fig. 2.2.

Figure 2.2: High-field planar structure that is stabilised at $h > 3$, referred to as V-shape configuration in the text. It is characterised by $\mathbf{l_2} = 0$, $\mathbf{l_1}$ with components both along the direction of the dashed line that is the direction of field and of the easy-axis in case of easy-axis HTAF, and transverse to this direction and $\mathbf{m}$ along the dashed line. The three arrows stand for the three spins of a triangular plaquette.
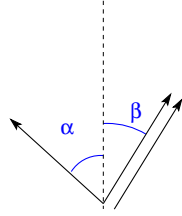
The natural question is then the nature of phase transitions occurring in the system. Such a treatment can be carried out discussing the order parameter symmetries. Considering the order parameter space, $S^1 \otimes \mathbb{Z}_3$, a discrete and a continuous symmetry have to be broken. Different scenarios are possible as Korshunov discussed it [60, 57, 58, 59]. Naturally there are three of them: either *(i)* the restoration of S^1 occurs before the restoration of the discrete symmetry or *(ii)* it is the opposite way round or *(iii)* there is a single transition that belongs to a new universality class. The latter case seems quite exotic and rather unlikely: the reason why it may have been suggested in some numerical studies is that numerical accuracy at that time was too limited to distinguish both transitions. Modern numerical investigations have ruled it out. First two scenarios involve excitations associated with each symmetry: vortices for the continuous symmetry, domain walls for the discrete symmetry. As a consequence it is possible to investigate the restoration of the compound symmetry analysing the behaviour of these excitations, or in other words tools used to investigate each transition can be used (spin stiffness and/or vorticity for S^1, correlation function and/or susceptibilities for $\mathbb{Z}_3$). A major difference between both scenarios is that in the second case fractional vortices form at kinks on domain walls [60, 57, 58], which implies the jump in spin stiffness is larger than it is in case of integer vortices, namely $(2q^2/\pi)T$ for $1/q$ vortices. This can be considered a definitive way to distinguish between both scenarios.

To discuss the succession of phase transition it is necessary to distinguish low-field and high-field regions as the involved spin configurations are different. In low-field region, as previously mentioned, thermal fluctuations stabilise up-up-down collinear phase, which thus appear as an intermediate phase between 120-degree configuration and both high-field configuration and high-temperature (paramagnetic) phase. This means that discrete symmetry-breaking occurs first (in this case $\mathbb{Z}_3$) then continuous symmetry-breaking (S^1). Indeed collinear structure only breaks $\mathbb{Z}_3$ symmetry and leaves S^1 symmetry unbroken. The latter breaks down in 120-degree configuration. Furthermore leading order parameters associated with each phase transition are dif-

ferent: $\mathbb{Z}_3$ symmetry-breaking is associated with the component along field direction whereas S^1 symmetry-breaking is associated with transverse component. As ordering occurs along different components in low-field region, the order of phase transition is clear and associated universality classes as well: the upper transition corresponds to the ordering along the field (up-up-down structure) and pertains to three-state clock model universality class (cf.[9]) whereas the lower transition corresponds to the ordering along a transverse direction (120-degree structure) and pertains to a BKT universality class.

At high fields the situation is less clear because there is only one ordered phase which corresponds to a planar spin configuration with spins on two sublattices identical and with a finite transverse magnetisation, so-called V-shape configuration (see Fig. 2.2). As $\mathbf{l}_2 = 0$ in this high-field configuration, there is a single order parameter involved in the breaking of two symmetries. In real space the ordering actually occurs along a single component, namely the transverse one; the ordering of parallel component is induced by the ordering of transverse component as can be seen considering the following term of Landau-Ginzburg functional that comes into play: $S_q^z \left(S_q^\perp\right)^2$, which indicates that transverse component acts as an ordering field on parallel component. As previously discussed the breaking of compound symmetry $\mathbb{Z}_3 \otimes S^1$ at once is quite unlikely: successive transitions corresponding to the successive breaking of each component of this compound symmetry are thus expected. The tricky question to answer to is then the order of these transitions. Korshunov demonstrates case (ii) implies the existence of fractional vortices centered at kinks on domain walls. Numerically it can be checked examining spin stiffness jump at binding-unbinding transition: the jump for a $1/q$ fractional vortex is indeed $(2q^2/\pi)T_{BKT}$. From this observation he draws the conclusion that scenario (i) necessarily occurs: the transition temperature for the binding-unbinding transition of fractional vortices is indeed much lower than the estimate for the transition associated with domain walls (percolation threshold), which is contradictory with scenario (ii). Consequently there is no fractional vortices and scenario (i) should occur. In next section a way to numerically find out the transition sequence is proposed.

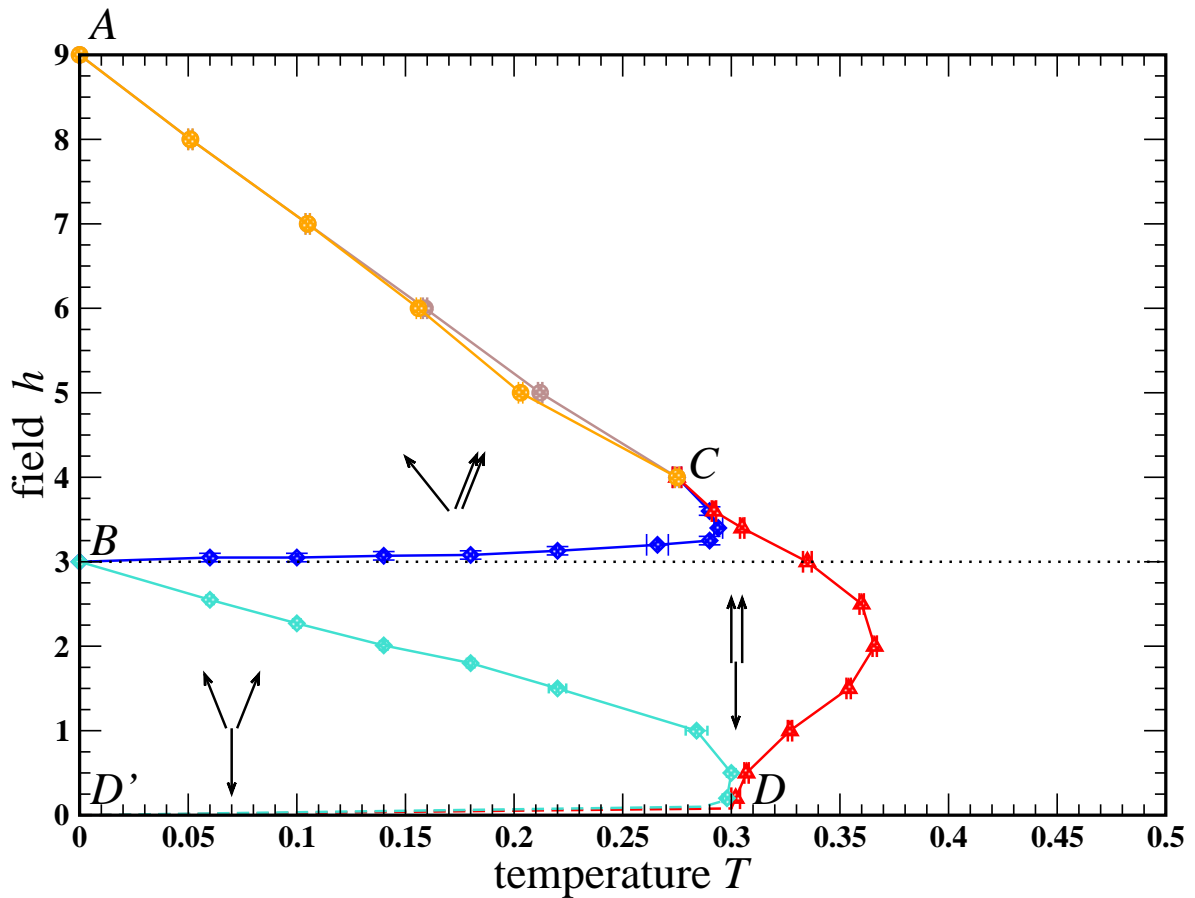**Figure 2.3:** Phase diagram of Heisenberg triangular antiferromagnet. Solid lines are a guide to the eye linking calculated points. Dashed lines indicate theoretically expected transitions for which precise numerical results have not yet been obtained. Spin structures are sketched by the configuration on a triangular plaquette with z axis assumed vertical and xy plane perpendicular to the plane of the sheet.

2.4   Finite-field behaviour: numerical determination

The phase diagram is numerically calculated using a hybrid algorithm that associates an optimised single-spin Monte Carlo algorithm with over-relaxation process (see App. E). The latter increases the portion of explored configuration space and therefore reduces the risk to remain trapped in a local minimum. With single-spin algorithm the risk is indeed quite important to get stuck in a local minimum, which hinders ergodicity property, an essential feature for Monte Carlo algorithm to be right. Our simulations have been carried out on finite-size rhombic clusters with periodic boundary conditions and linear sizes $24 \leqslant L \leqslant 120$ compatible with a three-sublattice pattern in order to avoid artificial frustration effects.

2.4.1   Preliminaries

Numerical calculation of a phase diagram consists in the identification of the relevant order parameters in the system according to symmetries at stake in the various phase transitions and the calculation of the most accurate numerical estimators of these order parameters or of observables reflecting them. Then it is possible to locate singularities in temperature or field dependence of these estimators, to use finite-size scaling to extract information about the precise location of phase transition and its nature (via the calculation of critical exponents). Both field and temperature sweeps have been carried out. In case of temperature sweeps the initial configuration is a random configuration in the paramagnetic region of phase diagram that is cooled down until the temperature range of interest. For field sweeps the initial configuration is a fully polarised configuration in the saturated phase.

Beside observables that are explicitly discussed and presented in the Monte Carlo numerical parts of this work, few calculations of the ordering vectors $\mathbf{l}_1$ and $\mathbf{l}_2$ have been carried out in terms of the third-order invariant $(l_1^\alpha + i l_2^\alpha)^3$. This approach is yet more adapted to mean-field analysis and within a Monte Carlo investigation the calculation of more directly accessible observables is more interesting, which is the reason why I only present results for these observables.

Let's discuss how this general program is here implemented. Of course one of the most straightforward idea is to track specific heat which can be defined as a measurement of energy variance:

$$c = \frac{\langle E^2 \rangle - \langle E \rangle^2}{N_s T^2} \tag{2.16}$$

where E is the internal energy and $N_s = L^2$ the number of spins in the considered cluster. Specific heat is however hardly suited to precisely locate such transitions as BKT (for the appearance of specific heat peak at a higher temperature T than T_{BKT}, see eg Fig. 9.4.3 in [20]) and often requires a fine sampling in the vicinity of phase transition to extract a precise estimate of transition temperature. However specific heat can be

helpful to identify the nature of a phase transition thanks to the determination of critical exponent α. Numerical estimators associated with other observables have therefore been considered as well: spin structure factor components; Binder's cumulant corresponding to spin structure factor; spin susceptibility; spin stiffness. Let's detail these different quantities. Spin structure factor is the Fourier transform of spin configuration at the ordering wave vector $\mathbf{q} = \mathbf{q}_0 = (4\pi/3, 0)$ and its components constitute relevant order parameters in this problem. In our numerical calculations we have calculated various even powers of its components; for example:

$$\left(m_{\mathbf{q}}^{\alpha}\right)^2 = \frac{1}{N_s^2} \sum_{i,j} \langle S_i^{\alpha} S_j^{\alpha} \rangle e^{i\mathbf{q}\cdot(\mathbf{r}_i - \mathbf{r}_j)} \tag{2.17}$$

A frequently used quantity to locate phase transitions (first and second order and infinite order as well) is Binder's cumulant that is a fourth-order quantity defined as follows:

$$U_A = \frac{\langle A^4 \rangle}{\langle A^2 \rangle^2} \tag{2.18}$$

where A is the order parameter of interest. At critical points Binder's cumulant becomes size-independent: as a consequence plots of Binder's cumulant versus temperature for different cluster sizes cross at a second-order phase transition, merge at a BKT transition (plots are on top of each other in low-temperature phase). In this case finite-size scaling is straightforward. As a fourth-order quantity Binder's cumulant is a statistical estimator that exhibits fluctuations that may be large especially in frustrated systems. A remedy is to consider a second-order quantity with similar properties: a ratio of spin-spin correlation functions fulfilling these requirements has been proposed by Tomita and Okabe [120, 112] (see App. D):

$$\Gamma^y = \frac{g(L/2, L, T)}{g(L/4, L, T)} \tag{2.19}$$

where $g(r, L, T) = L^{-d} \sum_i \langle \mathbf{S}_i \cdot \mathbf{S}_{i+r} \rangle$ is the spin-spin correlation function calculated on a cluster of linear size L, at temperature T for spins at distance r apart ($i + r$ short for neighbours at distance r of spin i). This ratio often exhibits better statistics than Binder's cumulant. As both observables are independent of any assumption on the nature of the transition (order, class of universality) they are quite useful a reference to check hypotheses made for the scaling of other parameters such as susceptibility.

Susceptibility is indeed a key element of various finite size scaling techniques to locate transitions and to calculate critical exponents, details of which are developed in App. D. Furthermore spin susceptibility is a second order quantity, which implies weaker fluctuations than for Binder's cumulant. Spin susceptibility characterises linear response of spins to a magnetic field. It is a second-order tensor the indexes of which

run over field directions in spin space. As there are here no off-diagonal terms, it then reads:

$$\chi_{\mathbf{q}}^{\alpha} = \frac{1}{N_s} \sum_{i,j} \frac{\langle S_i^{\alpha} S_j^{\alpha} \rangle}{T} \, e^{i\mathbf{q} \cdot (\mathbf{r}_i - \mathbf{r}_j)} \tag{2.20}$$

The most widely used means of studying BKT transition remains finite size scaling of spin stiffness ρ_S, which is associated with the very origin of this kind of transition, namely the unbinding of stable point defect, vortices. At BKT transition spin stiffness exhibits a jump the height of which is universal: $\rho_S = 2T_{BKT}/\pi$ in case of integer vortices ($\rho_S = 0$ in high-temperature phase). Spin stiffness is defined as a general elasticity coefficient in response to a weak nonuniform twist of spins $\delta\phi^{\alpha}(\mathbf{r})$ performed about a certain direction α in spin space. In our case it is sufficient to consider twists about $\hat{\mathbf{z}}$ direction, the direction of applied field, in spin space while all directions in lattice plane are equivalent thanks to sixfold rotational symmetry. A single parameter is thus left

$$\delta F = \frac{\rho_S}{2} \int \mathrm{d}^2 \mathbf{r} [\nabla \phi^z(\mathbf{r})]^2 \tag{2.21}$$

Choosing a twist with a uniform gradient along an arbitrary direction $\hat{\mathbf{e}}$ in the lattice plane, one obtains in spherical coordinates

$$\mathbf{S}_i \cdot \mathbf{S}_j = \cos(\theta_i)\cos(\theta_j) + \sin(\theta_i)\sin(\theta_j)\cos(\tilde{\varphi}_i - \tilde{\varphi}_j) \tag{2.22}$$

with $\tilde{\varphi}_i = \varphi_i + \delta\phi \, \hat{\mathbf{e}} \cdot \mathbf{r}_i$.

Calculating the change in the free energy up to second order in a small $\delta\phi$ and normalizing the result per unit area one obtains [92, 115, 127]:

$$\rho_S = -\frac{1}{L\sqrt{3}} \sum_{\langle i,j \rangle} \langle S_i^x S_j^x + S_i^y S_j^y \rangle + \frac{2}{LT\sqrt{3}} \left\langle \left\{ \sum_{\langle i,j \rangle} (S_i^x S_j^y - S_i^y S_j^x)[\hat{\mathbf{e}} \cdot (\mathbf{r}_i - \mathbf{r}_j)] \right\}^2 \right\rangle \tag{2.23}$$

2.4.2 Numerical results

As discussed in section 2.3, low-field and high-field regions have to be treated in different ways as the stabilised structures are different. Let's start with low-field region: collinear ordering and the ordering into 120-degree configuration are expected. The former happens along field direction $\hat{\mathbf{z}}$ and can thus be probed plotting Binder's cumulant associated with z-component of $S(\mathbf{q})$ versus temperature:

$$U_q^z = \frac{\langle (S_q^z)^4 \rangle}{\langle (S_q^z)^2 \rangle^2} \tag{2.24}$$

The crossing of plots for different cluster sizes indicates the transition into a long-range ordered phase. As HTAF adopts a planar ordering and up-up-down collinear structure
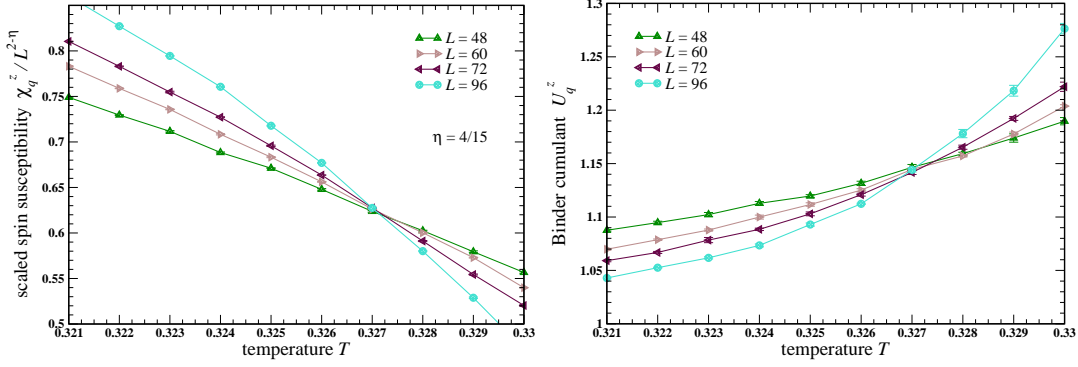
Figure 2.4: Scaling of spin susceptibility χ_q^z with critical exponent $\eta = 4/15$ corresponding to three-state clock-model universality class as $\chi_q^z/L^{2-\eta}$ yields a transition temperature $T_c = 0.327 \pm 0.001$ (left). The temperature obtained with Binder's cumulant U_q^z as shown on the right is the same. Both figures are drawn at field $h = 1.0$.

breaks $\mathbb{Z}_3$ symmetry the phase transition should pertain to three-state clock model universality class as is the case for XY model. With this viewpoint it is then possible to scale z-component of spin susceptibility (calculated as in (2.20) with $\alpha = z$) with the corresponding critical exponent η, $\eta = 4/15$ in this case. The transition temperature is obtained as the temperature of the crossing point of plots for different cluster sizes. Fig. 2.4 illustrates both methods at $h = 1.0$.

As the system is cooled down a BKT transition is expected for transverse spin component. This transition can be located using transverse spin susceptibility with $\eta = 1/4$ for its scaling as shown in Fig. 2.5. This method can be used both during temperature and field sweeps: given the shape of the transition line $\widehat{BDD'}$ into 120-degree phase it is indeed convenient to sweep field at fixed temperature in low-temperature region — the closer to straight angle is the angle between the sweeping line and the transition line, the sharper the location of the transition. Fig. 2.6 illustrates such a field sweep at $T = 0.06$ with both transverse spin susceptibility and Binder's cumulant; insets provide an enlarged view around the transitions. Defined in a natural way using (2.20), transverse spin susceptibility reads:

$$\chi_{\mathbf{q}}^{\perp} = \frac{1}{N_s^2} \sum_{i,j} \frac{\langle S_i^x S_j^x + S_i^y S_j^y \rangle}{T} \, e^{i\mathbf{q}\cdot(\mathbf{r}_i - \mathbf{r}_j)} \tag{2.25}$$

In the final diagram (see Fig. 2.3) transition lines $\widehat{D'D}$ at very low field appears as dashed lines: this expresses the difficulty to precisely locate transitions in the vicinity of zero-field. Even though hints of a transition can be sensed, statistical errors due to large fluctuations in this critical region (due to the nature of low-temperature zero-field phase, a severe slowing down of the convergence of Monte Carlo algorithm occurs) prevent us to fix for sure transition lines. However the argument earlier put forward
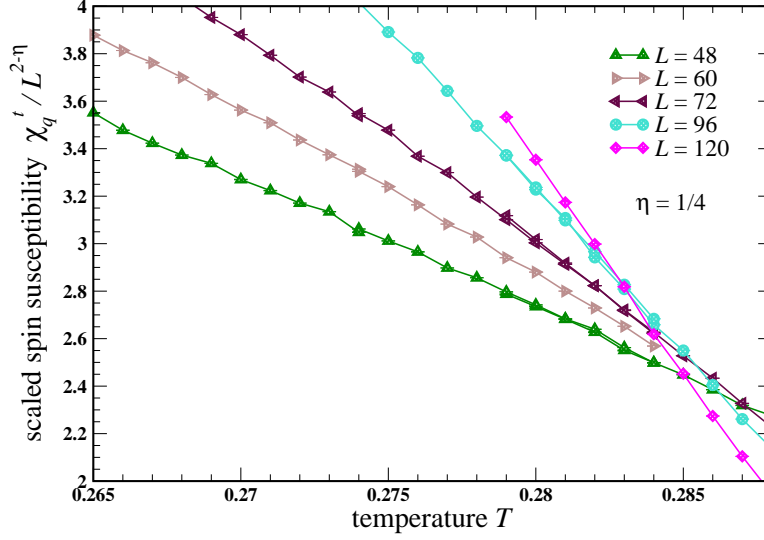
Figure 2.5: Scaling of spin susceptibility $\chi_q^{\perp}$ with critical exponent $\eta = 1/4$ corresponding to BKT universality class as $\chi_q^{\perp}/L^{2-\eta}$ at $h = 1.0$.

(an infinitesimal field cannot turn a massless phase into a massive one) lets us interpret these numerical hints as a further support for our proposition that transition lines go to $(T, h) = (0, 0)$.

Above $h = 3.0$ ordering occurs along transverse component. First a transition that can be easily investigated is the transition between up-up-down collinear phase and high-field phase: as previously explained there is no spin-flop first-order transition but a continuous transition. From symmetry analysis this transition is associated with S^1: it can thus be located the same way as the transition between collinear phase and 120-degree phase as can readily be seen in Fig. 2.6.

Concerning the ordering process from paramagnetic phase or saturated phase, the delicate problem of the breaking of compound $\mathbb{Z}_3 \otimes S^1$ symmetry for a single order-parameter, namely $\left(S_q^{\perp}\right)^2$, has to be dealt with. As stated among three possible scenarios one is expected to occur: first the breaking of discrete $\mathbb{Z}_3$ symmetry, then the breaking of continuous S^1 symmetry. To find out whether numerical results support or not this hypothesis it is necessary to extract the relevant information from data. Observables giving access to each symmetry separately have to be considered. As far as $\mathbb{Z}_3$ is concerned, scaling of transverse spin susceptibility can be used with critical exponent $\eta = 4/15$ corresponding to the class of universality of three-state clock model. This method yields a transition that is confirmed by the study of both the ratio of correlation functions $\Gamma^{\perp}$ and Binder's cumulant $U_q^{\perp}$ as illustrated in Fig. 2.7. As for BKT transition spin stiffness ρ_S is used. It is plotted versus temperature; the height of the jump in this case is incompatible with fractional vortices: integer vortices are at

stake. The temperature at the intersection of $\rho_S(T, L)$ with the line $(2/\pi)T$ is called T_L. The extrapolation to thermodynamic limit reads (cf App. D and Eq. D.21)

$$\frac{T_L - T_{BKT}}{T_{BKT}} = \frac{1}{2(\ln L + c)} \tag{2.26}$$

This requires a non-linear fitting with two parameters, T_{BKT} and $c = -\ln L_0$. Such a fit is illustrated in Fig. 2.7. In this way BKT transition is obtained at slightly lower temperature than the one associated with discrete symmetry breaking. These results support Korshunov's defense of scenario (i). Interestingly that in the case of isotropic HTAF the splitting between transitions is much tinier than in the case of easy-axis HTAF as can be seen in Fig. 3.8
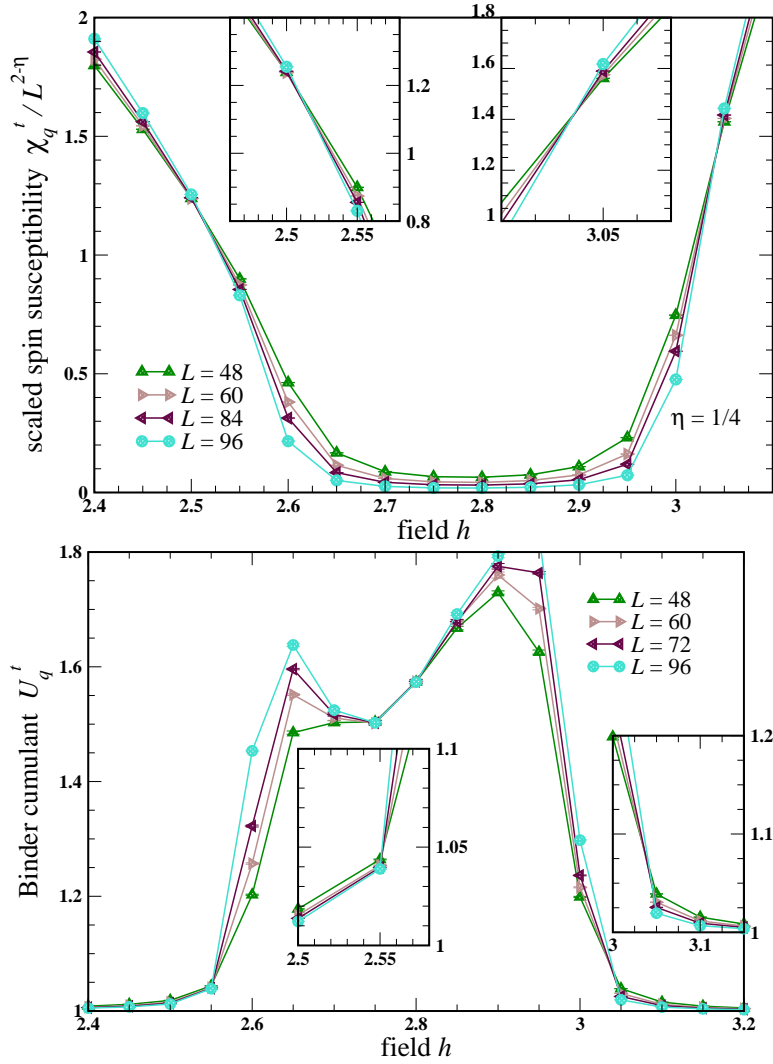
Figure 2.6: Field sweeping at $T = 0.06$. Scaling of spin susceptibility $\chi_q^{\perp}$ with critical exponent $\eta = 1/4$ corresponding to BKT universality class as $\chi_q^{\perp}/L^{2-\eta}$ (top). Insets give an enlarged view of crossing points that corresponds to BKT transitions: $h \leqslant 2.50$ corresponds to 120-degree phase, $2.50 \leqslant h \leqslant 3.04$ to collinear phase, and $3.04 \leqslant h$ to high-field phase. Binder's cumulant plotted versus temperature (bottom) confirms these transitions; insets offer an enlarged view on transition regions.
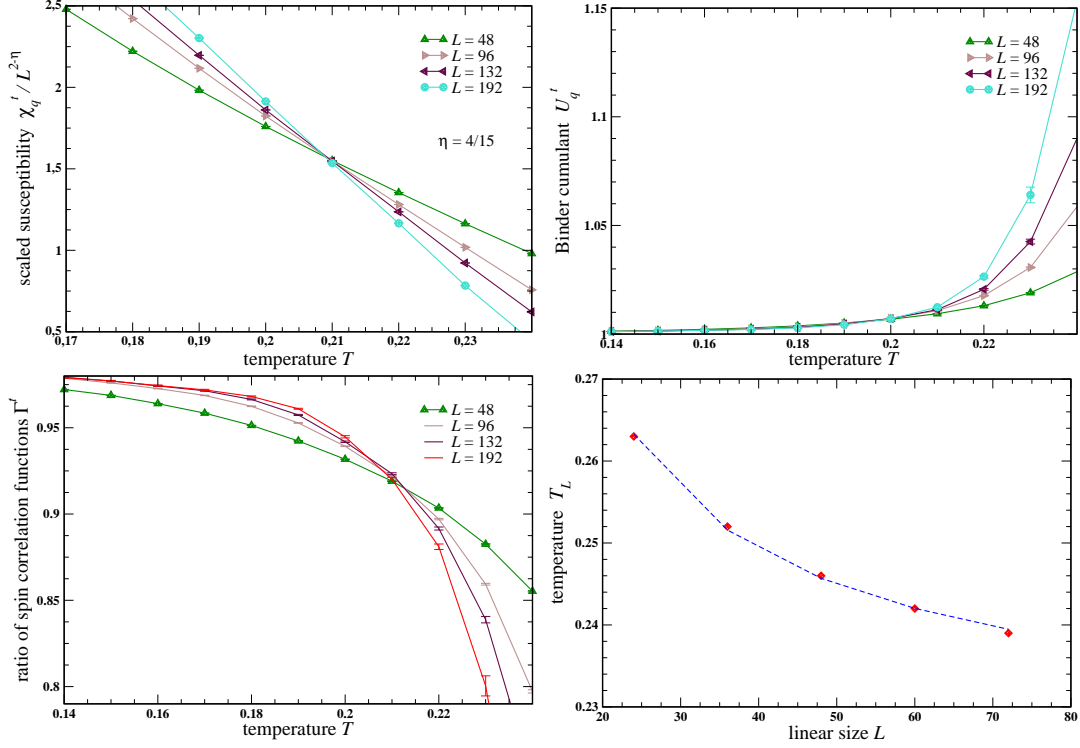
Figure 2.7: Comprehensive data for the location of transitions at $h = 5.0$. Scaling of spin susceptibility $\chi_q^\perp$ with critical exponent $\eta = 4/15$ corresponding to the universality class of three-state clock-model as $\chi_q^\perp / L^{2-\eta}$ (upper left). Binder's cumulant exhibits a merging of curves for different cluster sizes at the upper transition; it illustrates how hard it is to distinguish close transitions involving the same spin component using Binder's cumulant (upper right). The ratio of correlation functions $\Gamma^\perp$ sharply indicates the upper transition as a crossing for different cluster sizes; yet it also shows that here considered cluster sizes are somewhat too small to precisely locate BKT transition the presence of which can be seen in the merging of curves occurring for the largest sizes (lower left). BKT transition is located thanks to the scaling of T_L the temperature such that $\rho_S(T_L, L) = (2/\pi)T_L$ as described by Eq. D.21: non-linear fitting yields $T_{BKT} = 0.203 \pm 0.001$ and $c = -2.99 \pm 0.001$.

Chapter 3

Heisenberg Triangular Antiferromagnet with easy-axis single-ion anisotropy

In previous chapter a presentation of the phase diagram of HTAF is proposed. As seen one important characteristic of this diagram is the absence of ordering at zero field. This peculiarity is yet often absent in real compounds due to various perturbation terms; one of particular importance is single-ion anisotropy (see App. A for further details). When considering the easy-axis case as done in this chapter the system retains exactly the same symmetries as HTAF at finite field provided the field is applied along the anisotropy axis – hereafter I consider the case of a system with a global anisotropy axis rather than local anisotopy axes. As symmetries at finite field are the same as in HTAF the reader should refer to Sec. 2.3; at zero-field symmetries are specific to this anisotropic system and are discussed in Sec. 3.1: quite interesting a succession of transitions occurs, with three transitions (see [73] as well). At a mean-field level this succession reflects the change of sign of a sixth-order coefficient in Landau-Ginzburg expansion of free energy, which is associated with the discrete six-fold symmetry existing in the system. A mean-field analysis was carried out to further discuss symmetries and for its relevance for quasi-2d layered systems; it ascertains the stability of three-sublattice structures as structures with minimal energy as well. Mean-field treatment is carried out in Sec. 3.2. Then thermal fluctuations are taken into account through a Monte Carlo procedure and the whole phase diagram is calculated (see Fig. 3.8) both at zero field (Sec. 3.3) and finite field (Sec. 3.4).

3.1   Symmetries at zero field

Let's first write the Hamiltonian:

$$\mathcal{H} = \sum_{\langle i,j \rangle} \mathbf{S}_i \cdot \mathbf{S}_j - d \sum_i (S_i^z)^2 - h \sum_i S_i^z \qquad (3.1)$$

where terms are expressed in the units of the exchange constant J and spins are classical spins normalised to 1. In this chapter easy-axis anisotropy is considered, ie $d > 0$.

In contrast to zero-field spin configuration in Heisenberg triangular antiferromagnet, spin configurations in easy-axis Heisenberg antiferromagnet do exhibit a nonzero static magnetisation even at zero field:

$$\langle \mathbf{S}_i \rangle = \mathbf{l}_1 \cos (\mathbf{q} \cdot \mathbf{r}_i) + \mathbf{l}_2 \sin (\mathbf{q} \cdot \mathbf{r}_i) + \mathbf{m} \qquad (3.2)$$

where $\mathbf{q} = \mathbf{q}_0 = (4\pi/3, 0)$. Easy-axis anisotropy orients spin plane perpendicular to xy crystallographic plane and simultaneously distorts the spin structure. Finding directions and magnitudes of $\mathbf{l}_1$ and $\mathbf{l}_2$ then becomes quite nontrivial a task.
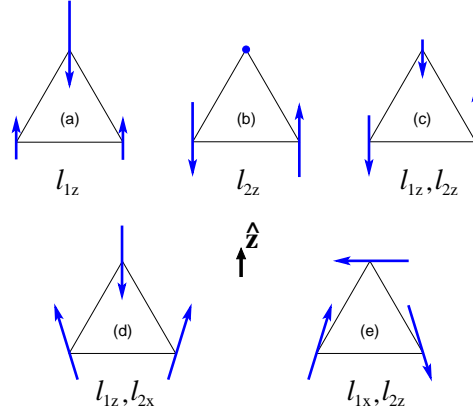
Figure 3.1: Possible three-sublattice planar configurations of the easy-axis triangular antiferromagnet. The direction of the easy-axis is indicated by $\hat{\mathbf{z}}$. Non-zero components of the order parameter (3.2) are indicated below each configuration.

The same way it was previously discussed (see Sec. 2.3) in order to elucidate symmetries of different phases, we note that a simple translation by a lattice vector $\mathbf{a}$ $\hat{T}_\mathbf{a}$ $(\mathbf{r}_i \to \mathbf{r}_i + \mathbf{a})$ transforms the antiferromagnetic order parameter according to

$$\hat{T}_\mathbf{a} \big[(\mathbf{l}_1 + i\mathbf{l}_2) \big] = (\mathbf{l}_1 + i\mathbf{l}_2) \, e^{-i\mathbf{q}_0 \cdot \mathbf{a}} \,, \qquad (3.3)$$

where the phase factor can take only three different values: $\mathbf{q}_0 \cdot \mathbf{a} = 0, \pm 2\pi/3$. Hence, besides the group S^1 of continuous rotations about $\hat{\mathbf{z}}$-axis the magnetic structure has an

inherent discrete symmetry $\mathbb{Z}_3$. Such an additional symmetry corresponds to permutations of the three sublattices. In zero magnetic field the time-reversal symmetry implies invariance with respect to $\mathbf{l}_i \rightarrow -\mathbf{l}_i$, which enlarges $\mathbb{Z}_3$ to $\mathbb{Z}_6$. The total symmetry group is, therefore,

$$G = S^1 \otimes \mathbb{Z}_6 \tag{3.4}$$

See also a similar discussion in Ref. [106]. The collinear phases shown in Figs. 3.1(a)-(c) preserve the axial symmetry S^1 but break in different ways the discrete symmetry group $\mathbb{Z}_6$. In terms of the order parameter angle φ defined by

$$l_{1z} = l \cos \varphi \ , \qquad l_{2z} = l \sin \varphi \ , \tag{3.5}$$

the state in Fig. 3.1(a) corresponds to commensurate values $\varphi = 2k\pi/6$ with an integer k, whereas the configuration in Fig. 3.1(b) has $\varphi = (2k + 1)\pi/6$. The third type of collinear state is described by an arbitrary angle φ and is shown schematically in Fig. 3.1(c). In such a state the phase φ remains unlocked and the sine and cosine harmonics introduced in (3.5) coexist with an arbitrary ratio.

For large enough values of $d > d_c = 1.5$ the magnetic anisotropy induces a highly degenerate collinear Ising state at zero temperature. Quantum fluctuations can lead, then, to interesting zero- and finite-temperature phases [25, 103]. This collinear ordering results from the disappearance of deformed 120-degree structures. It can be understood by a simple calculation of average energy per spin assuming a three-sublattice structure with 120-degree configuration as shown in Fig. 3.1(d). Let's introduce $\mathbf{m}_i = \langle \mathbf{S}_i \rangle$ the thermal average magnetisation of spins in the $i-$th sublattice. Then the average energy per spin ε reads:

$$\varepsilon = \mathbf{m}_1 \cdot \mathbf{m}_2 + \mathbf{m}_2 \cdot \mathbf{m}_3 + \mathbf{m}_3 \cdot \mathbf{m}_1 - \frac{d}{3}\left((m_1^z)^2 + (m_2^z)^2 + (m_3^z)^2\right) - \frac{h}{3}(m_1^z + m_2^z + m_3^z) \tag{3.6}$$

The energy of a deformed 120-degree as depicted in Fig. 2.1 at zero field can then be expressed in terms of the deviation angle θ as

$$\varepsilon = -2\cos\theta + \cos 2\theta - \frac{d}{3}(1 + 2\cos^2\theta) \tag{3.7}$$

The angle θ that minimises ε verifies

$$\cos\theta = \frac{1}{2(1 - d/3)} \tag{3.8}$$

which immediately shows the upper bound of d for such a structure to exist, namely $d_c = 3/2$. The Ising limit $d > d_c$ for interesting it may be is already well-documented and has not been the focus of my attention. Moderate anisotropy domain which has been overlooked for long presents quite interesting properties which are worth the discussion. As a consequence I only develop this case of moderate anisotropy, $0 < d < d_c$. In Sec. 3.2

$d = 1.0$ is used. Figures presented in Sec. 3.3 have been calculated with $d = 1.0$; yet results for zero-field within Monte Carlo approach have also been obtained for $d = 0.2$ that is the value used to build the whole phase diagram presented in Fig. 3.8.

Both 120-degree structures 3.1(d) and (e) are not energetically degenerate. Indeed evaluating (3.7) with (3.8) yields

$$\varepsilon_1 = -\frac{d}{3} - 1 - \frac{1}{2(1 - d/3)} \tag{3.9}$$

A similar procedure for configuration 3.1(e) leads to the following

$$\varepsilon_2 = -\frac{2d}{3} - 1 - \frac{1}{2(1 + d/3)} \tag{3.10}$$

Thence the energy difference

$$\Delta\varepsilon = \varepsilon_1 - \varepsilon_2 = -\frac{d^3}{1 - d^2} \tag{3.11}$$

This implies that both configurations are quasi-degenerate at low anisotropy as the removal of degeneracy is a third-order effect of anisotropy. Entropy can thus enable structure with the higher energy to be stabilised at finite temperatures as observed at mean-field level.

3.2   Real-space mean-field approach

Despite the break-down of mean-field in bidimensional system, such an approach is useful to assess symmetry analysis previously done: in this case mean-field calculations support a three-sublattice ordering. On a technical point of view the extension of real-space mean-field [7, 113, 19, 29] to a model with single-ion anisotropy presents some interest as well — for example to deal with pyrochlore magnets. These technical details can be found in Appendix B.

Mean-field Hamiltonian reads

$$\hat{\mathcal{H}}_{\mathrm{MF}} = -\sum_{\langle ij \rangle} \mathbf{m}_i \cdot \mathbf{m}_j + d \sum_i (S_i^z)^2 - \sum_i \mathbf{h}_i \cdot \mathbf{S}_i \ , \qquad \mathbf{h}_i = \mathbf{h} - \sum_{j(i)} \mathbf{m}_j \tag{3.12}$$

where $\mathbf{m}_i = \langle \mathbf{S}_i \rangle$. Mean-field treatment yields the following system of self-consistent equations (cf Eq. B.14):

$$
\begin{aligned}
m_i^{\perp} &= \frac{1}{2Z_i} \int_{-1}^{1} \mathrm{d}x \, \sqrt{1 - x^2} \, e^{dx^2/T} \, e^{h_i^z x/T} I_1(y_i) \ , \\
m_i^z &= \frac{1}{2Z_i} \int_{-1}^{1} \mathrm{d}x \, x \, e^{dx^2/T} \, e^{h_i^z x/T} \, I_0(y_i) \ , \\
Z_i &= \frac{1}{2} \int_{-1}^{1} \mathrm{d}x \, e^{dx^2/T} \, e^{h_i^z x/T} I_0(y_i) \ ,
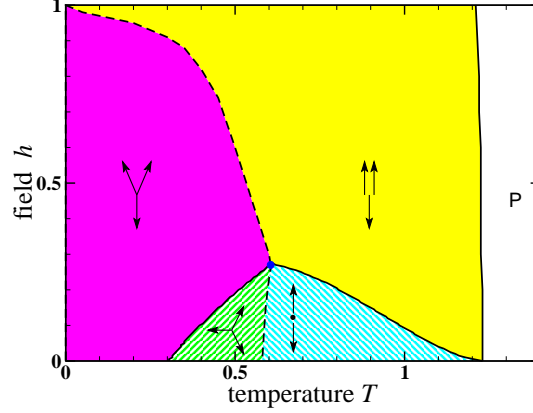\end{aligned}
\tag{3.13}
$$

Figure 3.2: Low-field part of mean-field phase diagram with **h** along the anisotropy axis and the anisotropy strength d taken as $d = 1$. Spin configurations for each phase are schematically indicated by arrows as in Fig. 3.1. Solid and dashed lines corresponds to first- and second-order transitions, respectively.

where $y_i = h_i^\perp \sqrt{1 - x^2}/T$ and $I_n(z)$ is the modified Bessel function of the n-th order:

$$I_n(z) = \frac{1}{\pi} \int_0^\pi d\alpha \, e^{z \cos \alpha} \cos^n \alpha \ . \tag{3.14}$$

In conjunction with the self-consistent constraint

$$\mathbf{h}_i = \mathbf{h} - \sum_{n.n.} \mathbf{m}_j \tag{3.15}$$

this system of equations can be iteratively solved on $L \times L$ clusters; in this study sizes L with $3 \leqslant L \leqslant 12$ have been used to check the stability of three-sublattice structure. Then to precisely locate phase boundaries the system (3.13,3.15) is solved assuming a three-sublattice structure.

Once convergence is achieved, various physical quantities are calculated including the free-energy

$$\mathcal{F}_{\mathrm{MF}} = -J \sum_{\langle ij \rangle} \mathbf{m}_i \cdot \mathbf{m}_j - T \sum_i \ln Z_i \ , \tag{3.16}$$

the internal energy $E_{\mathrm{MF}} = \langle \mathcal{H}_{\mathrm{MF}} \rangle$, and the antiferromagnetic order parameters. The latter cannot be calculated as such but have to be calculated using a third-order invariant, which takes into account the effect of translation (Eq. (3.3)): $(l_1^\alpha + i l_2^\alpha)^3$, where the real-part is zero if and only if $l_1^\alpha = 0$, and the imaginary part is zero if and only if $l_2^\alpha = 0$. By explicit calculations for clusters with $3 \leqslant L \leqslant 12$ at all temperatures and weak magnetic fields we have verified stability of the three-sublattice structure with $\mathbf{q}_0 = (4\pi/3, 0)$. After that a more detailed investigation of the H–T phase diagram has been performed with the three-sublattice ansatz. Precise location of phase boundaries

in Fig. 3.2 has been determined from temperature and field scans for the antiferromagnetic order parameters indicated in Fig. 3.1 as well as for the uniform magnetization. The behaviour of the specific heat has been also used to independently verify these results.

At the upper transition $T_{c1} \simeq 1.2$ in zero magnetic field only z-component of magnetic moments become ordered. In accordance with $\mathbb{Z}_6$ symmetry, selection between various collinear structures is determined by the following invariant in Landau free-energy:

$$\gamma_2 \big[(l_1^z + i l_2^z)^6 + \text{c. c.} \big] \; . \tag{3.17}$$

For negative $\gamma_2 < 0$ the pure l_1-state, Fig. 3.1(a), is energetically favored, while $\gamma_2 > 0$ corresponds to the l_2-state, Fig. 3.1(b). We have verified the positive sign of γ_2 in our case by a direct analytical expansion of Eqs. (3.13) (see App. C). Our numerical results also confirm that the l_2-state is stable below T_{c1}. Such a partially ordered phase has a vanishing moment on one of the antiferromagnetic sublattices. A similar phase has been discussed in relation to the intriguing phase diagram of $Gd_2Ti_2O_7$ [111]. Here, we provide an example, where a partially ordered phase is realized at the mean-field level in a simple spin model.

The second transition at $T_{c2} \simeq 0.6$ is related to the breaking of the rotational symmetry about $\hat{\mathbf{z}}$-axis. Below T_{c2} the third previously disordered magnetic sublattice becomes ordered with moments oriented within the xy plane. Simultaneously, moments of the other two sublattices start deviating from $\hat{\mathbf{z}}$-axis leading to a distorted triangular structure shown in Fig. 3.1(e). This distorted spin structure is characterized by $\mathbf{l}_2 \parallel \hat{\mathbf{z}}$ and $\mathbf{l}_1 \perp \mathbf{l}_2$. When temperature is further decreased the coefficient γ_2 in the effective anisotropy term changes sign at $T_{c3} \simeq 0.3$ and one finds a first-order transition into another distorted triangular structure shown in Fig. 3.1(d) with $\mathbf{l}_1 \parallel \hat{\mathbf{z}}$.

Note, that the related model with the exchange anisotropy [84, 106] has $\gamma_2 = 0$ in the mean-field approximation, which leads to an additional continuous degeneracy. As a result, only two finite-temperature transitions are found in this case: from the paramagnetic state to a degenerate collinear configuration shown in Fig. 3.1(c) and then to a degenerate distorted 120° configuration [84, 110]. Sheng and Henley [106] have discussed how different types of fluctuations, thermal, quantum, or random dilution, can induce a finite γ_2. For the model with the single-ion anisotropy one finds a different interesting possibility: the sign of the anisotropic term changes upon lowering temperature.

The two phases in Figs. 3.1(a) and (d) have a nonvanishing total magnetisation m^z. The coupling between ferro- and antiferromagnetic components is determined by the term

$$m^z (l_1^z + i l_2^z)^3 + \text{c. c.} \; , \tag{3.18}$$

which is invariant under $\mathbb{Z}_3$ transformations (3.3). In zero magnetic field this yields $m^z \sim (T_c - T)^{3/2}$ for states with $\mathbf{l}_1 \parallel \hat{\mathbf{z}}$. In contrast, states in Fig. 3.1(b) and 3.1(e) with

$\mathbf{l}_2 \parallel \hat{\mathbf{z}}$ have vanishing m^z. This difference is important to understand the finite-field behaviour, see Fig. 3.2. Magnetic field applied parallel to $\hat{\mathbf{z}}$-axis favours spin structures with a finite magnetisation and stabilises states with $l_1^z \neq 0$, which is why the two intermediate low-field phases are no longer pure l_2^z states. This feature is emphasised by hatches in Fig. 3.2. The collinear-noncollinear transitions are of the second order, whereas all other transition lines are of the first order. In the case of the transition from the paramagnetic state in external magnetic field the first-order nature of the transition follows from the presence of the cubic invariant (3.18), while in other cases the above conclusion is a consequence of the group-subgroup relation. The transition lines intersect at a multicritical point $(T^*, h^*) = (0.6, 0.25)$.

The mean-field phases and the structure of the phase diagram at fields larger than h^* are similar to the Heisenberg triangular antiferromagnet [84] so we do not go into further details. As we shall see in the next section, the true thermodynamic phases determined by Monte Carlo simulations of the model (3.1) differ from the mean-field solutions, which is often the case in $2d$. Still, the mean-field picture is expected to be qualitatively correct for $3d$ layered triangular antiferromagnets. By including a ferro- or antiferromagnetic interlayer coupling J' in the mean-field equations (3.12) and (3.13) we have verified that the predicted sequence of finite-temperature transitions remains valid up to $|J'/J| \sim 0.6$. For larger values of $|J'/J|$ we find a double transition with an intermediate l_1 collinear phase similar to the previously studied case of very strong J' [98].

3.3 Zero-field behaviour
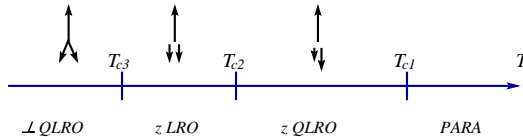
Figure 3.3: Sketch of zero-field diagram as obtained by symmetry analysis and Monte Carlo calculations.

The expected sequence of finite-temperature phases is schematically shown in Fig. 3.3 with three BKT-type transitions. A similar suggestion was made before for the triangular antiferromagnet with the exchange anisotropy [106], though no supporting numerical results were presented.

This scenario has been checked using Monte Carlo method on rhombic clusters with linear size $18 \leqslant L \leqslant 96$ for the same strength of anisotropy as in mean-field approach, namely $d = 1.0$, for comparison (calculations at $d = 0.2$ which have been used to establish phase diagram depicted in Fig. 3.8 are not presented for their being

similar). An extensive use of finite-size scaling techniques has been made to assess the value of critical exponents at the upper two transitions associated with the breaking of $\mathbb{Z}_6$ symmetry; at the lower one, that is of BKT type, spin stiffness has been used to precisely locate the transition. Further details on Monte Carlo technique here used can be found in App. E and Sec. 2.4.
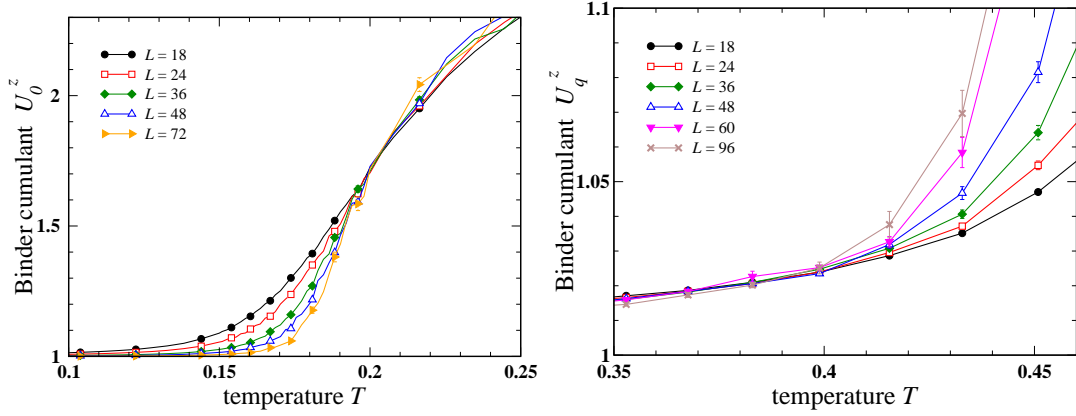
Figure 3.4: Results at $h = 0$ for the easy-axis HTAF with $d = 1.0$. Temperature dependence of Binder's cumulant associated with uniform magnetisation m^z for different cluster sizes (left): the crossing indicates T_{c2}. Temperature dependence of Binder's cumulant associated with antiferromagnetic order parameter $m_{\mathbf{q}}^z$ for different cluster sizes (right): the merging indicates T_{c1}.

To exploit data obtained during Monte Carlo calculations various observables and techniques can be used depending on the specific sought features as explained in Section 2.4. In this case as the first symmetry breaking is expected along $\hat{\mathbf{z}}$, observables along $\hat{\mathbf{z}}$ are used: Binder's cumulant only yields a rough estimate of transition temperatures as shows Fig. 3.4: $T_{c1} \approx 0.4$ and $T_{c2} \approx 0.2$. For these transitions to be more accurately located the scaling of spin susceptibility is finer. First the value of critical exponent η is checked using a procedure that doesn't require a precise location of the transition [70, 8]: it consists in the plotting of scaled susceptibility $\chi_{\mathbf{q}}^z / L^{2-\eta}$ versus Binder's cumulant U_q^z. In Fig. 3.5 the exponent η yielding the best fits is shown. The obtained values $\eta_1 = 0.26 \pm 0.01$ and $\eta_2 = 0.12 \pm 0.01$ are in very good agreement with renormalisation group predictions: $\eta_1 = 1/4$ and $\eta_2 = 4/6^2 = 1/9$ [40]. Next, scaled susceptibility is used to precisely locate transition temperatures as illustrated in Fig. 3.6.

Last, the third transition is associated with the breaking of S^1 and thence expected as BKT-like. To deal with a BKT transition spin stiffness is very well adapted as already discussed in Section 2.4. Furthermore the very fact that it exhibits a jump the height of which is a universal value, namely $2T_{BKT}/\pi$ for integer vortices, at the transition clearly identify the transition as BKT. Using this method with the simplest form of scaling to extract T_{c3} as illustrated in Fig. 3.7 the transition temperature is
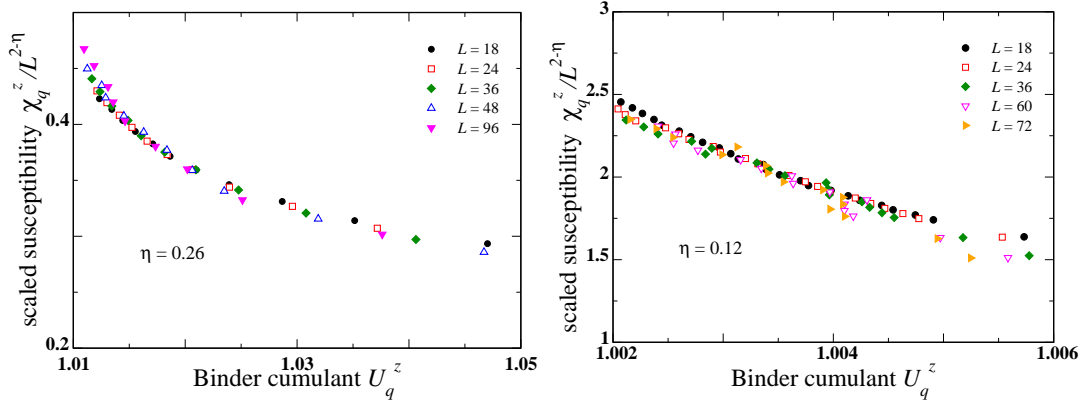
Figure 3.5: Results at $h = 0$ for the easy-axis HTAF with $d = 1.0$. Scaled susceptibility plotted versus Binder cumulant in the vicinity of T_{c1} (left) and T_{c2} (right). The indicated value of critical exponent η is the one that realises the best collapse of all data points onto a single curve.

$T_{c3} = 0.168 \pm 0.001$.

3.4 Finite-field behaviour

At finite field the symmetry of easy-axis HTAF Hamiltonian is the same as the symmetry of HTAF Hamiltonian: phase diagram should consequently look similar with the same stabilised phases and the same nature of transitions. Yet due to the anisotropy some differences are expected. As easy-axis anisotropy reduces transverse fluctuations the domain of ordered phases should stretch to higher temperatures. Concerning the very-low field region as zero-field behaviour in both systems is totally different the ways transition lines close at $h = 0$ are different as well: it can be expected in the case of easy-axis HTAF that lower BKT transition between up-up-down collinear structure and distorted 120-degree structure closes at the finite-temperature zero-field BKT transition that exists in this system. Similarly the upper transition between collinear and paramagnetic phases that belongs to three-state clock-model universality class closes at zero-field upper transition, that is associated whith $\mathbb{Z}_6$ symmetry: group-subgroup relation enables such a junction of transitions.

Another effect of anisotropy is to enlarge one-third magnetisation plateau at zero temperature. This appears as a splitting of the single transition existing in HTAF; the splitting can be estimated by linearising zero-temperature energy about equilibrium configurations in terms of small deviations. Let's start with the transition between distorted 120-degree structure and collinear one. Eq. (3.6) yields for up-up-down
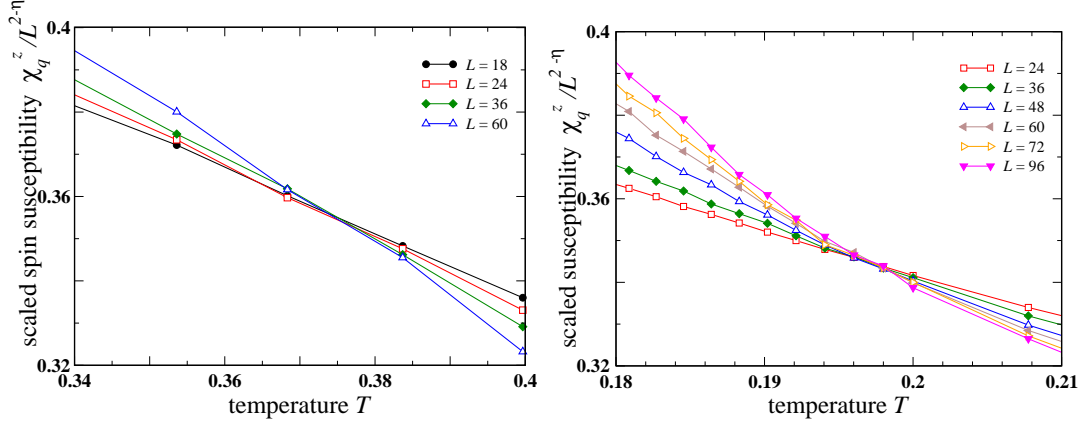
Figure 3.6: Results at $h = 0$ for the easy-axis HTAF with $d = 1.0$. Scaled susceptibility as a function of temperature; scaling with $\eta = 0.26$ at the upper transition (left) and with $\eta = 0.12$ at the second transition (right).

structure:

$$\varepsilon_{uud} = -1 - d - \frac{h}{3} \tag{3.19}$$

For a distorted 120-degree structure as depicted in Fig. 2.1 Eq. (3.6) yields

$$\varepsilon(\theta) = \cos 2\theta - 2\cos\theta - \frac{d}{3}\left(1 + 2\cos^2\theta\right) - \frac{h}{3}(-1 + 2\cos\theta) \tag{3.20}$$

Minimisation according to θ yields either $\theta = 0 \mod \pi$, which is up-up-down collinear structure, or

$$\cos\theta_0 = \frac{1 + h/3}{2(1 - d/3)} \tag{3.21}$$

and the associated energy

$$\varepsilon(\theta_0) = -\frac{(1 + h/3)^2}{2(1 - d/3)} + \frac{2d}{3} + \varepsilon_{uud} \tag{3.22}$$

A straightforward analysis shows that the first part of right-hand-side term is negative for $0 \leqslant d \leqslant d_c = 3/2$, where d_c is the upper limit of stability for a distorted 120-degree structure to exist; consequently the limit of stability is the one imposed by the expression of $\cos\theta_0$:

$$h_{c1} = 3 - 2d \tag{3.23}$$

For $d = 0.2$, which has been used for Monte Carlo simulations, $h_{c1} = 2.6$.

As for the upper bound of the splitting about $h = 3$ it is obtained linearising the energy of V-shape configuration (see Fig. 2.2) about $(\alpha, \beta) = (\pi, 0)$.

$$\varepsilon_V(\alpha, \beta) = 1 + 2\cos\alpha\cos\beta - 2\sin\alpha\sin\beta - \frac{d}{3}(2\cos^2\beta + \cos^2\alpha) - \frac{h}{3}(2\cos\beta + \cos\alpha) \tag{3.24}$$
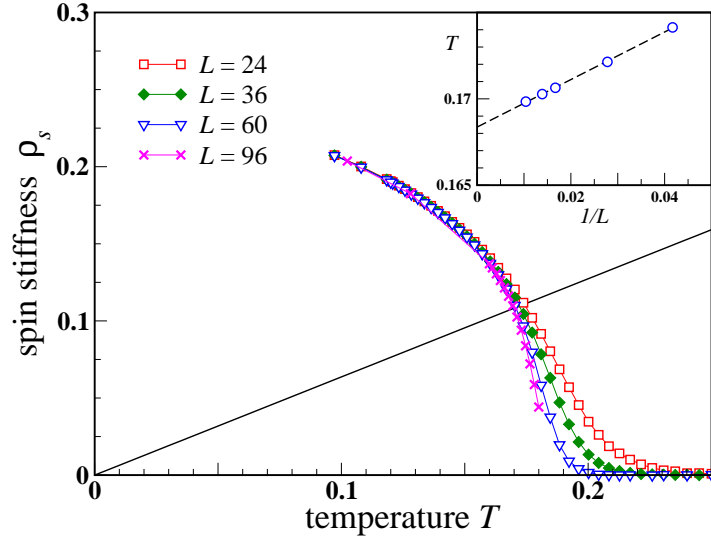
Figure 3.7: Results at $h = 0$ for the easy-axis HTAF with $d = 1.0$. Spin stiffness for different cluster sizes. T_{c3} is determined by the scaling of $T(L)$, where $T(L)$ such that $\rho_S(T(L), L) = 2T(L)/\pi$ – these are the temperatures of the crossing points between the solid line and curves representing ρ_S. The inset depicts the extrapolation made to $1/L = 0$.

Introducing $\gamma = \pi - \alpha$, the energy can be expanded as

$$\varepsilon_V = \varepsilon_{uud} + (\beta, \gamma) \begin{pmatrix} 1 + \frac{2d}{3} + \frac{h}{3} & -1 \\ -1 & 1 + \frac{d}{3} - \frac{h}{6} \end{pmatrix} \begin{pmatrix} \beta \\ \gamma \end{pmatrix} \tag{3.25}$$

This yields

$$h_{c2} = \frac{3 + \sqrt{9 + 8(2d^2 + 9d)}}{2} \tag{3.26}$$

For $d = 0.2$, $h_{c2} = 3.95$.

Zero-field saturation field is also reduced due to easy-axis anisotropy. The saturation field can be determined developing ε_V around $(\alpha, \beta) = (0, 0)$:

$$\varepsilon_V = \varepsilon_{sat} + (\alpha, \beta) \begin{pmatrix} -1 + \frac{d}{3} + \frac{h}{6} & -1 \\ -1 & -1 + \frac{2d}{3} - \frac{h}{3} \end{pmatrix} \begin{pmatrix} \alpha \\ \beta \end{pmatrix} \tag{3.27}$$

where $\varepsilon_{sat} = 3 - d - h$ is the energy of a fully polarised configuration. Hence the saturation field:

$$h_{sat} = 9 - 2d \tag{3.28}$$

For $d = 0.2$ this is $h_{sat} = 8.6$

Numerical determination of transitions is carried out with a similar Monte Carlo algorithm as previously described; the observables I used are the same as in the case
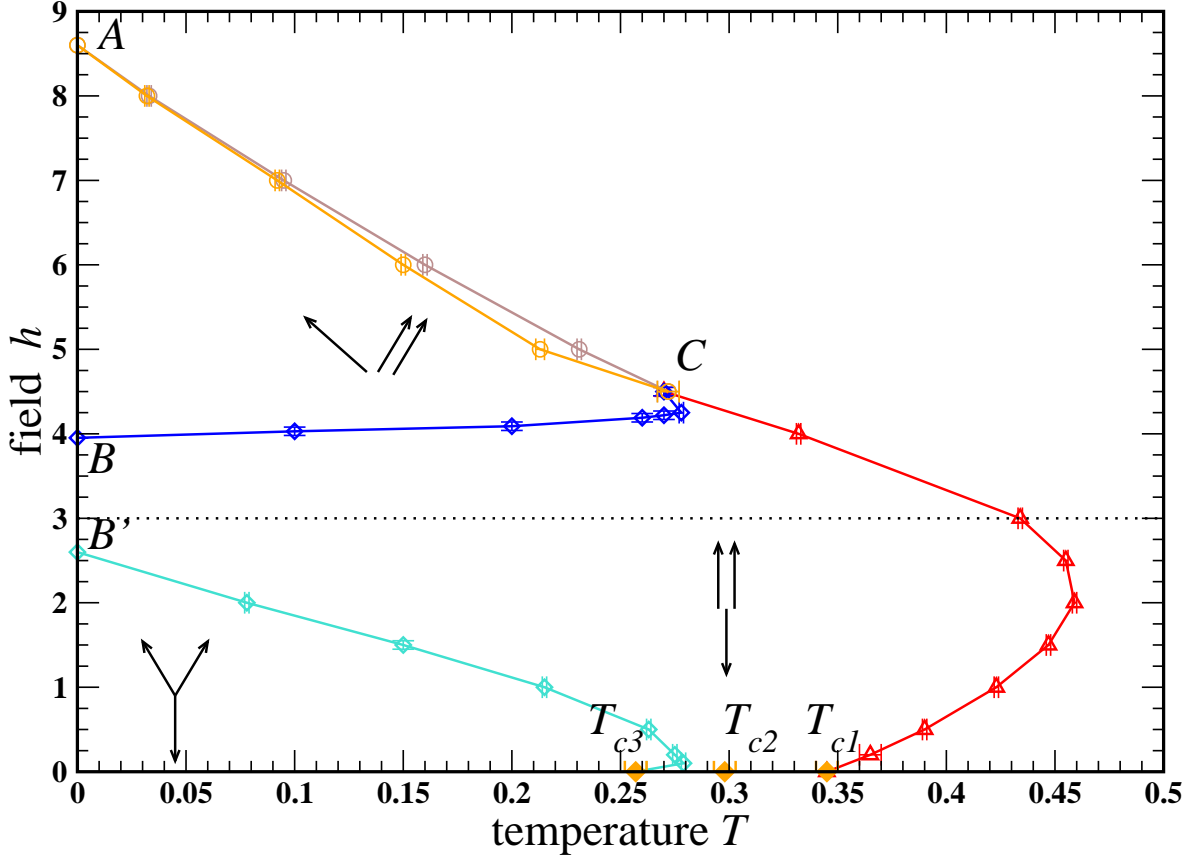
Figure 3.8: Phase diagram of easy-axis HTAF calculated for $d = 0.2$. Solid lines are a guide to the eye linking calculated points. Spin structures are sketched by the configuration on a triangular plaquette with z axis assumed vertical and xy plane perpendicular to the plane of the sheet.

of HTAF as the transitions belong to the same classes of universality. Let's review the different transitions and illustrate for each of them their determination. At low field upper transition $\widehat{CT_{c1}}$ is investigated monitoring z spin component susceptibility χ_q^z, scaled as $\chi_q^z/L^{2-\eta}$ with $\eta = 4/15$ that is the critical exponent for the class of universality of three-state clock model, and Binder's cumulant U_q^z.

The lower transition $\widehat{B'T_{c3}}$ corresponds to the ordering of transverse component: it is thus located using transverse spin component susceptibility $\chi_q^\perp$, scaled as $\chi_q^\perp/L^{2-\eta}$ with Fisher's exponent equal to $1/4$ that is the value for a BKT transition; Binder's cumulant $U_q^\perp$ is used for cross-checking.

Transition $\widehat{BC}$ between up-up-down phase and high-field phase can be located using transverse spin component susceptibility $\chi_q^\perp$ scaled as $\chi_q^\perp/L^{2-\eta}$ with $\eta = 1/4$ that is the value for a BKT transition, and cross-checking with Binder's cumulant $U_q^\perp$. Given the
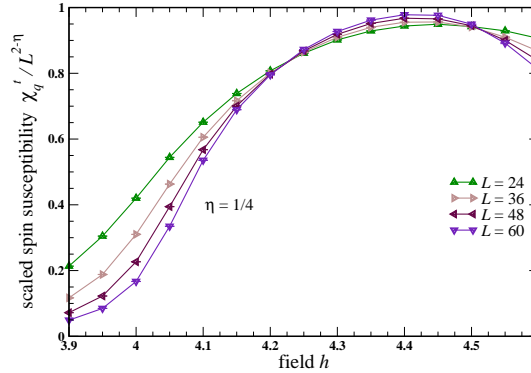
Figure 3.9: This plot depicts scaled spin susceptibility along transverse component $\chi_q^\perp/L^{2-\eta}$ in a field scan at $T = 0.27$. Two transitions can clearly be seen: this denotes the roundig of the transition line backward to multicritical C point.

quasi horizontal shape of the transition it is more adapted to sweep field at constant temperature rather than the opposite; Fig. 3.9 illustrates such a sweep in the vicinity of C point, which clearly shows the double transition that reflects the rounded shape of the transition line in this vicinity.

Double transition associated with the breaking of $S^1 \otimes \mathbb{Z}_3$ between paramagnetic or saturated phase presents the same hardship to be located as is the case in HTAF due to the breaking along a single spin component. As in that case, phase transition associated with the breaking of S^1 is located thanks to finite-size scaling of spin stiffness whereas the transition associated with discrete symmetry breaking is located thanks to the scaling of transverse spin component susceptibility $\chi_q^\perp/L^{2-\eta}$ with $\eta = 1/4$. Binder's cumulant can be used to further confirm the location of the upper transition: the lower one cannot be seen with this observable as the range of its value for different cluster sizes is dramatically reduced so that plots for different cluster sizes appear on top of each other. Such a procedure is illustrated in Fig. 3.10. As can readily be observed comparing Figs. 3.8 and 2.3 the separation between two transitions $\widehat{BC}$ is larger in case of the easy-axis HTAF than in case of HTAF, which is a consequence of the reduced linear energy of domain walls in the anisotropic system where transverse spin fluctuations are hindered.

Another point of interest is to question the evolution of zero-field behaviour at tiny field. As previously seen an intermediate critical phase exists for $T_{c2} \leqslant T \leqslant T_{c1}$: this phase probably extends to finite fields for very weak fields scaling with d^3 which is the order of degeneracy between configurations with and without phase locking (angle φ in Eq. 3.5). This is however a field range out of reach for this numerical investigations.
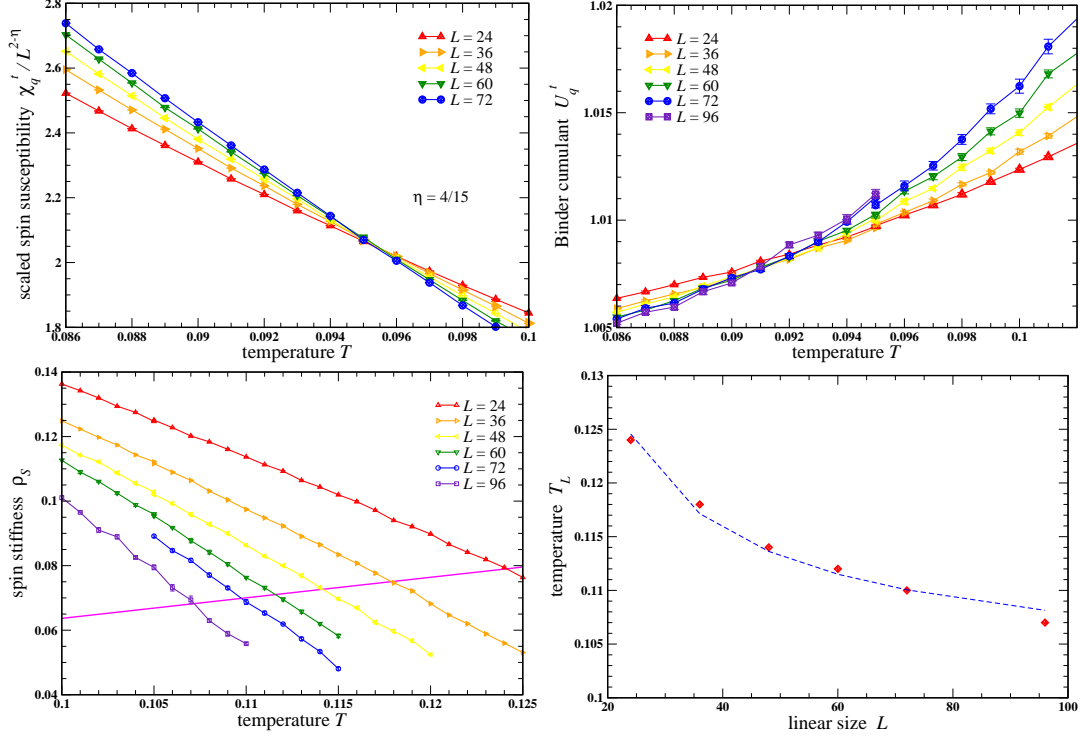
Figure 3.10: Location of successive transitions at $h = 7.0$. Upper transition associated with the breaking of $\mathbb{Z}_3$ is located thanks to the scaling of transverse component of spin susceptibility $\chi_q^\perp / L^{2-\eta}$ with $\eta = 4/15$ (upper left); cross-checking with Binder's cumulant $U_q^\perp$ (upper right). Lower transition associated with the breaking of S^1 is located using spin stiffness: temperature T_L such that $\rho_S(T_L, L) = (2/\pi)T_L$ (lower left) is scaled according to Eq. D.21 (lower right): the obtained parameters for this nonlinear fit are $T_{BKT} = 0.092$ and $c = -1.25$.

Chapter 4

Heisenberg Triangular Antiferromagnet with easy-plane single-ion anisotropy

Determining the phase diagram of Heisenberg triangular antiferromagnet with easy-plane single-ion anisotropy necessarily induces an interest in the phase diagram of XY triangular antiferromagnet: the former shares the same symmetries as the latter which is the paradigmatic model of this class of systems. Even though XY triangular antiferromagnet has been studied a lot since the 1980's either directly [85, 66, 46, 26, 57, 60, 56, 67, 68, 134, 69, 91, 90] or indirectly by the study of closely related bidimensional models such as fully frustrated XY model, associated with Josephson junction arrays at half flux per plaquette [107, 108, 37, 59], and $XX0$ model [16, 15, 90], a detailed discussion of its whole phase diagram is still welcome as it clarifies many questions left so far unanswered as far as I know.

In this chapter the phase diagram of XY triangular antiferromagnet (XY TAF) is thus discussed in some details (see Fig. 4.1) before dealing with Heisenberg triangular antiferromagnet with easy-plane single-ion anisotropy (easy-plane HTAF). First zero-field behaviour is described (Sec. 4.1); then the discussion of finite-field phase diagram is split into two parts: the first one deals with moderate fields and the delicate question of the connection of finite-field transition lines with zero-field transition points (Sec. 4.2); the second one presents high-field behaviour, which means between one-third magnetisation field and saturation field (Sec. 4.3). Last the diagram of Heisenberg triangular antiferromagnet with easy-plane single-ion anisotropy is presented (Sec. 4.4).
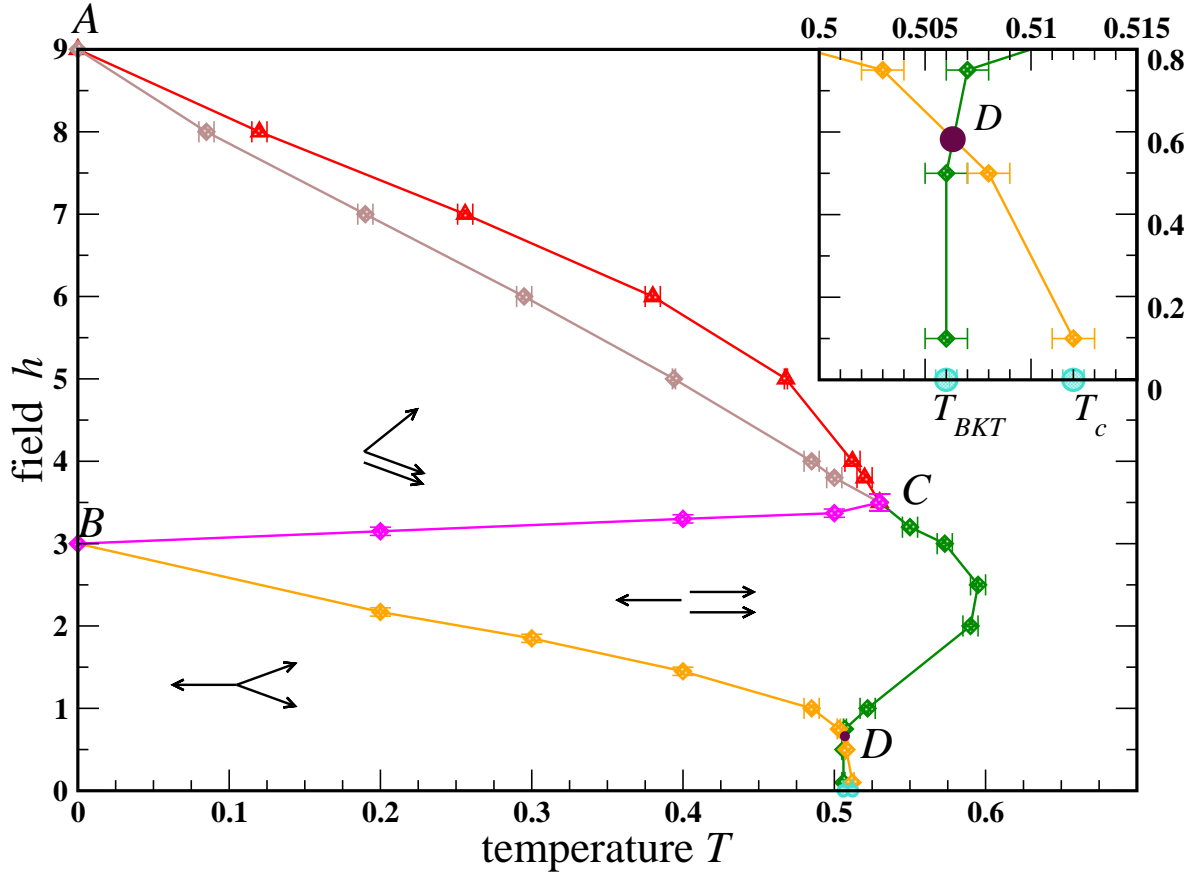
Figure 4.1: Phase diagram of *XY* TAF. Lines are guides to the eye between calculated points. The inset offers an enlarged view about low-field multicritical point *D*. Spin structures are sketched by the configuration on a triangular plaquette with x axis assumed horizontal and y axis vertical in the plane of the sheet. Transition line $\widehat{AC}$ is split into two with an intermediate critical phase.

4.1   *XY* triangular antiferromagnet at zero-field

Even though a continuous symmetry cannot be broken in bidimensional systems as demonstrated by Mermin and Wagner [77], another kind of phase transition is possible: it is induced by stable topological excitations as found out by Berezinskii on the one hand [10, 11], and by Kosterlitz and Thouless on the other hand [61] – which is referred to as a BKT transition. Interestingly some bidimensional systems intertwine both continuous and discrete symmetries, which creates highly non-trivial phase transition scenarios. This is the case of classical *XY* TAF at zero field:

$$\mathcal{H} = \sum_{\langle ij \rangle} \mathbf{S}_i \cdot \mathbf{S}_j \tag{4.1}$$

where the Hamiltonian has been normalised by the coupling exchange and by spin as well so that $\mathbf{S}_i$ in the above expression is a classical bidimensional unit vector. At low-temperature this Hamiltonian admits a 120-degree structure that can be described as:

$$\langle \mathbf{S}_i \rangle = \mathbf{l}_1 \cos\left(\mathbf{q} \cdot \mathbf{r}_i\right) + \mathbf{l}_2 \sin\left(\mathbf{q} \cdot \mathbf{r}_i\right) \tag{4.2}$$

with $(\mathbf{l}_1, \mathbf{l}_2)$ a pair of orthogonal vectors and $\mathbf{q} = (4\pi/3, 0)$ the three-sublattice ordering wave vector. Beside continuous S^1 symmetry associated with the global rotation of spins, that is the rotation of the pair $(\mathbf{l}_1, \mathbf{l}_2)$, a discrete $\mathbb{Z}_2$ symmetry comes into the game, which corresponds to the direct or indirect character of the basis $(\mathbf{l}_1, \mathbf{l}_2)$. In real space it corresponds to the fact spins in this non-collinear structure can rotate either clockwise or anticlockwise around a triangle. This extra discrete symmetry, called chirality, was pointed out in 1984's pioneering works [85, 66]. Due to the discrete character of $\mathbb{Z}_2$, its breaking does induce a long-range order. The subsequent questions are then: what is the nature of the ordering? Does chiral order come with quasi-long range magnetic order? Does a magnetically disordered chiral phase exist? If an early agreement was reached on the existence of a quasi-long range magnetically ordered phase with long-range chiral order, the scenario for ordering has remained a controversial issue for more than twenty years with proponents of two transitions [85, 68, 134, 69, 91] opposing those in favour of a single one belonging to a new universality class [66, 67]. This latter proposition was made possible by the hardship to numerically resolve both transitions as they are quite close by – the latest estimate [95] published before this work [74] yields $T_{chiral} = 0.512(1)$ and $T_{BKT} = 0.508(1)$, which agrees both with certain older results and with our own ones, and participates to today's consensus on the number of transitions. Renormalisation group approaches for frustrated magnets are at best difficult, at worst misleading, especially in the vicinity of $d = 2$, which is the one of interest here. While a general agreement on the BKT nature of the lower transition exists, the nature of the upper transition is regularly debated [85, 66, 69, 93, 91]. The point is that critical exponents are notoriously hard to compute. Symmetry arguments make Ising universality class the most natural, which was pointed up from the very beginning [85]. Yet numerical investigations have failed so far to calculate critical exponents matching those of Ising universality class (see Table II in [95] for a summary of results). As often noted misleading finite-size effects could be responsible for these difficulties [91, 112]. In the following, specific heat is studied as the logarithmic scaling of its peak value with cluster linear size L is a clear argument in favour of Ising universality class.

To investigate chiral ordering the most adapted parameter is chiral susceptibility:

$$\chi_\kappa = \langle \kappa^2 \rangle - \langle \kappa \rangle^2 \tag{4.3}$$

where chirality κ reads

$$\kappa = \frac{1}{L^2\sqrt{3}} \left[\sum_\Delta \varepsilon_\Delta \left(\mathbf{S}_1 \times \mathbf{S}_2 + \mathbf{S}_2 \times \mathbf{S}_3 + \mathbf{S}_3 \times \mathbf{S}_1 \right) \right] \cdot \hat{\mathbf{z}} \tag{4.4}$$

with summation running over triangles, spins numbered clockwise around a triangle, and $\varepsilon_\Delta = \pm 1$ taking into account staggered ordering. In this definition κ is really a scalar: the cross product are all along $\hat{\mathbf{z}}$ as spins are strictly within xy plane. With this definition κ is a non-zero Ising variable in phases with chiral order: introducing spin structure (4.2) in (4.4) yields (there are $2L^2$ triangles)

$$\kappa = (\mathbf{l}_1 \times \mathbf{l}_2) \cdot \hat{\mathbf{z}} \qquad\qquad (4.5)$$

which is zero in phases without chiral order ($\mathbf{l}_1$ and $\mathbf{l}_2$ collinear or one of the two zero) and is ± 1 in 120-degree phase, even if distorted (distortion doesn't change $\mathbf{l}_1$ and $\mathbf{l}_2$ but $\mathbf{m}$). Chiral susceptibility can be scaled as $\chi_\kappa / L^{2-\eta}$, which quantity plotted against temperature (see App. D) yields the transition temperature. Of course this requires η to be known, which is a matter of concern especially in this case as the nature of chiral transition is much debated. As explained in App. D it is possible to determinate η plotting $\chi_\kappa / L^{2-\eta}$ vs U_κ adjusting η so that data points for different cluster sizes collapse onto a single curve. Yet in this case due to the closeness of transitions it appears this method is not satisfactory with cluster sizes here used. As critical exponents differ very moderately between several class of universality in $2d$, sorting out this question can indeed be quite tricky. The argument here put forward makes use of a specificity of Ising universality class that does dramatically distinguish it from other universality classes: $\alpha = 0$, which implies specific heat is logarithmically divergent. Obtained results tend to exclude $\alpha > 0$ as can be seen in log-log plot presented in Fig. 4.2: the clear downward bending cannot be compatible with $\alpha > 0$. My viewpoint is that numerical estimations of other critical exponents are not yet satisfactory because too small systems are used. Large clusters would be welcome not to yield high precision estimates as is the case in most problems but right ones: as discussed in [91] and supported by Fig. 6 in that article, too small clusters most probably exhibit a misleading behaviour and an idea about thermodynamic limit can be gained only using very large clusters. Consequently the assumption $\eta = 1/4$ according to Ising universality class value is used due to theoretical arguments above mentioned, in agreement with symmetry considerations, and numerical support gained from the analysis of specific heat. Fig. 4.3 shows this scaling and the associated temperature: $T_{chiral} = 0.512 \pm 0.001$.

As far as magnetic ordering temperature is concerned usual means of locating a BKT transition can be used: spin stiffness, spin susceptibility, and Binder's cumulant. Spin susceptibility χ_q, which is the total spin susceptibility

$$\chi_{\mathbf{q}} = \frac{1}{N_s^2} \sum_{i,j} \frac{\langle S_i^x S_j^x + S_i^y S_j^y \rangle}{T} \, e^{i\mathbf{q}\cdot(\mathbf{r}_i - \mathbf{r}_j)} \qquad\qquad (4.6)$$

is used as illustrated in Fig. 4.3.
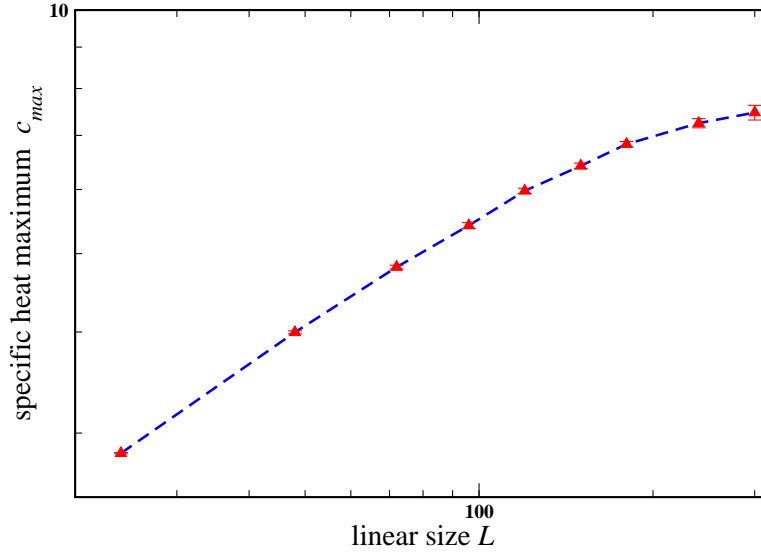
Figure 4.2: Maximum of the specific heat at $h = 0$ plotted vs cluster linear size L in a log-log plot: if critical exponent α were positive data points should align on a straight line. As can be observed a clear downward bending exists that prevents $\alpha > 0$.

4.2 Low fields: competing $\mathbb{Z}_2$ and $\mathbb{Z}_3$ symmetry breaking

Let's now apply a magnetic field along x direction:

$$\mathcal{H} = \sum_{\langle i,j \rangle} \mathbf{S}_i \cdot \mathbf{S}_j - h \sum_i S_i^x \tag{4.7}$$

At finite field XY triangular antiferromagnet retains a continuous degeneracy. Indeed Hamiltonian (4.7) can be written taking into account a three-sublattice pattern as:

$$\mathcal{H} = \frac{1}{2} \sum_\Delta \left(\mathbf{S}_1 + \mathbf{S}_2 + \mathbf{S}_3 - \frac{h\hat{\mathbf{x}}}{3} \right)^2 + const. \tag{4.8}$$

This expression clearly shows that ground-states are characterised by the following set of constraints:

$$\mathbf{S}_1 + \mathbf{S}_2 + \mathbf{S}_3 = \frac{h\hat{\mathbf{x}}}{3} \tag{4.9}$$

From this relation the value of saturation field is immediately obtained as $h = 9$. As there are three degrees of liberty (three bidimensional unit vectors) and two constraints, one free parameter remains: a continuous degeneracy persists. As this degeneracy is not related to a symmetry in the Hamiltonian (4.7), it can be expected thermal fluctuations
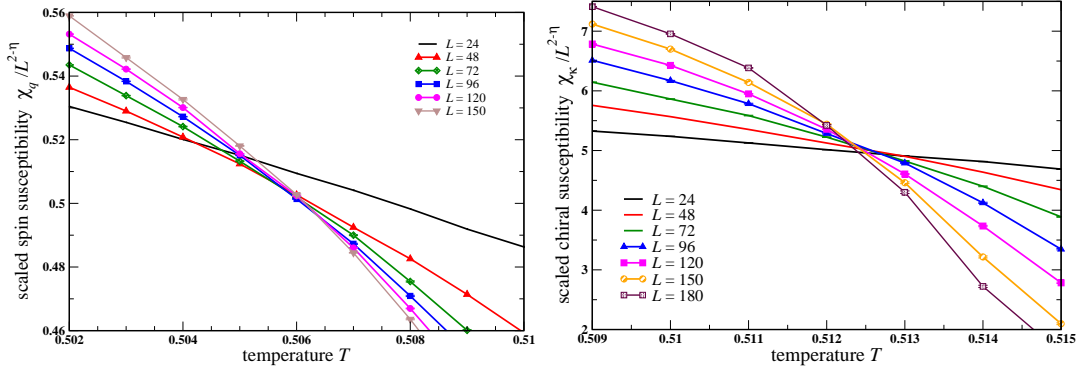
Figure 4.3: The upper transition temperature is located thanks to chiral susceptibility (right); the lower one with spin susceptibility (left).

lift it. This is indeed the case [46, 57, 102]: symmetry is reduced to the composite discrete $\mathbb{Z}_2 \otimes \mathbb{Z}_3$ symmetry.

As mentioned in the introduction to this chapter the discussion first focuses on low-field part of the diagram, namely for $h < 3$. At $h = 3$ one-third magnetisation plateau appears in magnetisation curves: it corresponds to an up-up-down structure as can be seen from (4.9). This collinear structure is stable at $T = 0$ and $h = 3$ as shown in [46]. At finite temperature thermal fluctuations do widen the field range of stability of up-up-down structure mainly towards $h < 3$ as increased fluctuations of spin component transverse to applied field destabilise 120-degree structure. Hence a twofold symmetry-breaking scenario: first $\mathbb{Z}_3$ is broken with the collinear ordering; then $\mathbb{Z}_2$ symmetry with the ordering into 120-degree structure. This scenario implies the successive symmetry-breakings occur along different components: $\mathbb{Z}_3$ along field direction $\hat{\mathbf{x}}$ and $\mathbb{Z}_2$ in transverse direction – or according to chiral order parameter: in this case both magnetic ordering along $\hat{\mathbf{y}}$ and chiral ordering happen simultaneously as 120-degree structure has an inherent chiral symmetry. Such a separation makes it easier to numerically assess the scenario as there is a clear distinction among order parameters, which may otherwise be problematic in case of multiple ordering along a single component. According to the exact results of the hard hexagon model [9] the upper transition belongs to three-state clock model universality class.

Let's now detail how this numerical investigation has been done. For the upper transition χ_q^x can be scaled as $\chi_q^x/L^{2-\eta}$ using $\eta = 4/15$, the value of the universality class of three-state clock model where

$$\chi_q^\alpha = \frac{\langle (S_q^\alpha)^2 \rangle - \langle S_q^\alpha \rangle^2}{T} \quad \text{with } \alpha \in \{x, y\} \tag{4.10}$$

This assumption theoretically grounded in Baxter's results, can also be numerically supported in various ways using Binder's cumulant or the ratio of correlation functions

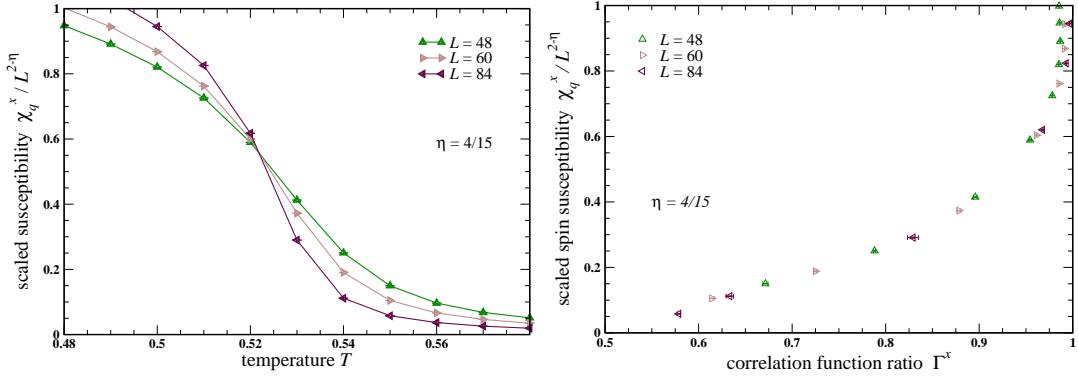**Figure 4.4:** Upper transition location at $h = 1.0$ Scaled spin susceptibility $\chi_q^x / L^{-(2-\eta)}$ with $\eta = 4/15$ is used to locate the upper transition (left). The correctness of the value of η is checked plotting scaled spin susceptibility $\chi_q^x / L^{-(2-\eta)}$ vs the ratio of correlation function Γ^x. The value of three-state clock-model universality class is fully satisfactory to have data points collapse onto a single curve (right).

Γ^x (see App. A, Eq. (2.19), and the discussion on the properties of this ratio): either of them can be used to locate transition temperature as well, and even though Binder's cumulant may be less accurate the estimate thus obtained should be reasonably close to the one resulting from the scaling of susceptibility; second to calculate η as explained in App. D. Such a mix of techniques is illustrated in Figs. 4.4 and 4.5 at $h = 1.0$.

The lower transition can be investigated in two different ways: according to chirality or to magnetic ordering along transverse direction. Both yield the same transition, in strong support for the explicited scenario that implies simultaneous chiral and transverse magnetic ordering at the lower transition as shows Fig. 4.6. Techniques are the same as previously explained at zero field for chirality; concerning transverse magnetic ordering χ_q^y is scaled using $\eta = 1/4$ (Ising universality class).

A delicate problem arises when drawing the phase diagram down to zero field: zero-field symmetry-breaking pattern is different from the one above described at moderate finite field. How can both be connected? Finite-field upper transition is a $\mathbb{Z}_3$ symmetry-breaking line: it cannot join zero-field upper transition which is a $\mathbb{Z}_2$ symmetry-breaking point. On the contrary finite-field lower transition that corresponds to chiral ordering can join zero-field upper transition: this is even the most natural scenario as it is the simplest way to divide (T, h) plane into a chirally ordered part and a disordered one. This scheme implies the existence of a multicritical point D defined by (T_D, h_D) with $h_D \neq 0$. At D an inversion between $\mathbb{Z}_3$ and $\mathbb{Z}_2$ symmetry-breakings takes plase: for $h > h_D$ the former occurs first whereas for $h < h_D$ the latter does, which implies that a magnetically disordered chiral phase is expected at very low field. Numerical evidences of this scheme are sought using chiral susceptibility χ_κ on the one hand and spin susceptibility along $\hat{\mathbf{x}}$ χ_q^x on the other hand. Binder's cumulant and y component
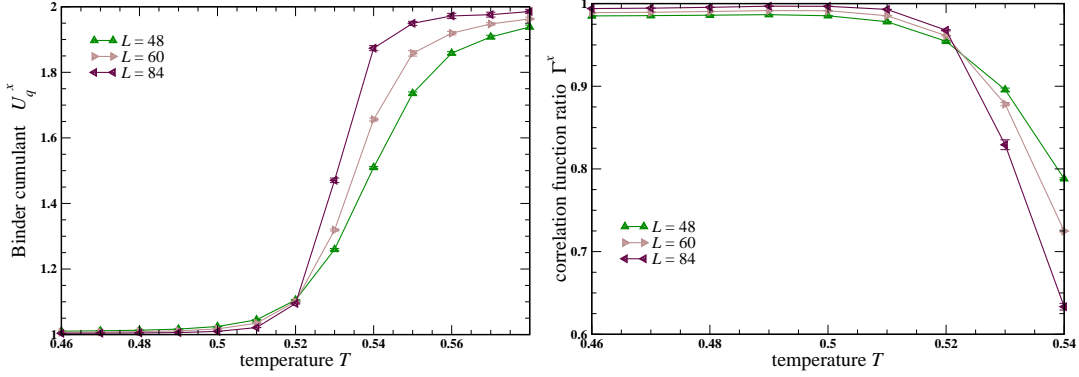
Figure 4.5: Upper transition location at $h = 1.0$. Binder's cumulant U_q^x (left) is compared with the ratio of correlation functions Γ^x (right). In this case both exhibit similar precision and yield following transition temperature: 0.520 ± 0.005.
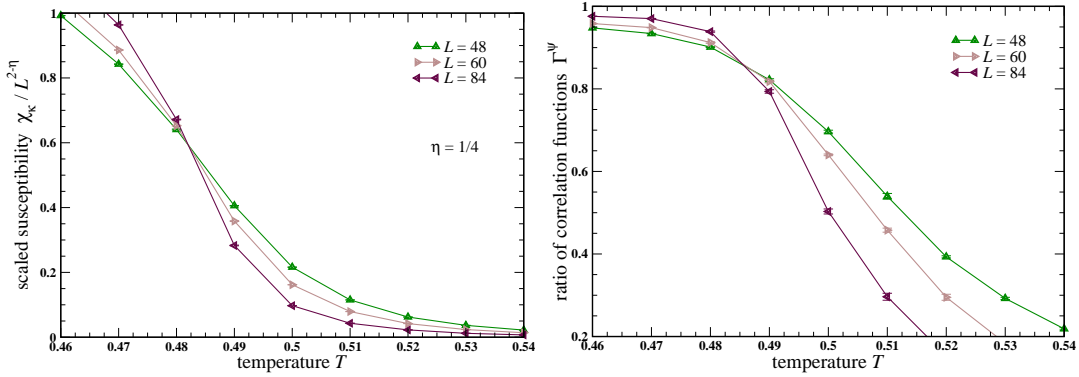
Figure 4.6: Lower transition at $h = 1.0$. Finite-size scaling of chiral susceptibility (4.3) (left) to locate Ising transition into chiral ordered phase and ratio of correlation functions Γ^y (right) to illustrate simultaneous ordering along transverse direction.

quantities are monitored as well. For illustration results at $h = 0.1$ are proposed in Fig. 4.7. Measurements at $h = 0.75$ and $h = 0.5$ assures $0.5 \leqslant h_D \leqslant 0.75$. At $h = 0.75$ the location of transitions carried out in a similar way to the case $h = 0.1$ yields $T_{chiral} = 0.503 \pm 0.001$ and $T_{\mathbb{Z}_3} = 0.507 \pm 0.001$ (see Fig. 4.8) whereas at $h = 0.5$ the order is reversed: $T_{chiral} = 0.509 \pm 0.001$ and $T_{\mathbb{Z}_3} = 0.506 \pm 0.001$ (see Fig. 4.9). In the latter case chiral transition can be located only with chiral susceptibility or observables built upon susceptibility: magnetic ordering is indeed disconnected from chiral ordering in this regime as can readily be seen noticing there is no difference between x and y component in their ordering temperature (see Fig. 4.10). As a consequence an intermediate magnetically disordered chiral phase exists in this regime.

Last point not yet discussed about this low-field region is the way the lower transition
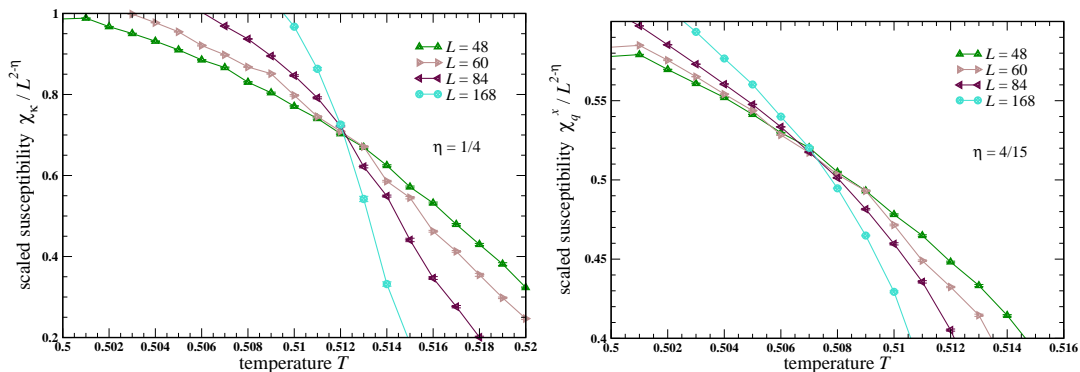
Figure 4.7: Finite-size scaling of chiral susceptibility (4.3) (left) to locate Ising transition into chiral ordered phase and finite-size scaling of χ_q^x (right) to locate the transition associated with the breaking of $\mathbb{Z}_3$ symmetry; both at $h = 0.1$.

terminates at zero field. Actually it is fully admissible that it terminates at zero-field BKT transition as $\mathbb{Z}_3$ is a subgroup of S^1. As low-field spin-wave expansion of the free-energy yields a three-fold-anisotropy-like term [46, 74], which is irrelevant about BKT transition in [40], finite-field transition line necessarily closes at zero-field BKT transition.

4.3 Breaking of $\mathbb{Z}_6$ symmetry at high fields

For $h > 3$ the behaviour is quite different. Indeed up-up-down structure is no longer stable as constraint (4.9) clearly shows: in this equation there are indeed two regimes depending on whether $h \leqslant 3$ or $h \geqslant 3$. In the latter regime stable structures exhibit both the breaking of sublattice symmetry (which means the breaking of $\mathbb{Z}_3$) and of the symmetry along transverse direction (therefore breaking of $\mathbb{Z}_2$) [46, 57]. These structures can be described as

$$\langle \mathbf{S}_i \rangle = \mathbf{l}_1 \cos\left(\mathbf{q} \cdot \mathbf{r}_i\right) + \mathbf{m} \tag{4.11}$$

where $\mathbf{m}$ is uniform magnetisation. Only y component is critical. This has a striking consequence on the breaking of composite $\mathbb{Z}_2 \otimes \mathbb{Z}_3$ discrete symmetry: it is broken as a whole $\mathbb{Z}_6$ symmetry. If Korshunov already proposed such a possibility for this high-field transition [57], the proposition hadn't found any further support, either theoretical or numerical, before the results here presented (see also [74]). The hallmark of such symmetry-breaking as compared to other possible symmetry-breakings in this system is the existence of an intermediate critical phase with algebraically decaying correlation functions between disordered and ordered phase [40]. As a consequence the most convincing evidence for this scenario is the existence of the intermediate critical phase.

Figure 4.8: Location of $\mathbb{Z}_2$ and $\mathbb{Z}_3$ symmetry breakings at $h = 0.75$. The former is associated with chiral ordering and is thus located using chiral susceptibility χ_κ scaled as $\chi_\kappa/L^{2-\eta}$ with $\eta = 1/4$ (Ising universality class). The latter corresponds to the breaking of lattice translational symmetry along the applied field and is thus located using spin susceptibility scaled as $\chi_q^x/L^{2-\eta}$ with $\eta = 4/15$ (three-state clock model universality class). These results show $h_D \leqslant 0.75$.

Such an evidence can be obtained from the use of the ratio of correlation functions introduced in Eq. (2.19) Γ^y, which has the same properties as Binder's cumulant but lower noise as it is a second-order quantity (see App. D). In case of $\mathbb{Z}_6$ symmetry-breaking as is here investigated, this ratio shows both upper and lower transitions which is not the case with Binder's cumulant. This is neatly illustrated in Fig. 4.12 at $h = 5.0$ where the width of the intermediate phase is rather large. For transition temperatures to be more accurately calculated the scaling of spin susceptibility χ_q^y can then be used with $\eta = 1/4$ at the upper transition and $\eta = 4/6^2 = 1/9$ at the lower one [40]. Figs. 4.11 and 4.12 shows the results for h=5.0.

Another transition remains for the discussion: the one between high-field phase and collinear phase. From the latter to the former a $\mathbb{Z}_2$ symmetry-breaking occurs. As shown by Kawamura there is no spin-flop transition but a continuous one. Hence the transition is expected to be of Ising type. Results obtained through field scans across the transition for transverse spin susceptibility and Binder's cumulant support this assumption.

In the proposed phase diagram another multicritical point, called C in Fig. 4.1, appears. I haven't investigated it in details. What can be said is that transition line $\widehat{CD}$ and upper transition line $\widehat{AC}$ merge at C with different slopes as they correspond to different representations. Lower transition line $\widehat{AC}$ is also expected to merge at C: indeed the splitting of the transition with the existence of an intermediate critical phase is observed in all the measurements; the occurrence of a first-order transition in the small field range $3.4 \leqslant h \leqslant 3.8$ seems improbable. Last Ising line $\widehat{BC}$ ends at multicritical point C as well.
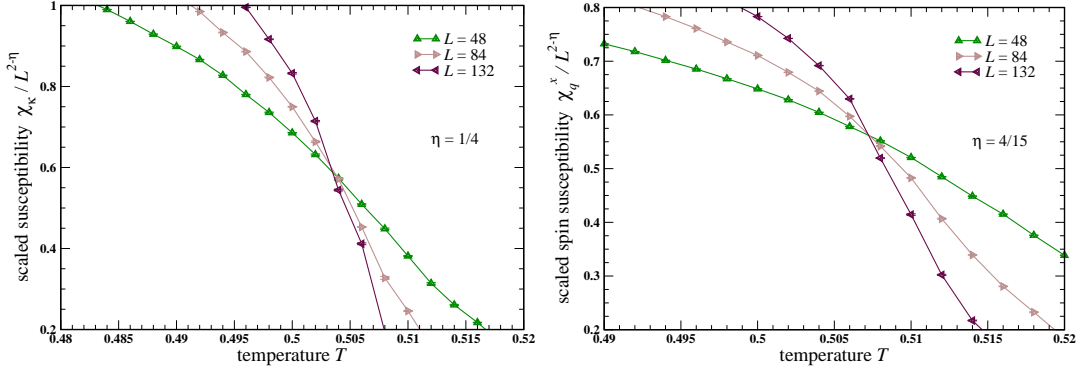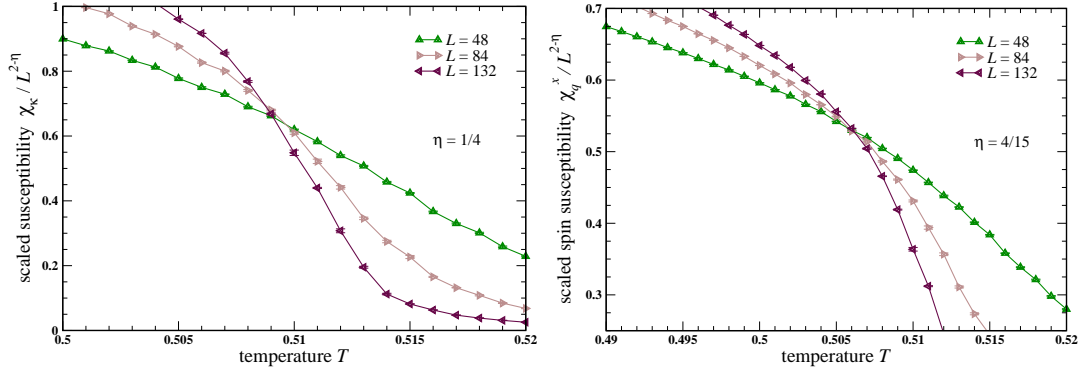
Figure 4.9: Location of $\mathbb{Z}_2$ and $\mathbb{Z}_3$ symmetry breakings at $h = 0.5$. The former is associated with chiral ordering and is thus located using chiral susceptibility χ_κ scaled as $\chi_\kappa/L^{2-\eta}$ with $\eta = 1/4$ (Ising universality class). The latter corresponds to the breaking of lattice translational symmetry along the applied field and is thus located using spin susceptibility scaled as $\chi_q^x/L^{2-\eta}$ with $\eta = 4/15$ (three-state clock model universality class). These results show $h_D \geqslant 0.5$.
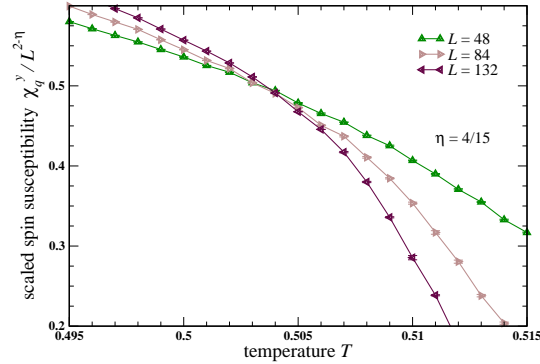
Figure 4.10: Scaling of spin susceptibility along y direction χ_q^y as $\chi_q^y/L^{2-\eta}$ with $\eta = 4/15$ which corresponds to the breaking of lattice translational invariance associated with magnetic ordering. Comparison with scaled susceptibility along x direction $\chi_q^x/L^{2-\eta}$ with $\eta = 4/15$ in Fig. 4.9 shows that for $h \leqslant h_D$ the lower transition corresponds to magnetic ordering along both component, which is an evidence of the existence of an intermediate magnetically disordered chiral phase in this regime.
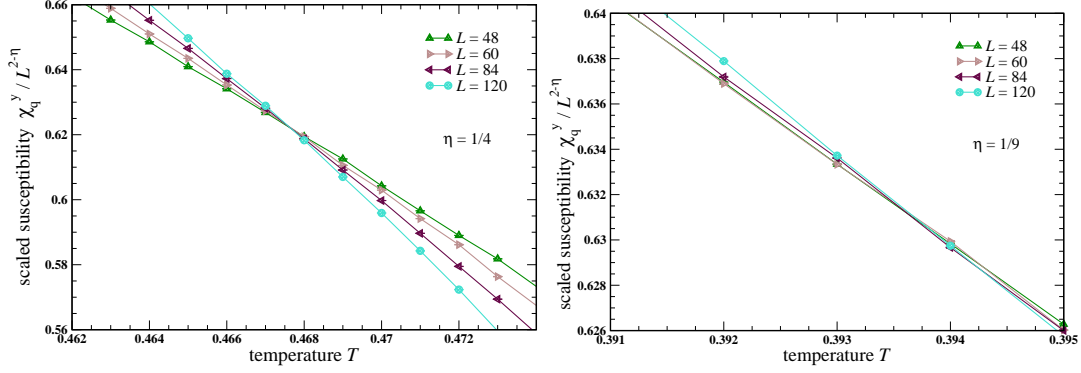
Figure 4.11: Scaled spin susceptibility $\chi_q^y L^{-(2-\eta)}$ with $\eta = 1/4$ (upper transition; left panel) and $\eta = 1/9$ (lower transition; right panel) to locate double transition of $\mathbb{Z}_6$ symmetry breaking at h=5.0.
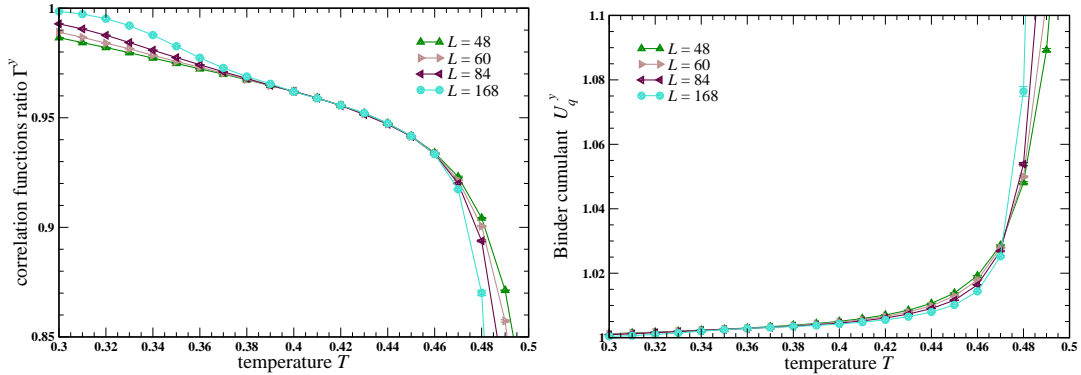
Figure 4.12: Correlation ratio (2.19) for critical y component at $h = 5.0$ (left). The intermediate phase with algebraically decaying correlations corresponds to the intermediate temperature range over which plots for different cluster sizes L merge. Long-range ordered phase with exponentially decaying correlation can also be identified as the lowest temperature range with separated plots; the highest one corresponds to paramagnetic phase. For comparison Binder's cumulant is shown as well (right).

4.4 Heisenberg triangular antiferromagnet with easy-plane single-ion anisotropy
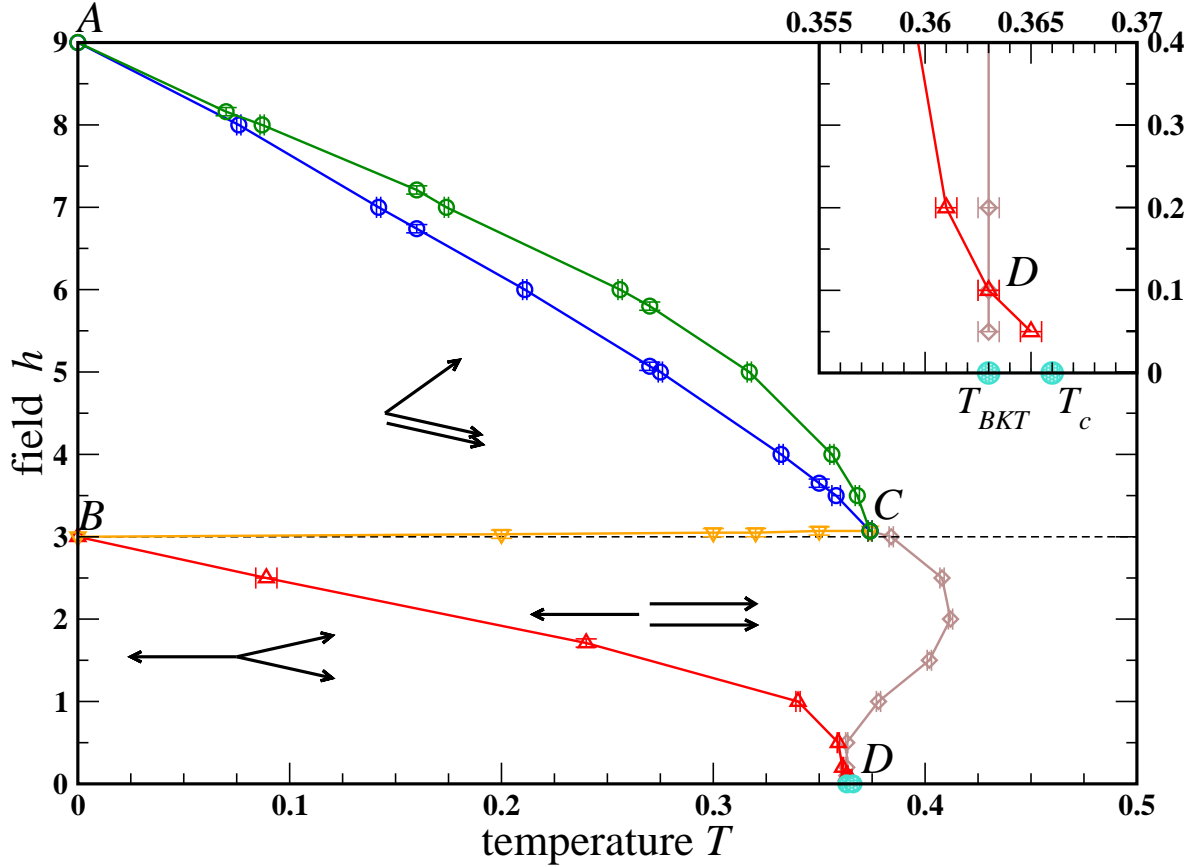
Figure 4.13: Phase diagram of easy-plane HTAF calculated at $d = -0.2$. Lines are guides to the eye between calculated points. The inset offers an enlarged view about low-field multi-critical point D. Spin structures are sketched by the configuration on a triangular plaquette with x axis assumed horizontal and y axis vertical in the plane of the sheet. Transition line $\widehat{AC}$ is split into two with an intermediate critical phase.

The Hamiltonian of Heisenberg triangular antiferromagnet with easy-plane single-ion anisotropy reads

$$\mathcal{H} = \sum_{\langle i,j \rangle} \mathbf{S}_i \cdot \mathbf{S}_j - d \sum_i (S_i^z)^2 - h \sum_i S_i^x \tag{4.12}$$

with $d < 0$. It belongs to the same universality class as XY triangular antiferromagnet: same symmetries are involved. Given the extra fluctuations in $\hat{\mathbf{z}}$ direction the whole

phase diagram should shrink to lower temperatures. Phase transitions have been located as in XY triangular antiferromagnet: details of this location are therefore not repeated hereafter, which would not bring anything new.The phase diagram has been calculated at $d = -0.2$: it is depicted in Fig. 4.13.

The splitting of zero-field transitions exhibits little dependence on the strength d of the anisotropy as shows the comparison between $d = -0.2$ and $d = -0.4$: for $d = -0.2$, $T_{chiral} = 0.366 \pm 0.0005$ and $T_{BKT} = 0.362 \pm 0.0005$; for $d = -0.4$, $T_{chiral} = 0.392 \pm 0.0005$ and $T_{BKT} = 0.389 \pm 0.0005$. Even when comparing with XY model that can be seen as $d = -\infty$ limit for which $T_{chiral} = 0.512 \pm 0.0005$ and $T_{BKT} = 0.506 \pm 0.0005$, the splitting looks almost constant. This observation suggests the splitting has little to do with spin fluctuations and consequently with the formation of domain walls but is rather mainly due to the screening of vortex-vortex interaction due to domain walls: as a consequence, this screening effect being independent of spin fluctuations, the splitting exhibits little dependence on anisotropy strength d.

Chapter 5

Conclusion

In this doctoral dissertation I have presented a determination of the whole phase diagram of classical Heisenberg triangular antiferromagnet (HTAF) in the strict $2d$ case and of its anisotropic derivatives. For the latter ones the case of single-ion anisotropy was chosen for both its experimental relevance and its expected more altering character. In the case of easy-plane anisotropy, the extensive study of XY (XY TAF) model has appeared necessary as it is the paradigmatic model of the relevant class of universality and its thorough study was still to be done.

After a statement of the motivations for such a study, I successively presented the case of HTAF, of easy-axis HTAF and, last, of XY TAF and easy-plane TAF. However surprising it may seem sixty years after the first study of a classical antiferromagnetic spin system on the triangular lattice, the phase diagram of the systems here considered had not yet been completely built. In case of HTAF and XY TAF, parts of the diagram had been discussed but the overall picture was still unsatisfactory and important features that are not refinements were at best lacking support, at worst fully ignored.

Let's review the results presented in this dissertation for each system. Zero-field behaviour of HTAF had been studied a lot and with convincing care for me not to undertake another study of it. This system is governed by a continuous symmetry and shouldn't order at finite temperature as a consequence of Mermin-Wagner theorem. Interestingly Kawamura challenged this viewpoint discussing the topological excitations of HTAF and not only showed two temperature regimes for these exist, which his opponents agree on, but precisely exposed the reason for the change of regime to be a transition. His line of arguments parallels the one of Berezinskii, Kosterlitz, and Thouless in their discussion of the phase transition now known after their names (BKT transition): the transition is topological by nature; yet it is distinct of BKT transition by the decoupling of spin excitations and vortex excitations, which induces a low-temperature phase quite peculiar, coined as spin gel by Kawamura. In any case finite-field behaviour that I studied was astonishingly lacking a precise discussion. The first surprising feature of so-far published diagrams was the closing of finite-field transition

lines at a finite-temperature multicritical point which is contradictory with the massless nature of zero-field phases as opposed to the massive nature of low-temperature finite-field phase. Other important features had already been presented: the existence of an up-up-down collinear phase separating the so-called 120-degree phase from both para-magnetic phase and high-field phase; the selection of a planar high-field phase rather than the umbrella structure. A tricky issue had been laid aside, namely the nature of the transition at high field between the ordered phase and the saturated/paramagnetic phase. A compound $S^1 \otimes \mathbb{Z}_3$ symmetry has to be broken. The hardship lies in the fact there is a single order parameter, namely transverse spin component. It appears that both symmetries are separately broken, first the discrete $\mathbb{Z}_3$ then the continuous S^1. Numerical determination of this sequence is somehow delicate as the symmetry discussion underpinning this study.

The easy-axis HTAF as presented here in the case of a single-ion anisotropy term exhibits quite rich a zero-field behaviour with triple BKT-like transition. This results from the specific compound $S^1 \otimes \mathbb{Z}_6$ symmetry of the system. The upper two transitions are associated with the breaking of the discrete $\mathbb{Z}_6$ symmetry and delimit an intermediate massless critical phase characteristic of $\mathbb{Z}_p$ models with $p \geqslant 4$ (as p goes to ∞ the lower transition temperature tends to zero to yield the limiting case, namely XY model). They are BKT-like but not real BKT transitions. The third transition is the BKT transition associated with the breaking of continuous S^1 symmetry. As for finite-field the behaviour is similar to the one of HTAF as expected by their common $S^1 \otimes \mathbb{Z}_3$ symmetry. In the case of easy-axis HTAF the diagram stretches to higher temperatures thanks to reduced spin fluctuations. Furthermore the anisotropy creates distinct features: first the splitting of zero-temperature one-third magnetisation transition with a finite field range of existence for the up-up-down collinear phase; second saturation field is lowered.

XY TAF presents quite rich a diagram as well. At zero-field it exemplifies the emergence of a discrete symmetry in a continuous model as introduced by Villain: here this discrete $\mathbb{Z}_2$ symmetry is the well-known chirality. If the successive breaking of $\mathbb{Z}_2$ symmetry and S^1 symmetry has been fully demonstrated the precise nature of the upper transition still excites controversy due to the notorious difficulty to calculate critical exponents at this transition. In this dissertation I support the viewpoint this transition belongs to Ising class of universality. Finite-field behaviour exhibits interesting patterns. If Korshunov had carefully discussed them, refinements and numerical evidences were necessary. The first feature to be discussed is the existence of a low-field multicritical point that delimits the magnetically disordered chiral phase. Indeed zero-temperature intermediate magnetically disordered chiral phase survive at finite-field up to a multicritical point. It is delimited by transition lines that both emerge from zero-field transitions: the upper one is $\mathbb{Z}_2$ symmetry-breaking chiral transition, the lower one is $\mathbb{Z}_3$ symmetry-breaking transition associated with lattice translational symmetry-breaking. The emergence of a $\mathbb{Z}_3$ line from a BKT transition is fully allowed in terms of

symmetry as $\mathbb{Z}_3$ is a subgroup of S^1; it is here both supported by numerical results and by the observation that the coupling of spin-waves with field in this region presents a three-fold anisotropy character.At this multicritical point transition lines are inverted: above the multicritical point an intermediate up-up-down collinear phase is stabilised above the low-temperature low-field long-range-ordered 120-degree phase. The second feature to be put forward is the nature of the transition at high-field into the ordered phase from the paramagnetic/saturated one. The compound $\mathbb{Z}_3 \otimes \mathbb{Z}_2$ symmetry is broken as a whole $\mathbb{Z}_6$ symmetry, which implies the existence of an intermediate massless critical phase. The easy-plane HTAF exhibits the same behaviour as XY TAF without much specificity.

Hence this dissertation sheds light on the behaviour of paradigmatic geometrically frustrated magnets. Specifically I have refined finite-field diagram of HTAF and of easy-axis HTAF pointing out a double transition at high field. For XY TAF the diagram is now precise: I clarify the breaking of emergent $\mathbb{Z}_6$ symmetry at high field and the extension to finite field of the magnetically disordered chiral phase. One point still remains an open question that needs to be assigned, namely very low-field behaviour of HTAF. The dissertation exemplifies the wealth of intricate transitions the intertwining of various discrete symmetries or of discrete symmetries with a continuous one can induce. It also shows that a balanced blend of topological and symmetry arguments with not too complicated yet astutely devised numerical simulations can bring much information and pave the way for more sophisticated machinery to refine details of the overall picture presented here. This theoretical dissertation naturally finds an experimental extension: special attention should be given to the following compounds that are quite well described by models previously discussed. HTAF emblematic system is $NiGa_2S_4$ [135]. Yet the most interesting systems are easy-axis HTAF such as $Rb_4Mn(MoO_4)_3$ [39] or $Rb_4Fe(MoO_4)_2$ [54].

Appendix A

Single-ion anisotropy

As this dissertation presents systems in which the interplay between anisotropy and geometric frustration plays a leading role a short reminder on magnetic anisotropy in crystals doesn't seem useless (the reader is referred to reference textbooks for detailed calculations which are not the purpose of this appendix meant as a reminder; see for example [136, 62]). Magnetic properties of a crystal results from the behaviour of electrons in the partially filled outer shells of atoms. Two classes of elements are here of interest for their magnetic properties: iron-group transition elements (electrons on $3d$ shell) on the one hand and rare-earth compounds (electrons on $4f$ shell) on the other hand. In both families it is possible to derive a single-ion anisotropy term even though the energy hierarchy is different between both. What are the relevant energetic terms to be considered in order to describe spins in a crystal? There are three terms: crystal field, spin-orbit coupling LS and Zeeman energy. They respectively read

$$V_{cf}(i) = -e \sum_j V(\mathbf{r}_j) = -e \sum_j \frac{1}{|\mathbf{r}_j - \mathbf{r_i}|} \tag{A.1}$$

with e the electric charge of the electron

$$V_{LS} = \lambda \, \mathbf{L} \cdot \mathbf{S} \tag{A.2}$$

and

$$V_Z = \mu_B (\mathbf{L} + 2\mathbf{S}) \cdot \mathbf{h} \tag{A.3}$$

where μ_B is Bohr magneton.

In iron-group elements spin-orbit coupling is much weaker than crystal field and can hence be treated as a perturbation around the structure obtained from crystal field. Perturbation theory to the second-order for Zeeman and LS terms then yields

$$\mathcal{H} = \sum_{\mu\nu} 2\mu_B h_\nu (\delta_{\mu\nu} - \lambda\Lambda_{\mu\nu})S_\nu - \lambda^2 S_\mu \Lambda_{\mu\nu} S_\nu - \mu_B h_\mu \Lambda_{\mu\nu} h_\nu \tag{A.4}$$

where the tensor $(\Lambda_{\mu\nu})$ is defined as

$$\Lambda_{\mu\nu} = \sum_n \frac{\langle 0|L_\mu|n\rangle\langle n|L_\nu|0\rangle}{E_n - E_0} \tag{A.5}$$

The second term that is the anisotropy term can be developed using x, y, and z crystal directions as principal axis as

$$\mathcal{H} = \frac{1}{3}\left(\Lambda_z - \frac{1}{2}(\Lambda_x + \Lambda_y)\right)(3S_z^2 - S(S+1)) + \frac{1}{2}(\Lambda_x - \Lambda_y)(S_x^2 + S_y^2) \tag{A.6}$$

or in shortened notations

$$DS_z^2 + E(S_x^2 + S_y^2) \tag{A.7}$$

with the constant term dropped.

On the contrary in rare-earth elements spin-orbit coupling is the leading interaction. As a consequence levels first split according to $\mathbf{J} = \mathbf{L} + \mathbf{S}$ values and levels are then split by crystal field term. In an hexagonal geometry using the development of crystal field term with Legendre polynomial on J states let us obtain

$$
\begin{aligned}
V_{cf} =\ & \alpha A_{20}\langle r^2\rangle[3J_z^2 - J(J+1)] \\
+\ & \beta A_{40}\langle r^4\rangle[35J_z^4 - 30J(J+1)J_z^2] \\
+\ & \gamma A_{60}\langle r^6\rangle[231J_z^6 - 315J(J+1)J_z^4 \\
& +105J^2(J+1)^2 J_z^2 - 5J^3(J+1)^3 + 735J_z^4 \\
& -525J(J+1)J_z^2 + 40J^2(J+1)^2 + 294J_z^2 - 60J(J+1)] \\
+\ & \gamma A_{66}\langle r^6\rangle\frac{1}{6}[(J_x + iJ_y)^6 + (J_x - iJ_y)^6]
\end{aligned} \tag{A.8}
$$

where α, β, and γ are coefficient depending on J, L, S and l; A_{20}, A_{40}, A_{60}, and A_{66} are symmetry coefficients in the polynomial expansion. Rare-earth compounds generally exhibit strong anisotropy and the description with the formalism of single-ion anisotropy appears the best suited.

In this work single-ion anisotropy term is used in the form of DS_z^2 which is fully enough to make non-trivial interplay with geometric frustration appear and to correctly describe real compounds (see chap. 6 in [62] and references therein).

Appendix B

Real-space mean-field theory

In this appendix real-space mean-field theory is presented in the case of Heisenberg spin systems. In the first section models with only spin exchange and Zeeman terms are treated. In the second section models with single-ion anisotropy are carefully discussed.

B.1 Heisenberg Model

Here we treat explicitly an isotropic magnetic system with Heisenberg interaction between neighbouring spins.

B.1.1 Single spin in an external field

Let us begin with a single spin in an external magnetic field described by the Hamiltonian $\hat{\mathcal{H}} = -\mathbf{h} \cdot \mathbf{S}$, where $\mathbf{S}$ is either a unit classical vector or a quantum spin S. We need to calculate the partition function corresponding to the above Hamiltonian.

(i) In the classical case the partition function is given by an integral:

$$Z = \int \frac{\sin\theta \mathrm{d}\theta \mathrm{d}\varphi}{4\pi} \, e^{h\cos\theta/T} = \frac{1}{2} \int_{-1}^{1} \mathrm{d}x \, e^{-hx/T} = \frac{T}{h} \, \sinh\frac{h}{T} \tag{B.1}$$

Local magnetization can be obtained by differentiating the free energy $F = -T \ln Z$:

$$m = \langle \cos\theta \rangle = -\frac{\partial F}{\partial h} = T\frac{Z_h'}{Z} = \coth\frac{h}{T} - \frac{T}{h} \; . \tag{B.2}$$

(ii) In the quantum case the partition function is obtained by summation of a finite series:

$$Z = \mathrm{Tr}\, e^{-\hat{\mathcal{H}}/T} = e^{hS/T} + e^{h(S-1)/T} + \ldots + e^{-hS/T} = \frac{\sinh h(S + \frac{1}{2})/T}{\sinh h/2T} \; . \tag{B.3}$$

The magnetization is expressed as

$$m = \left(S + \frac{1}{2}\right) \coth \frac{h(S + \frac{1}{2})}{T} - \frac{1}{2} \coth \frac{h}{2T} \ . \tag{B.4}$$

B.1.2   Lattice model

Consider the following spin Hamiltonian:

$$\hat{\mathcal{H}} = \sum_{\langle ij \rangle} J_{ij} \, \mathbf{S}_i \cdot \mathbf{S}_j - \mathbf{h} \cdot \sum_i \mathbf{S}_i \ . \tag{B.5}$$

The mean field approach amounts to neglecting correlations between spin fluctuations on adjacent sites:

$$
\begin{aligned}
\mathbf{S}_i \cdot \mathbf{S}_j &= \big[\mathbf{m}_i + (\mathbf{S}_i - \mathbf{m}_i)\big] \cdot \big[\mathbf{m}_j + (\mathbf{S}_j - \mathbf{m}_j)\big] \\
&\approx \mathbf{m}_i \cdot \mathbf{m}_j + \mathbf{m}_j \cdot (\mathbf{S}_i - \mathbf{m}_i) + \mathbf{m}_i \cdot (\mathbf{S}_j - \mathbf{m}_j) \\
&= \mathbf{S}_i \cdot \mathbf{m}_j + \mathbf{S}_j \cdot \mathbf{m}_i - \mathbf{m}_i \cdot \mathbf{m}_j
\end{aligned}
\tag{B.6}
$$

where $\mathbf{m}_i = \langle \mathbf{S}_i \rangle$ is a thermodynamic average of an on-site spin. The mean field Hamiltonian, then, is

$$\hat{\mathcal{H}}_{\mathrm{MF}} = -\sum_{\langle ij \rangle} J_{ij} \, \mathbf{m}_i \cdot \mathbf{m}_j - \sum_i \mathbf{h}_i \cdot \mathbf{S}_i \ , \tag{B.7}$$

where

$$\mathbf{h}_i = \mathbf{H} - \sum_j J_{ij} \, \mathbf{m}_j \ . \tag{B.8}$$

The problem of interacting spins is, thus, reduced to a set of single-spin problems supplied by the self-consistency equations:

$$\mathbf{m}_i = \frac{\mathbf{h}_i}{h_i} \left[\coth \frac{h_i}{T} - \frac{T}{h_i}\right] \quad \text{or} \quad \mathbf{m}_i = \frac{\mathbf{h}_i}{h_i} \left[\left(S + \frac{1}{2}\right) \coth \frac{h_i(S + \frac{1}{2})}{T} - \frac{1}{2} \coth \frac{h_i}{2T}\right] \tag{B.9}$$

with local fields defined by Eq. (B.8).

After the solution of self-consistent equations is found the internal energy E_{MF} and the free energy F_{MF} are calculated by

$$E_{\mathrm{MF}} = \sum_{\langle ij \rangle} J_{ij} \, \mathbf{m}_i \cdot \mathbf{m}_j - \sum_i \mathbf{h}_i \cdot \mathbf{m}_i \quad \text{and} \quad F_{\mathrm{MF}} = -\sum_{\langle ij \rangle} J_{ij} \, \mathbf{m}_i \cdot \mathbf{m}_j - T \sum_i \ln Z_i \ , \tag{B.10}$$

where Z_i is given by Eqs. (B.1) or (B.3) depending on the nature of spins.

B.2 Anisotropic Model

The above expressions with very little modifications can be transferred to anisotropic systems with anisotropy coming from interspin interactions (anisotropic exchange, Dzyaloshinskii-Moria interaction, dipolar interactions). In the presence of single-ion anisotropy the basic equations must be modified significantly. Below we treat explicitly the case of classical spins.

B.2.1 Classical spins problem

The single-site Hamiltonian is

$$\hat{\mathcal{H}} = D(\mathbf{n} \cdot \mathbf{S})^2 - \mathbf{h} \cdot \mathbf{S} \tag{B.11}$$

where D is a single-ion anisotropy constant and $\mathbf{n}$ is an anisotropy axis. We split local magnetic field into two parts: component parallel to anisotropy axis $h^{\parallel} = \mathbf{h} \cdot \mathbf{n}$ and transverse component: $h^{\perp} = \sqrt{h^2 - (h^{\parallel})^2}$. In the classical case the partition function is given by

$$Z = \int \frac{\sin\theta \mathrm{d}\theta \mathrm{d}\varphi}{4\pi}\, e^{-E(\theta,\varphi)/T}\ , \qquad E(\theta,\varphi) = D\cos^2\theta - h^{\parallel}\cos\theta - h^{\perp}\sin\theta\cos\varphi \tag{B.12}$$

while the resulting magnetization has two components in the direction parallel and perpendicular to the axis $\mathbf{n}$:

$$\begin{aligned}
\mathbf{m} &= m^{\parallel}\mathbf{n} + m^{\perp}\big[\mathbf{h} - \mathbf{n}(\mathbf{h}\cdot\mathbf{n})\big]/h^{\perp} \\
m^{\parallel} &= \frac{1}{Z}\int \frac{\sin\theta \mathrm{d}\theta \mathrm{d}\varphi}{4\pi}\, \cos\theta\, e^{-E(\theta,\varphi)/T} \\
m^{\perp} &= \frac{1}{Z}\int \frac{\sin\theta \mathrm{d}\theta \mathrm{d}\varphi}{4\pi}\, \sin\theta\cos\varphi\, e^{-E(\theta,\varphi)/T}
\end{aligned} \tag{B.13}$$

Partial integration over azimuthal angle simplifies Eqs.. (B.12) and (B.13) to

$$\begin{aligned}
Z &= \frac{1}{2}\int_{-1}^{1} \mathrm{d}x\, e^{-Dx^2/T}\, e^{h^{\parallel}x/T} I_0(y) \\
m^{\parallel} &= \frac{1}{2Z}\int_{-1}^{1} x\mathrm{d}x\, e^{-Dx^2/T}\, e^{h^{\parallel}x/T} I_0(y) \\
m^{\perp} &= \frac{1}{2Z}\int_{-1}^{1} \mathrm{d}x\, \sqrt{1-x^2}\, e^{-Dx^2/T}\, e^{h^{\parallel}x/T} I_1(y)
\end{aligned} \tag{B.14}$$

where $y = (h^{\perp}\sqrt{1-x^2})/T$ and $I_0(z)$ and $I_1(z)$ are the modified Bessel functions of zeroth and first order:

$$I_0(z) = \frac{1}{\pi}\int_0^{\pi} e^{z\cos\varphi}\mathrm{d}\varphi\ , \qquad I_1(z) = \frac{1}{\pi}\int_0^{\pi} e^{z\cos\varphi}\cos\varphi\mathrm{d}\varphi\ . \tag{B.15}$$

The lattice Hamiltonian is written as

$$\hat{\mathcal{H}} = D \sum_i (\mathbf{n}_i \cdot \mathbf{S}_i)^2 + \sum_{\langle ij \rangle} J_{ij}\, \mathbf{S}_i \cdot \mathbf{S}_j - \mathbf{h} \cdot \sum_i \mathbf{S}_i \ , \tag{B.16}$$

where the anisotropy axis can be either uniform or staggered. The mean-field approximation leads to the following Hamiltonian:

$$\hat{\mathcal{H}}_{\mathrm{MF}} = - \sum_{\langle ij \rangle} J_{ij}\, \mathbf{m}_i \cdot \mathbf{m}_j + D \sum_i (\mathbf{n}_i \cdot \mathbf{S}_i)^2 - \sum_i \mathbf{h}_i \cdot \mathbf{S}_i \ , \qquad \mathbf{h}_i = \mathbf{h} - \sum_j J_{ij}\, \mathbf{m}_j \tag{B.17}$$

supplied by the mean-field equations (B.14). The free-energy is still given by the above Eq. (B.10), while an expression for the internal energy becomes

$$E_{\mathrm{MF}} = \sum_{\langle ij \rangle} J_{ij}\, \mathbf{m}_i \cdot \mathbf{m}_j - \sum_i \mathbf{h}_i \cdot \mathbf{m}_i + D \sum_i \langle (m_i^{\parallel})^2 \rangle \ . \tag{B.18}$$

Here, square of the parallel component of the on-site moment is given by

$$\langle (m^{\parallel})^2 \rangle = \frac{1}{2Z} \int_{-1}^{1} x^2 \mathrm{d}x\, e^{-Dx^2/T}\, e^{h^{\parallel} x/T} I_0(y) \ . \tag{B.19}$$

B.2.2   Quantum case S=1

Let's now introduce the case of a quantum system. Single-ion anisotropy is relevant for $S \geqslant 1$ as $(\mathbf{S} \cdot \hat{\mathbf{n}})^2 = const$ in case of $S = 1/2$. Provided we consider the anisotropy axis along z the single-site anisotropy can be written

$$\hat{\mathcal{H}} = D(\hat{S}_z)^2 - h^{\parallel} \hat{S}_z - h^{\perp} \frac{\hat{S}_+ + \hat{S}_-}{2} \tag{B.20}$$

In the case of spin $S = 1$ this can be written as

$$\hat{\mathcal{H}} = \begin{pmatrix} h^{\parallel} + D & -\frac{h^{\perp}}{\sqrt{2}} & 0 \\ -\frac{h^{\perp}}{\sqrt{2}} & 0 & -\frac{h^{\perp}}{\sqrt{2}} \\ 0 & -\frac{h^{\perp}}{\sqrt{2}} & -h^{\parallel} + D \end{pmatrix} \tag{B.21}$$

Introducing the characteristic polynomial the eigenvalues can be calculated and the magnetisation deduced

$$\chi_{\hat{\mathcal{H}}}(E) = -E^3 + 2DE^2 + (h^2 - D^2)E - D(h^{\perp})^2 \tag{B.22}$$

$$E_k = 2\sqrt{\frac{-p}{3}} \cos\left(\frac{1}{3} \arccos\left(\frac{-q}{2}\sqrt{\frac{27}{-p^3}}\right) + \frac{2k\pi}{3}\right) - \frac{2D}{3} \tag{B.23}$$

where $p = -(D^2/3 + h^2)$ and $q = 2D^3/27 + D(-2(h^\parallel)^2/3 + (h^\perp)^2/3)$. Then using $m^{\parallel,\perp} = -T\partial_{h^{\parallel,\perp}} \ln Z$ and $\partial_{h^{\parallel,\perp}} \chi_{\hat{\mathcal{H}}}(E_k) = 0$

$$Z = \sum_k e^{-E_k/T}, \quad m^\parallel = \frac{1}{Z} \sum_k \frac{-2h^\parallel E_k e^{-E_k/T}}{3E_k^2 - 4DE_k + D^2 - h^2}, \quad m^\perp = \frac{1}{Z} \sum_k \frac{-(2E_k - D)h^\perp e^{-E_k/T}}{3E_k^2 - 4DE_k + D^2 - h^2}$$

$$(B.24)$$

Using the mean field approximation the lattice Hamiltonian can be expressed as in (B.17), which enables to use the above results for the single-site.

Appendix C

Zero-field upper transition in mean-field treatment: sign of γ_2

In this appendix the sign of one of the sixth-order coefficients in Landau-Ginzburg functional about zero-field upper transition is determined using mean-field description. For the determination of some phenomenological parameters it is necessary to use the description of a layered system and consider the specific case of fully decoupled layers to obtain the sign of γ_2 in case of the purely $2d$ system.

Let's recall mean-field equations:

$$m_i^\perp \;=\; \frac{1}{2Z_i} \int_{-1}^{1} \mathrm{d}x \, \sqrt{1-x^2} \, e^{Dx^2/T} \, e^{h_i^z x/T} I_1(y_i) \tag{C.1}$$

$$m_i^z \;=\; \frac{1}{2Z_i} \int_{-1}^{1} \mathrm{d}x \, x \, e^{Dx^2/T} \, e^{h_i^z x/T} \, I_0(y_i) \tag{C.2}$$

$$Z_i \;=\; \frac{1}{2} \int_{-1}^{1} \mathrm{d}x \, e^{Dx^2/T} \, e^{h_i^z x/T} I_0(y_i) \tag{C.3}$$

where $y_i = h_i^\perp \sqrt{1-x^2}/T$, $\mathbf{h}_i = \mathbf{h} - \sum_{n.n.} \mathbf{m}_j$, and $I_n(z)$ is the modified Bessel function of the n-th order:

$$I_n(z) = \frac{1}{\pi} \int_0^{\pi} \mathrm{d}\alpha \, e^{z\cos\alpha} \, \cos^n\alpha \;. \tag{C.4}$$

At the upper transition from paramagnetic phase to collinear one $h_i^\perp = 0$, which implies $y_i = 0$, and $m_i^\perp = 0$ as well: Eq. (C.1) can be dropped. For clarity we hereafter drop the index z: $h_i^z = h_i$, etc. Let's expand Eqs. (C.3) and (C.2) in powers of h_i around $h_i = 0$. For calculations to remain legible abridged notations are introduced as follows:

$$K_n = \int_{-1}^{1} \mathrm{d}x \, x^n e^{\frac{dx^2}{T}} \quad \forall n \in \mathbb{N}, K_{2n+1} = 0 \tag{C.5}$$

For our purpose following integrals will be used:

$$
\begin{aligned}
K_0 &= \frac{\sqrt{\pi}\,\mathrm{erfi}\left(\sqrt{d/T}\right)}{\sqrt{d/T}} \\[2mm]
K_2 &= \frac{e^{d/T}}{d/T} - \frac{K_0}{2d/T} \\[2mm]
K_4 &= \frac{2d/T - 3}{2(d/T)^2}e^{d/T} + \frac{3K_0}{4(d/T)^2} \\[2mm]
K_6 &= \frac{15 - 10d/T + 4(d/T)^2}{4(d/T)^3}e^{d/T} - \frac{15}{8(d/T)^3}K_0
\end{aligned}
$$

where erfi designates the imaginary error function defined as

$$
\mathrm{erfi}(z) = \frac{\mathrm{erf}(iz)}{i} \quad \text{with} \quad \mathrm{erf}(z) = \frac{2}{\sqrt{\pi}}\int_0^z \mathrm{d}u\, e^{-u^2} \tag{C.6}
$$

With these notations the expansion to fourth-order of Eq. (C.3) reads

$$
Z_i = \frac{K_0}{2}\left[1 + \frac{K_2}{2K_0 T^2}h_i^2 + \frac{K_4}{24K_0 T^4}h_i^4\right] + \mathcal{O}(h_i^6) \tag{C.7}
$$

thus

$$
\frac{1}{Z_i} = \frac{1}{Z_i}\left[1 - \frac{K_2}{2K_0 T^2}h_i^2 + \frac{6K_2^2 - K_0 K_4}{24K_0^2 T^4}h_i^4\right] + \mathcal{O}(h_i^6) \tag{C.8}
$$

To calculate m_i, let's start with the calculation of the integral in Eq. (C.2):

$$
\int_{-1}^{1}\mathrm{d}x\, x e^{\frac{dx^2 + h_i x}{T}} = \frac{K_2}{T} + \frac{K_4}{6T^3}h_i^3 + \frac{K_6}{120T^5}h_i^5 + \mathcal{O}(h_i^7) \tag{C.9}
$$

Then combining with Eq. (C.8) Eq. (C.2) becomes

$$
m_i = b_1 h_i + b_3 h_i^3 + b_5 h_i^5 + \mathcal{O}(h_i^7) \tag{C.10}
$$

where

$$
b_1 = \frac{K_2}{K_0 T} \tag{C.11}
$$

$$
b_3 = \frac{K_0 K_4 - 3K_2^2}{6K_0^2 T^3} \tag{C.12}
$$

$$
b_5 = \frac{K_6 K_0^2 - 15K_0 K_2 K_4 + 30K_2^2}{120K_0^3 T^5} \tag{C.13}
$$

Now self-consistent equations are derived in the context of layered systems with an interlayer coupling λ, with $\lambda > 0$ for antiferromagnetic coupling and $\lambda < 0$ for ferromagnetic coupling. Let's write down the definition of local fields in the case of an antiferromagnetic coupling (six-sublattice structure: m_1, m_2, m_3 on one layer, m_1', m_2', m_3' on the other):

$$\begin{cases} m_1 &= l_1 \\ m_2 &= \frac{-l_1 - \sqrt{3}l_2}{2} \\ m_3 &= \frac{-l_1 + \sqrt{3}l_2}{2} \end{cases} \qquad \begin{cases} m_1' &= -l_1 \\ m_2' &= \frac{l_1 + \sqrt{3}l_2}{2} \\ m_3' &= \frac{l_1 - \sqrt{3}l_2}{2} \end{cases} \tag{C.14}$$

and

$$\begin{cases} h_1 &= -3(m_2 + m_3) - 2\lambda m_1' = (3 + 2\lambda)l_1 \\ h_2 &= -3(m_1 + m_3) - 2\lambda m_2' = -(3 + 2\lambda)\frac{l_1 + \sqrt{3}l_2}{2} \\ h_3 &= -3(m_1 + m_2) - 2\lambda m_3' = -(3 + 2\lambda)\frac{l_1 - \sqrt{3}l_2}{2} \end{cases} \qquad \begin{cases} h_1 &= -(3 + 2\lambda)l_1 \\ h_2 &= (3 + 2\lambda)\frac{l_1 + \sqrt{3}l_2}{2} \\ h_3 &= (3 + 2\lambda)\frac{l_1 - \sqrt{3}l_2}{2} \end{cases} \tag{C.15}$$

where antiferromagnetic order parameters have been introduced:

$$\mathbf{m}_i = \mathbf{l}_1 \cos(\mathbf{q}_0 \cdot \mathbf{r}_i) + \mathbf{l}_2 \sin(\mathbf{q}_0 \cdot \mathbf{r}_i) \tag{C.16}$$

As a consequence solving Eq. (C.10) is equivalent to solving the following polynomial equation:

$$\left(\tilde{b}_1 - 1 + \tilde{b}_3 x^2 + \tilde{b}_5 x^4 \right) x = 0 \tag{C.17}$$

where the term $\mathcal{O}(x^7)$ has been dropped, $x \in \{l_1, (l_1 \pm \sqrt{3}l_2)/2\}$, and renormalised coefficients b_i's read (one can easily check that the treatment of ferromagnetic and antiferromagnetic couplings are equivalent, hence the introduction of $|\lambda|$ to encompass both situations in the following)

$$\tilde{b}_k = (3 + 2|\lambda|)^k b_k \tag{C.18}$$

Solutions to Eq. (C.17) are either $x = 0$ or solutions to $\left(\tilde{b}_1 - 1 + \tilde{b}_3 x^2 + \tilde{b}_5 x^4 \right)$ that can be written as

$$y_\pm = \frac{-b_3 \pm \sqrt{B}}{2(3 + 2|\lambda|)^2 b_5} \tag{C.19}$$

where

$$B = b_3^2 - 4 \left(b_1 - \frac{1}{3 + 2|\lambda|} \right) b_5 \tag{C.20}$$

Then solutions can be expressed in terms of l_1 and l_2:

$$l_1 = l_2 = 0 \tag{C.21}$$

$$\begin{cases} l_1 &= \varepsilon \sqrt{y_+} \\ l_2 &= \frac{1}{\sqrt{3}} \varepsilon \sqrt{y_+} \end{cases} \tag{C.22}$$

$$\begin{cases} l_1 & = & \varepsilon\sqrt{y_-} \\ l_2 & = & \frac{1}{\sqrt{3}}\varepsilon\sqrt{y_-} \end{cases} \tag{C.23}$$

where $\varepsilon = \pm 1$.

Of course conditions of positivity for B and $y_\pm$ have been taken into account: on the temperature range $[1.04, 1.30]$ $B > 0$ $y_\pm > 0$.

Let's now turn to Landau-Ginzburg free energy functional:

$$F = \alpha(l_1^2 + l_2^2) + \beta_{12}(l_1^2 + l_2^2)^2 + \gamma_1(l_1^2 + l_2^2)^3 + \gamma_2[(l_1 + il_2)^6 + cc] \tag{C.24}$$

In this expression there is only a single fourth-order term as the development is made about a collinear phase in which case both fourth-order terms have the same expression. At equilibrium

$$\begin{cases} \partial_{l_1} F & = & 0 \\ \partial_{l_2} F & = & 0 \end{cases} \tag{C.25}$$

which yields

$$\begin{cases} \alpha + 2\beta_{12}(l_1^2 + l_2^2) + 3(\gamma_1 - 4\gamma_2)l_1^4 + 3(\gamma_1 + 4\gamma_2)l_2^4 + 6\gamma_1 l_1^2 l_2^2 & = & 0 \\ 3\gamma_2 l_1^4 + 3\gamma_2 l_2^4 - 10\gamma_2 l_1^2 l_2^2 & = & 0 \end{cases} \tag{C.26}$$

In terms of l_1 and l_2 solutions read:

$$l_1 = l_2 = 0 \tag{C.27}$$

or

$$l_1 = 0 \quad \text{and} \quad l_2 = \pm\sqrt{\frac{-\beta_{12} \pm \sqrt{\delta'}}{3(\gamma_1 - 2\gamma_2)}} \tag{C.28}$$

or

$$l_1 = \pm\sqrt{\frac{-\beta_{12} \pm \sqrt{\delta}}{3(\gamma_1 + 2\gamma_2)}} \quad \text{and} \quad l_2 = 0 \tag{C.29}$$

or

$$l_1 = \pm\sqrt{\frac{-\beta_{12} \pm \sqrt{\delta}}{12(\gamma_1 + 2\gamma_2)}} \quad \text{and} \quad l_2 = \pm\sqrt{\frac{-\beta_{12} \pm \sqrt{\delta}}{4(\gamma_1 + 2\gamma_2)}} \tag{C.30}$$

or

$$l_1 = \pm\sqrt{\frac{-\beta_{12} \pm \sqrt{\delta}}{4(\gamma_1 - 2\gamma_2)}} \quad \text{and} \quad l_2 = \pm\sqrt{\frac{-\beta_{12} \pm \sqrt{\delta}}{12(\gamma_1 - 2\gamma_2)}} \tag{C.31}$$

where $\delta = \beta_{12}^2 - 3\alpha(\gamma_1 - 2\gamma_2)$ and $\delta' = \beta_{12}^2 - 3\alpha(\gamma_1 - 2\gamma_2)$.

From the comparison of both sets of solutions it is then possible to extract an expression for γ_2, which is the purpose of these calculations:

$$\gamma_2 = \frac{b_5}{4}\left(\frac{4}{3\alpha}\left(b_1 - \frac{1}{3 + 2|\lambda|}\right) - \frac{1}{2}(3 + 2|\lambda|)^2\right) \tag{C.32}$$

Taking $|\lambda| = 0$ in Eq. (C.32) yields $\gamma_2 > 0$ in the vicinity of the upper transition at zero field, $T_{c1} \approx 1.2$ QED.

Appendix D

Finite-size scaling

A striking paradox lies at the very heart of our experience of phase transitions: trusting our senses they do occur in systems around us, trusting our reason they are mathematically possible only for infinite systems. As often physics just stands in between as shows the introduction of the thermodynamic limit, which can be understood as a way to take an infinite limit to describe physical systems that are necessarily finite. Yet such a solution encounters its limits of accuracy as we start dealing with systems characterised by small extent in one or several dimensions. Systems used in numerical works do exhibit strong alterations to thermodynamic behaviour as they are often of very limited sizes. Then it is necessary to question the way thermodynamic limit is approached and what the correction terms are. In the late 1960's Fisher initiated the answering to this concern. If I don't aim at reproducing this work hereafter, which is quite clearly exposed in original papers [31, 32, 30] and the textbook review by Barber [8], I will remind most important assumptions that lay the foundation for this analysis of correction terms for finite-size systems, otherwise called finite-size scaling. Interestingly what could be perceived a hindrance to numerical investigation of phase transitions has in fact been turned into *the* way to extract information on phase transitions from calculations on finite-size systems. Of course it doesn't mean misleading results in finite-size clusters can always be circumvented.

D.1   Fundamentals

D.1.1   Geometry and boundary conditions

First the system under consideration has to be precised, especially the boundary conditions that are adopted. There are three different geometries dealt with in scaling theories:

- G_1: A completely finite system of volume $V = L^d$ in d dimensions $(d' = 0)$

- G_2: A d-dimensional layer of infinite dimension in $d' = d - 1$ dimensions and of finite thickness L

- G_3: A system finite in $d - 1$ dimensions and infinite in the last one with a cross-section area characterized by length L ($d' = 1$)

G_1 corresponds to the situation of real systems and clusters used in Monte Carlo numerical investigations as presented in this work. G_2 is of interest mainly for analytical calculations and enable to study dimensional crossover phenomena. G_3 is the geometry used in transfer matrix method and phenomenological renormalisation group or in quantum systems, with time as the infinite dimension.

When considering finite systems boundary conditions have to be assigned: these can be expressed using a function φ defined on a $d' \times (d - d')$ space (the first component corresponds to dimensions along which the system is infinite, the second to those along which it is finite) with $(\hat{\mathbf{e}}_i)_{1 \leqslant i \leqslant d - d'}$ a basis of the second component:

- Periodic boundary conditions: $\forall i, u, v, \quad \varphi(\mathbf{u}, \mathbf{v} + L\hat{\mathbf{e}}_i) = \varphi(\mathbf{u}, \mathbf{v})$

- Open boundary conditions (or free surface): $\forall u, v, \quad \varphi(\mathbf{u}, \mathbf{v}) = 0 \quad \text{if} \quad v \notin [0, L]^d$

- Twisted boundary conditions, among which antiperiodic ones: $\forall i, u, v, \quad \varphi(\mathbf{u}, \mathbf{v} + L\hat{\mathbf{e}}_i) = -\varphi(\mathbf{u}, \mathbf{v})$

Each set of conditions presents advantages depending on the use: for example the latter ones are often introduced in the study of helicity modulus, aka stiffness. Open boundary conditions may be helpful when carrying out analytical calculations. The reason why periodic boundary conditions are used in most numerical works is the quick convergence of functions towards thermodynamic limit. Let's indeed assume thermodynamic limit exists:

$$f_\infty(T, \rho) = \lim_{\substack{N \to \infty \\ V \to \infty \\ \rho = N/V = const}} \frac{F(T, V, N)}{V} \tag{D.1}$$

where F is the free energy, T the temperature, V the volume, N the number of particles and ρ the density. Then free surface boundary conditions yield surface terms:

$$F(T, V, N) = V f_\infty(T, \rho) + A f_x(T, \rho) + o(A) \tag{D.2}$$

where A designates the area of the boundary. Periodic boundary conditions induce an exponential convergence:

$$F(T, V, N) = V f_\infty(T, \rho) + \mathcal{O}\left(e^{-L\Gamma(T)}\right) \tag{D.3}$$

This expansion however breaks down in the vicinity of critical temperature T_c as $\lim_{T \to T_c} \Gamma(T) = 0$, which explains the so-called critical slowing-down about phase transition in numerical calculations.

D.1.2 Alteration of singularities in finite systems

As previously seen finite size induces corrections to thermodynamic functions and especially a rounding of singularities. Let's consider a diverging thermodynamic quantity and discuss the behaviour of its estimate in finite-size systems for which no singularity appears (typically in geometry G_1 that is relevant for Monte Carlo numerical works). Its estimate on finite systems exhibits a peak instead of a divergence, the height of which increases with $l = L/a$ (a is a typical microscopic lengthscale of the system), located at $T_m(l)$ that tends to T_c, the thermodynamic critical temperature, as [31, 32]

$$\frac{T_m(l) - T_c}{T_c} \sim \frac{b}{l^\lambda} \tag{D.4}$$

Another temperature of interest is the temperature $T^*(l)$ at which the quantity evaluated on a finite-size system starts departing significantly from the thermodynamic function. T^* tends to T_c as [31, 32]

$$\frac{T^*(l) - T_c}{T_c} \sim \frac{c}{l^\theta} \tag{D.5}$$

Fisher and Ferdinand put forward the following argument to assign a value to θ [31]: T^* is such that $\xi(T^*) = L$. In other words once the correlation length spans the whole system it is no longer possible for criticality to grow. This argument yields $\theta = 1/\nu$ as $\xi(T) \sim (T - T_c)^{-\nu}$. For λ the situation is less clear; yet a similar line of reasoning leads to $\lambda = 1/\nu$.

D.1.3 Scaling

After having described the rounding of singularities in finite systems, next point is to explain how to nevertheless extract information on thermodynamic singularity, ie on transition, from finite-size data. This is the aim of finite-size scaling. Finite-size scaling is based on the following Ansatz [32, 30]: in the vicinity of the bulk critical temperature T_c the behaviour of a system with at least one large but finite dimension is determined by

$$y = \frac{L}{\xi(T)} \tag{D.6}$$

with ξ the bulk correlation length. Then considering a thermodynamic quantity $P_L(T)$ of the finite system with an algebraic singularity in the infinite system $P_\infty \underset{t\to 0}{\sim} c_\infty t^{-\rho}$ where $t = (T - T_c)/T_c$ is the reduced temperature, the finite-size scaling hypothesis reads

$$P_L(T) \sim l^\omega R_P(y) \tag{D.7}$$

or in terms of the reduced temperature as can be derived transforming scaling variable
(D.6) introducing the algebraic divergence of ξ ($\xi(T) \sim (T - T_c)^{-\nu}$)

$$P_L(T) \sim l^\omega Q_P(l^\theta \dot{t}) \tag{D.8}$$

where $\dot{t} = T - T_c(L)$ and $T_c(L)$ is a pseudo-critical temperature – in fact as long as
the shift exponent $\lambda \geqslant 1/\nu$ there is a certain flexibility in the definition of this pseudo-
critical temperature based either on T^* or T_m; it is even possible to substitute $t = T - T_c$
to $\dot{t}$ in certain formulas as done in the following section where this formalism is actually
used. Then for these definitions to be coherent and reconcile with the infinite limit
exponents have to respect

$$\omega = \rho\theta = \frac{\rho}{\nu} \tag{D.9}$$

In the case here considered (no transition in the finite system) $\lim_{x \to 0} Q_P(x) = Q_0$ so that

$$P_l(T_c(l)) \underset{l \to \infty}{\sim} Q_0 l^{\rho/\nu} \tag{D.10}$$

This relation states that the way estimates of thermodynamic quantities vary with
system size depends on thermodynamic critical exponents. It constitutes the heart of
finite-size scaling techniques to estimate critical exponents and critical temperature.

The preceding calculations are applicable in case of an algebraic singularity in the
infinite system. In case the thermodynamic quantity under scrutiny exhibits a loga-
rithmic divergence as is the case of specific heat in bidimensional Ising model:

$$P_\infty(T) \sim c_\infty \ln t \tag{D.11}$$

then Eq. (D.8) cannot be used. Scaling is however possible introducing a non-critical
temperature T_0 and then write [32]

$$(P_L(T) - P_L(T_0)) \sim \left(Q_P(l^\theta t) - Q_P(l^\theta t_0)\right) \tag{D.12}$$

Matching limiting cases yields once again the scaling equation of practical use:

$$P_L(T_c(L)) \underset{\substack{l \to \infty \\ \dot{t} \to 0}}{\sim} -\frac{c_\infty}{\nu} \ln l + \mathcal{O}(1) \tag{D.13}$$

D.2   Expressions of direct interest in this study

This section aims at summarizing the quantities used in the numerical calculations
of this work. It starts with a specification of the general expressions introduced in the
previous section before a discussion of other interesting probes to locate and characterise
transitions, namely Binder's cumulant and a ratio of correlation functions astutely

chosen. The way procedures to locate transitions based on these equations can be built is extensively discussed.

In preceding section as already mentioned some results can be expressed in terms of the critical temperature of the infinite system. In particular (D.10) can be written in terms of T_c. Hence for specific heat the exponent ρ is α; for susceptibility (D.10) reads

$$\chi(T_c, l) \underset{l \to \infty}{\sim} Q_0 l^{2-\eta} \tag{D.14}$$

where $\gamma/\nu = 2 - \eta$, when $d = 2$, has been used. This has been extensively used to locate T_c as it shows that $\chi(T_c, l) l^{-(2-\eta)}$ is size independent: in other words T_c is the temperature of the intersection points of plots of $\chi(T_c, l) l^{-(2-\eta)}$ versus temperature for different cluster sizes.

Another consequence of scaling was drawn by Binder when he introduced the cumulant now often referred to after his name [12]. For the purpose of scaling scalar factors introduced in the original paper can be taken off:

$$U_A(T, L) = \frac{\langle A^4 \rangle}{\langle A^2 \rangle^2} \tag{D.15}$$

where A is the order parameter of interest (eg: S_q^α with $\alpha \in \{x, y, z\}$, chirality κ, etc.). Applying scaling to fourth and second moments that appear in this definition yields the following

$$U_A(T, L) = f_A(y) \tag{D.16}$$

A straightforward and important consequence of this expression is that $U_A(T_c, L)$ is size-independent $(f_A(y) \underset{y \to 0}{\longrightarrow} f_A^0)$: plots of Binder's cumulant versus temperature for different L cross at T_c in case of a second-order transition, merge in case of a BKT transition. Another consequence is that it can be used to estimate critical exponents [70]. Let's illustrate the method with susceptibility: expression (D.7) used for χ_A (where A is the order parameter of interest) shows that $\chi_A/L^{2-\eta}$ is a function of y; given (D.16) it results that plotting $\chi_A/L^{2-\eta}$ versus U_A with η as a free parameter can be used to estimate η: for the right value plots are indeed L-independent, which means all data points collapse on a single curve.

An improvement has recently been brought with the consideration of a ratio of correlation functions [120, 112] which has similar properties to Binder's cumulant with the great advantage of better accuracy as it is a second-order quantity. Let's consider spin-spin correlation function

$$g(r, L, T) = \frac{1}{L^d} \sum_i \langle \mathbf{S}_i \cdot \mathbf{S}_{i+r} \rangle \tag{D.17}$$

where the abridged notation $i + r$ indexes neighbours of spin i at distance r. Scaling form of g introduces another length ratio beside $y = L/\xi$:

$$g(r, L, T) \sim r^{-(d-2+\eta)} Q\left(\frac{r}{L}, y\right) \tag{D.18}$$

As a consequence

$$\Gamma = \frac{g(L/2, L, T)}{g(L/4, L, T)} = \left(\frac{L/2}{L/4}\right)^{-(d-2+\eta)} \frac{Q\left(\frac{L/2}{L}, y\right)}{Q\left(\frac{L/4}{L}, y\right)} = \tilde{Q}(y) \tag{D.19}$$

As it is a second-order expression statistical noise affects less severely this quantity. It can then be used in a similar way to Binder's cumulant and can also help identifying an intermediate algebraic phase that is otherwise invisible using Binder's cumulant.

Last, the case of BKT transition has to be addressed. In numerical calculations one of the most efficient ways to study a BKT transition is spin stiffness ρ_S (see Eq. 2.23). At a BKT transition spin stiffness exhibits a jump the height of which is universal, equal to $\rho_S(T_{BKT}) = (2q^2/\pi)T_{BKT}$ for a transition driven by $1/q$ vortices. For integer vortices ($q = 1$) it thus reads $\rho_S(T_{BKT}) = (2/\pi)T_{BKT}$. Renormalisation group flow yields the following scaling for spin stiffness [127, 94]:

$$\rho_S(T, L) = \rho_S^\infty(T)\left(1 + \frac{1}{2(\ln L + c)}\right) \tag{D.20}$$

From this formula a way to extrapolate T_{BKT} can be devised: if T_L is such that $\rho_S(T_L, L) = (2/\pi)T_L$ then

$$\frac{T_L - T_{BKT}}{T_{BKT}} = \frac{1}{2(\ln L + c)} \tag{D.21}$$

Often an approximate expansion in terms of $1/L$ can be used instead due to negligible correction terms.

Appendix E

Monte Carlo algorithms

To study thermal averages in equilibrium statistical mechanics a powerful method arose with the development of numerical simulations, viz. Monte Carlo simulation: it uses a stochastic trajectory to explore the phase space. This method is quite efficient as it enables to study any classical system even if analytically intractable and offers results that can often be compared with experiments. Concerning quantum systems the situation is less favourable due to the notorious sign problem. Quantum Monte Carlo techniques are quite distinct of classical Monte Carlo and won't be dealt with hereafter: only classical Monte Carlo algorithms are indeed of interest for the present work.

This appendix is not meant to provide an extensive presentation on Monte Carlo algorithms, as may be found in [13, 45], but to review the basics about classical Monte Carlo.

E.1 Back to basics

Let's consider a system with Hamiltonian $\mathcal{H}$. We are interested in calculating such properties of this system as $\langle A \rangle_T$ (canonical ensemble) where A is an observable (internal energy, magnetisation, etc.) and the average is a thermal one. In other words we want to average an observable over phase space Ω respecting a certain distribution of states ω in this space (typically $\omega(\mathbf{x}) = \exp\left[-\beta\mathcal{H}(\mathbf{x})\right]$):

$$\langle A \rangle_T = \frac{\int_\Omega d\mathbf{x} \quad A(\mathbf{x})\omega(\mathbf{x})}{\int_\Omega d\mathbf{x} \quad \omega(\mathbf{x})} \tag{E.1}$$

For such an average to be calculated an efficient integrating algorithm has to be used: in high dimensions the most efficient one is a Monte Carlo integration. Monte Carlo algorithms are based on the use of a pseudo-random variable: most of the time it is enough to use variables provided by a well-designed random number generator rather

than using a list of 'true' random numbers obtained, eg, through nuclear radiations and thus we won't make any distinction in the following. In our work we implemented a random number generator proposed by Marsaglia [72].

If phase space were to be explored in a fully random manner the number of Monte Carlo steps required for a good accuracy would be awfully huge as the distribution of states in the phase space appears to be too peaked to make a simple sampling method efficient. It is thus most desirable to devise an importance sampling that could preferably sample regions according to the equilibrium distribution ω: a Markov chain offers such a possibility in a way perfectly adapted for numerical calculations as it has no memory: the evolution only depends on the current state and the transition matrix T defining the chain. Let's remind what a Markov chain is and review the conditions for a Markov process to converge to a given distribution ω. For simplicity we hereafter present the case of a Markov chain in a finite space : going to infinite discrete or even continuous limit can be done in a natural way for spaces relevant to physical systems.

First let's recall what a stochastic matrix is: let T be a matrix; then T is said to be a stochastic matrix if all its row vectors are probability distributions. A Markov chain is a stochastic process defined as a sequence of random variables $(X_n)_{n \geqslant 1}$ on a space $\mathcal{S}$ such that $P(X_{n+1} = i | X_n = j) = T_{ij}$ with (T_{ij}) a stochastic matrix. To initiate the process, an initial distribution λ is chosen. We note (X, λ, T) such a Markov process. For our purpose the initial distribution λ doesn't matter as we aim at gaining information on the stationary distribution π of the process, which is such that $T\pi = \pi$ and that we want verifying $\pi = \omega$. The existence of a stationary distribution is guaranteed by the ergodic theorem: let (X, λ, T) be a Markov process over a finite space $\mathcal{S}$ with T an aperiodic and irreducible stochastic matrix, then there exists a unique stationary distribution π. Furthermore, for any initial distribution λ and bounded function f over $\mathcal{S}$, then

$$\lim_{N \to \infty} \frac{1}{N} \sum_{i \in (X_n)_{n=1}^N} f(i) = \sum_{i \in \mathcal{S}} \pi_i f(i) \quad \text{almost surely} \tag{E.2}$$

An aperiodic and irreducible transition matrix for a Markov process prevents any finite period of return for all states after a certain rank in the process and assures that any state is reachable from any other state during the process. As a consequence, the chain can be assumed independent of the initial distribution λ after a certain rank depending on its speed of convergence towards its stationary distribution. λ-dependent initial steps are typically called thermalisation steps and are discarded for measurement.

The next question is how to construct the transition matrix T such that its stationary distribution is the given distribution $\pi = \omega$. There are various ways of dealing with this problem: we will concentrate on processes that can be described with a transition matrix reading:

$$T_{ij} = P_{ij} A_{ij} + \delta_{ij} \sum_k P_{kj}(1 - A_{kj}) \tag{E.3}$$

where P is a proposal matrix and A an acceptance matrix. Time can be introduced

in such a Markov chain through a characteristic time τ_0 associated with an elementary step, multiplying T_{ij} by τ_0^{-1}. Provided P is a symmetric stochastic matrix and A, a matrix with elements in $[0,1]$, respecting detailed balance with respect to π:

$$\forall(i,j), \ A_{ij}\pi_j = A_{ij}\pi_i \tag{E.4}$$

then the Markov chain associated with T admits π as its stationary distribution and property (E.2) applies. Different choices then exist for both P and A [45, 71]. Let's first discuss the choice of the acceptance matrix A. Among the most widely used methods are Hastings' ones [38]:

$$A_{ij} = f(i,j)\min\left(\frac{\pi_j f(j,i)}{\pi_i f(i,j)}, 1\right) \tag{E.5}$$

where f is an appropriate auxiliary function. The well-known algorithm proposed by Metropolis *et al.* [78] corresponds to $f = 1$ in (E.5) with Boltzmann's distribution as π.

Various proposal matrices have been devised. In the case of non-frustrated systems cluster algorithm are certainly among the most efficient ones; alas in case of the frustrated systems considered in this work they cannot be used. Therefore we present here the solution we have adopted to update continuous Heisenberg or XY spins, namely a single-spin restricted motion scheme.

A naïve approach for Heisenberg spins consists in generating a random vector uniformly distributed on $\mathcal{S}^2$. This can be achieved using an angular representation: $\mathrm{d}z = \sin(\theta)\mathrm{d}\theta$ and $\mathrm{d}\phi$ are uniform distributions. Then one can proceed as follows:

```
z    =   p1
phi  =   p2*pi
r    =   sqrt(1 - p1**2)
x    =   r cos(phi)
y    =   r sin(phi)
```

where p1 and p2 are random numbers uniformly distributed in $[-1,1]$ obtained before this sequence by calling a random number generator. This method is quite heavy in calculations as it calls two trigonometric functions and one root square. Another straightforward method is a von Neumann rejection procedure:

```
(1) z = p1
    y = p2
    x = p3
    r = sqrt(x**2+y**2+z**2)
    if(r.gt.1) then goto (1)
    x = x/r
    y = y/r
    z = z/r
```

This is also quite CPU consuming as it uses a square root and has a poor acceptance ratio a: $a \approx V_{sphere}/V_{cube} \approx 52\%$.

Marsaglia proposed another approach based on the fact that a uniform angular distribution (α, β) also yields a uniform distribution of the radius $\alpha^2 + \beta^2$. As a consequence if (α, β) is uniformly drawn in $[-1, 1] \times [-1, 1]$, a rejection method then yield a uniform distribution on the unit-radius circle with an acceptance ratio $a \approx A_{disc}/A_{square} \approx 72\%$. This uniformly distributed random variable $\alpha^2 + \beta^2 \in [0, 1]$ is then used to build z. x and y are proportional to α and β respectively: one has just to renormalise the latter variables. The algorithm reads:

```
(1)  random(p1)
     random(p2)
     if((p1**2+p2**2).gt.1.d0) goto (1)
     z = 1 - 2*(p1**2 + p2**2)
     a = sqrt(2*(1+z))
     x = a*p1
     y = a*p2
```

Landau and Binder [64] introduced in the context of the unfrustrated anisotropic Heisenberg model on the square lattice a method to avoid the dramatic plummeting of acceptance ratio at low temperature, namely restricted motion. They base this proposition on the fact that nearby configurations are likely to have close-by energies. This method can be adapted to frustrated systems and to the specific proposal generator we use. This improvement devised by Zhitomirsky can easily be understood in terms of local coordinates: sampling in a small cone about the spin to be updated is equivalent to a reduction of the interval of distribution of z which amounts to replace $z = 1 - 2(\alpha^2 + \beta^2)$ by $z = 1 - \delta_s(\alpha^2 + \beta^2)$ with $\delta_s \in]0, 2[$ adjusted to keep an acceptable acceptance rate. Such a restriction restricts the dynamics in phase space, which may be a matter of concern when phase space is very craggy: it is then possible to be locally trapped out of equilibrium in a metastable configuration.

For XY spins to avoid the use of trigonometric functions one can use two random variables for cartesian coordinates; for restricted motion to be implemented no such equivalent of what is shown above for Heisenberg spins is known to us: at most considering local framework proposals can be restricted to the half plane in which the spin is pointing.

E.2 Out of traps: over-relaxation

When dealing with systems like frustrated magnets it is quite common to encounter the problem of trapping as previously described. Unfortunately most clever updating schemes designed for simple systems such as Ising ferromagnet don't work for frustrated

magnets. A way out is provided by the mixing with quite different a technique, namely over-relaxation. It consists in proposing a new state the action of which is not increasing as compared with the current one; the new state is related to the current one by a symplectic transformation [24]. This evolution can be made micro-canonical as proposed hereafter. For simplicity when we refer to over-relaxation we mean micro-canonical over-relaxation.

Let's illustrate how over-relaxation works in Heisenberg spin systems. In case the model can be written in terms of a local field:

$$\mathcal{H} = \sum_i \mathbf{h}_i \cdot \mathbf{S}_i \tag{E.6}$$

where $\mathbf{h}_i$ is a function independent of $\mathbf{S}_i$, any rotation of $\mathbf{S}_i$ around $\mathbf{h}_i$ is a micro-canonical evolution. The most efficient rotation to calculate thermal averages is π rotation around $\mathbf{h}_i$ [24, 42, 43]:

$$\begin{aligned} \mathbf{S}'_i &= -\mathbf{S}_i + 2\mathbf{S}_i^{\parallel} \\ &= -\mathbf{S}_i + 2\mathbf{h}_i \frac{\mathbf{h}_i \cdot \mathbf{S}_i}{h_i^2} \end{aligned} \tag{E.7}$$

Such an evolution enables the evolution to a far-away state in phase space enhancing ergodicity, hence convergence. Furthermore this is a deterministic step as it doesn't require any random number. In case of Heisenberg models with a single-ion anisotropy term, two different terms control the evolution of a given spin: the local field and the anisotropic term. Let's illustrate what a micro-canonical evolution looks like in this case.

$$\mathcal{H} = \sum_i \left(\mathbf{h}_i \cdot \mathbf{S}_i - d(\hat{\mathbf{n}} \cdot \mathbf{S}_i)^2 \right) \tag{E.8}$$

To keep both terms constant in (E.8), a possible action is to reflect $\mathbf{S}_i$ with respect to the plane $(\hat{\mathbf{n}}, \mathbf{h}_i)$:

$$\begin{aligned} \mathbf{S}'_i &= \mathbf{S}_i - 2\mathbf{S}_i^{\perp} \\ &= \mathbf{S}_i - 2\frac{(\hat{\mathbf{n}} \times \mathbf{h}_i) \cdot \mathbf{S}_i}{(\hat{\mathbf{n}} \times \mathbf{h}_i)^2} (\hat{\mathbf{n}} \times \mathbf{h}_i) \end{aligned} \tag{E.9}$$

If investigations using pure over-relaxation algorithms exist (eg. [42]), which requires careful treatment of the updating process in order to obtain an ergodic evolution, it is often interesting to combine over-relaxation into Monte Carlo so that it is still possible to work in the canonical ensemble that presents some advantages eg in the use of finite-size scaling techniques. A typical mixed algorithm consists in the insertion of an over-relaxation step after each Monte Carlo step. In our work an over-relaxation step was devised as a sequential single-spin change according to (E.7) or (E.9) depending on the case. In a pure over-relaxation algorithm sequential updating has to be avoided for ergodicity considerations; in our algorithm as Monte Carlo steps breaks sequential updating it is not a matter of concern.

E.3   Estimating errors

As in any numerical work it is necessary to estimate errors on the obtained estimates. Two kinds of errors have to be considered [13]: statistical errors and controllable systematic errors. Concerning the latter, once errors due to a bad random number generator have been removed, there remains those due to finite-size clusters and finite-length Markov chains. As explained in Appendix D, the first group of errors can be turned into a powerful source of information; regarding the second group one can interpret the Markov chain as a dynamical process: one can then discuss of relevant parameters affecting the error as further explained below. Let's consider N successive measurements of A. The expectation value of the squared error can be written [13]:

$$\langle(\delta A)^2\rangle = \langle[\,\frac{1}{N}\sum_{\mu=1}^{N}(A_\mu - \langle A\rangle)\,]^2\rangle \tag{E.10}$$

where the abridged notation $A_\mu = A(\mathcal{S}_\mu)$ is used.

The handling of errors is not as trivial as in the case of the average of independent random variables. In Markov chains, states are highly correlated. Let's introduce the autocorrelation time τ_A that indicates the typical time over which configurations are correlated. Shifting to a time representation with $t = \delta t\,\mu$ where $\delta t = n\tau_0$, τ_A can be defined as follows:

$$\tau_A = \int_0^\infty dt \quad \varphi_A(t) \tag{E.11}$$

with

$$\varphi_A(t) = \frac{\langle A(0)A(t)\rangle - \langle A\rangle^2}{\langle A^2\rangle - \langle A\rangle^2} \tag{E.12}$$

Then (E.10) can be written:

$$\langle(\delta A)^2\rangle = \frac{1}{N}\left(\langle A^2\rangle - \langle A\rangle^2\right)\left\{1 + \frac{2}{\delta t}\int_0^{t_N} dt \quad \left(1 - \frac{t}{t_N}\right)\varphi_A(t)\right\} \tag{E.13}$$

where $t_N = N\delta t$. If $t_N \gg \tau_A$ then $\langle(\delta A)^2\rangle$ reads:

$$\frac{1 + 2\tau_A/\delta t}{N}\left(\langle A^2\rangle - \langle A\rangle^2\right) \tag{E.14}$$

If $\delta t \gg \tau_A$ ie $n \gg \tau_A/\tau_0$ (in other words measurements are carried out every n elementary steps with n much larger than the autocorrelation for the observable A acting on the states of the Markov chain), autocorrelations can be neglected, and the error on the average can be estimated by the standard formula:

$$\langle(\delta A)^2\rangle \approx \langle A^2\rangle - \langle A\rangle^2 \tag{E.15}$$

On the contrary if $\delta t \ll \tau_A$ the error reads:

$$\left\langle (\delta A)^2 \right\rangle \approx \frac{2\tau_A}{t_N} \left(\langle A^2 \rangle - \langle A \rangle^2 \right) \tag{E.16}$$

In this case the only relevant parameter is τ_A/t_N which means either the length of the Markov chain as to be improved or τ_A reduced to reduce statistical error. At a second-order transition this is a matter of concern as τ_A diverges for several observables, especially the order parameter. The divergence of τ_A is called critical slowing-down. In our simulation we have coped with critical slowing-down by increasing the length of Markov chain, ie t_N.

So far we have discussed how to estimate statistical error in a single finite-length Markov chain. Another way to further improve data statistics is to carry out measurements on several independent Markov chains, respecting the above considerations for each of them. In fact it is a way to increase t_N in a reasonable manner regarding available computing facilities. Note that the effective overall t_N is larger than the sum of the individual ones thanks to the independence between different Markov chains. Results presented in this work are typically the average of ten to twenty independent runs.

Appendix F

French summary

Cette thèse de doctorat est consacrée à l'étude d'un modèle paradigmatique de système magnétique géométriquement frustré, à savoir le modèle antiferromagnétique de Heisenberg sur réseau triangulaire et à ses variantes anisotropes — occasion de proposer un diagramme complet du modèle antiferromagnétique XY sur réseau triangualaire, en relation avec le cas d'anisotropie de plan facile. Les cas d'anisotropie d'axe facile et de plan facile sont envisagées pour une anisotropie mono-ionique (cf Ann. A) du fait de sa pertinence expérimentale et de son caractère attendu plus altérant que celui de l'anisotropie d'échange.

Le chapitre 2 est consacré à la détermination du diagramme de phase du modèle antiferromagnétique de Heisenberg sur réseau triangulaire (Fig. 2.3). Il commence par un rappel sur l'origine du modèle de Heisenberg comme modèle de description de spins localisés dans un système cristallin ; suit une discussion des états fondamentaux du modèle de Heisenberg classique et l'introduction d'une paramétrisation de la structure de spins, Éq. 2.6 (Sec. 2.1). Le comportement à champ nul qui n'a pas fait l'objet d'une nouvelle étude est discuté à travers une revue des résultats obtenus et l'explication des lignes d'opposition existant entre les différents travaux et la prise de position en faveur de l'interprétation proposée par Kawamura d'une transition de phase topologique (Sec. 2.2). La nature des symétries gouvernant le comportement sous champ est ensuite présentée, à savoir une symétrie composite $S^1 \otimes \mathbb{Z}_3$, avec les implications en terme de transitions de phases (Sec. 2.3). À faible champ, la symétrie discrète $\mathbb{Z}_3$ est d'abord brisée, laissant apparaÓtre un ordre colinéaire, au cours d'une transition qui appartient à la classe d'universalité du modèle vectoriel de Potts à trois états ; la brisure de la symétrie continue S^1 a ensuite lieu lors d'une transition de type BKT vers une phase à ordre algébrique formée par la configuration à 120 degrés (voir Fig. 2.1). Un élément mis en avant dans cette étude est qu'a contrario de ce qui se trouvait publié jusqu'alors les deux lignes de transition à faible champ (brisure de $\mathbb{Z}_3$ et de S^1) précédemment discutées ne peuvent pas se terminer à un point multicritique à température finie en champ nul mais doivent rejoindre le point $(T, h) = (0, 0)$: cela résulte du caractère

sans masse des phases à champ nul par contraste avec le caractère massique de la phase de basse température à champ fini : un champ infinitésimal ne peut pas rendre le système massique. À haut champ la brisure de symétrie est encore successive mais plus difficile à mettre en évidence comme les transitions sont gouvernées par le comportement selon la seule composante transverse pour stabiliser une structure planaire en forme de V (Fig. 2.2). En Sec. 2.4 l'étude numérique réalisée pour construire le diagramme de phase Fig. 2.3 est présentée. Cette présentation commence par une brève esquisse de l'algorithme utilisé (cf Ann. E). Sont ensuite introduites les observables utilisées pour localiser les transitions, à savoir la chaleur spécifique, le cumulant de Binder, un rapport de fonction de corrélation de spin et la susceptibilité $\chi_{\mathbf{q}}^{\alpha}$ renormalisée selon $\chi_{\mathbf{q}}^{\alpha}/L^{2-\eta}$ (cf Ann. D). Enfin les résultats sont explicités.

Dans le chapitre 3 le diagramme de phase du modèle antiferromagnétique de Heisenberg sur réseau triangulaire avec anisotropie d'axe facile est déterminé (le diagramme est calculÈ pour $d = 0.2$, Fig 3.8). Si la symétrie sous champ est identique à celle du modèle isotrope, celle à champ nul est différente, à savoir $S^1 \otimes \mathbb{Z}_6$: les implications en sont discutées en Sec. 3.1. Une présentation en champ moyen est ensuite proposée (Sec. 3.2) pour son apport en termes de discussion des symétries, sa pertinence pour les composés laminaires et l'intérêt du développement d'une théorie correcte de champ moyen dans l'espace réel en présence d'une anisotropie mono-ionique (cf Ann. B & C) qui n'existe pas à ma connaissance dans la littérature et qui se révèle utile par exemple pour l'étude de certains systèmes pyrochlores. La détermination du diagramme de phase par une technique Monte Carlo est enfin présentée en deux temps : à champ nul (Sec. 3.3) une succession de trois transitions est observée, les deux premières associées à la brisure de la symétrie discrète $\mathbb{Z}_6$ avec une phase critique intermédiaire ; sous champ (Sec. 3.4) les brisures de symétries sont similaires au cas isotrope. Dans ce dernier cas certaines spécificités apparaissent cependant : la terminaison des lignes de transition au point de transition en champ nul situés à température finie (aux deux points extrémaux en fait), la scission de la transition à température nulle au champ de tiers d'aimantation permettant un élargissement de la zone d'existence de la phase colinéaire autrement réduite à un point dans le cas isotrope ; la réduction du champ de saturation.

Le sujet du chapitre 4 est la détermination du diagramme de phase du modèle antiferromagnétique bidimensionnel sur réseau triangulaire : le modèle paradigmatique en est le système de spins XY (Fig. 4.1); dans la continuité de l'étude proposée du modèle de Heisenberg et de ses variantes anisotropes, le cas de l'anisotropie de plan facile est aussi considérée. Après l'introduction des spécificités du modèle XY à champ nul avec l'émergence d'une symétrie chirale, la localisation des deux transitions correspondant à la brisure successive de la symétrie chirale ($\mathbb{Z}_2$) puis de la symétrie continue (S^1) est présentée. La nature de la transition chirale est discutée et des arguments sont mis en avant soutenant l'appartenance à la classe d'universalité d'Ising (Sec. 4.1). La détermination des transitions sous champ est ensuite explicitée en deux temps. Tout d'abord

le cas des champs faibles est étudié (Sec. 4.2) puis celui des champs forts (Sec. 4.3). À faible champ l'existence d'un point multicritique auquel les lignes de transition de phase s'inverse est mise en évidence : au-dessus de ce point la symétrie discrète composite $\mathbb{Z}_2 \otimes \mathbb{Z}_3$ se brise successivement selon la translation du réseau (phase collinéaire) puis la chiralité ; en-dessous de ce point une phase chirale intermédiaire désordonnée magnétiquement apparaît qui prolonge celle existant à champ nul ; les lignes de transitions de phase rejoignent les transitions à champ nul, ce qui est une évidence pour la transition chirale, les transitions étant de même nature. Dans le cas de la ligne associée à la brisure de $\mathbb{Z}_3$ cette terminaison est non seulement autorisée comme $\mathbb{Z}_3$ est un sous-groupe de S^1 mais encore attendue comme le développement de l'énergie libre des ondes de spin à faible champ donne un terme dominant présentant une anisotropie d'ordre trois qui est inessentielle (ou non pertinente) dans le voisinage d'une transition BKT. À haut champ l'ordre se fait selon la seule composante transverse ce qui entraîne la brisure de la symétrie comme une symétrie $\mathbb{Z}_6$: ainsi une phase critique intermédiaire existe. Pour compléter l'étude du modèle de Heisenberg et de ses variantes anisotropes, le cas du système avec anisotropie de plan facile qui appartient à la même classe d'universalité que le système XY est discuté en Sec. 4.4. Il n'y a pas de spécificité particulière, si ce n'est une contraction selon l'axe des températures, ce qui est attendu étant donné des fluctuations de spins possibles selon la troisième direction. Le diagramme est présenté en Fig. 4.13 pour le cas $d = -0.2$.

Bibliography

[1] ALEXANDER, S., AND PINCUS, P. Phase transitions of some fully frustrated models. *Journal of Physics A: Mathematical and General 13* (1980), 263–273.

[2] ANDERSON, P. W. Ordering and antiferromagnetism in ferrites. *Physical Review 102*, 4 (1956), 1008–1013.

[3] ANDERSON, P. W. The resonating valence bond state in La_2CuO_4 and superconductivity. *Science 235* (1987), 1196–1198.

[4] AZARIA, P., AND DELAMOTTE, B. The renormalization group approach to frustrated Heisenberg spin systems. In *Magnetic Systems with Competing Interactions*, H. T. Diep, Ed. World Scientific Publishing Co., 1994, pp. 51–119.

[5] AZARIA, P., DELAMOTTE, B., AND JOLICOEUR, T. Nonuniversality in helical and canted-spin systems. *Physical Review Letters 64*, 26 (JUN 25 1990), 3175–3178.

[6] AZARIA, P., DELAMOTTE, B., JOLICOEUR, T., AND MOUHANNA, D. Spin stiffness of canted antiferromagnets. *Physical Review B 45*, 21 (JUN 1 1992), 12612–12615.

[7] BAK, P., AND VON BOEHM, J. Ising model with solitons, phasons, and "the devil's staircase". *Phys. Rev. B 21*, 11 (Jun 1980), 5297–5308.

[8] BARBER, M. N. Finite-size scaling. In *Phase Transitions and Critical Phenomenal*, C. Domb and J. L. Lebowitz, Eds. Academic Press, New York, 1983, pp. 146–268.

[9] BAXTER, R. Hard hexagons - exact solution. *Journal of Physics A-Mathematical and General 13*, 3 (1980), L61–L70.

[10] BEREZINSKII, V. L. Destruction of long-range order in one-dimensional and 2-dimensional systems having a continuous symmetry group 1 - Classical systems. *Soviet Physics JETP-USSR 32*, 3 (1971), 493.

[11] BEREZINSKII, V. L. Destruction of long-range order in one-dimensional and 2-dimensional systems possessing a continuous symmetry group .2. Quantum systems. *Soviet Physics JETP-USSR 34*, 3 (1972), 610.

[12] BINDER, K. Critical properties from Monte-Carlo coarse graining and renormalization. *Physical Review Letters 47*, 9 (1981), 693–696.

[13] BINDER, K. Applications of Monte Carlo methods to statistical physics. *Reports on Progress in Physics 60*, 5 (MAY 1997), 487–559.

[14] BLOCH, I., DALIBARD, J., AND ZWERGER, W. Many-body physics with ultracold gases. *Reviews of Modern Physics 80*, 3 (JUL-SEP 2008), 885–964.

[15] CAPRIOTTI, L., CUCCOLI, A., TOGNETTI, V., AND VAIA, R. Monte Carlo study of the classical Heisenberg antiferromagnet with easy-plane anisotropy on a triangular lattice. *Journal of Applied Physics 85*, 8, Part 2B (APR 15 1999), 6073–6075. 43rd Annual Conference on Magnetism and Magnetic Materials, Miami, Florida, NOV 09-12, 1998.

[16] CAPRIOTTI, L., VAIA, R., CUCCOLI, A., AND TOGNETTI, V. Phase transitions induced by easy-plane anisotropy in the classical Heisenberg antiferromagnet on a triangular lattice: A Monte Carlo simulation. *Physical Review B 58*, 1 (JUL 1 1998), 273–281.

[17] CARDY, J. General discrete planar models in 2-dimensions - duality properties and phase-diagrams. *Journal of Physics A-Mathematical and General 13*, 4 (1980), 1507–1515.

[18] CASTELNOVO, C. Coulomb physics in spin ice: From magnetic monopoles to magnetic currents. *ChemPhysChem 11*, 3 (FEB 22 2010), 557–559.

[19] CÉPAS, O., AND SHASTRY, B. Field-driven transitions in the dipolar pyrochlore antiferromagnet $Gd_2Ti_2O_7$. *Physical Review B 69*, 18 (MAY 2004).

[20] CHAIKIN, P. M., AND LUBENSKY, T. C. *Principle of Condensed Matter Physics*. Cambridge University Press, Cambridge, 1995.

[21] CHANDRA, P., AND DOUÇOT, B. Possible spin-liquid state at large S for the frustrated square Heisenberg lattice. *Physical Review B 38* (1988), 9335–9338.

[22] CHUBUKOV, A. V., AND GOLOSOV, D. I. Quantum-theory of an antiferromagnet on a triangular lattice in a magnetic-field. *Journal of Physics-Condensed Matter 3*, 1 (JAN 7 1991), 69–82.

[23] COLLINS, M., AND PETRENKO, O. Triangular antiferromagnets. *Canadian Journal of Physics 75*, 9 (SEP 1997), 605–655.

[24] CREUTZ, M. Overrelaxation and Monte-Carlo simulation. *Physical Review D 36*, 2 (JUL 15 1987), 515–519.

[25] DAMLE, K. Low temperature ordering in easy-axis S=1 kagome and triangular lattice antiferromagnets. *Physica A-Statistical Mechanics and its Applications 384*, 1 (OCT 1 2007), 28–33. International Conference on Statistical Physics, Raichak, India, JAN 05-09, 2007.

[26] DOTSENKO, V. S., AND UIMIN, G. V. Phase-transitions in two-dimensional antiferromagnetic XY-models in external-field. *Journal of Physics C-Solid State Physics 18*, 25 (1985), 5019–5032.

[27] EINHORN, M. B., SAVIT, R., AND RABINOVICI, E. A physical picture for the phase-transitions in Z_n symmetric models. *Nuclear Physics B 170*, 1 (1980), 16–31.

[28] ELITZUR, S., PEARSON, R., AND SHIGEMITSU, J. Phase structure of discrete abelian spin and gauge systems. *Physical Review D 19*, 12 (1979), 3698–3714.

[29] ENJALRAN, M., AND GINGRAS, M. Theory of paramagnetic scattering in highly frustrated magnets with long-range dipole-dipole interactions: The case of the $Tb_2Ti_2O_7$ pyrochlore antiferromagnet. *Physical Review B 70*, 17 (NOV 2004).

[30] FISHER, M., AND BARBER, M. Scaling theory for finite-size effects in critical region. *Physical Review Letters 28*, 23 (1972), 1516.

[31] FISHER, M., AND FERDINAND, A. Interfacial boundary and size effects at critical points. *Physical Review Letters 19*, 4 (1967), 169.

[32] FISHER, M. E. Theory of critical point singularities. In *Critical Phenomena, Proceedings of the 51st Enrico Fermi Summer School*, M. S. Green, Ed. Academic Press, New York, 1971, pp. 1–99.

[33] FUJIKI, S., SHUTOH, K., AND KATSURA, S. Possibility of the Kosterlitz-Thouless phase-transition in the two-dimensional fully frustrated Ising-model. *Journal of the Physical Society of Japan 53*, 4 (1984), 1371–1379.

[34] GOLDSTONE, J. Field theories with superconductor solutions. *Nuovo Cimento 19*, 1 (1961), 154–164.

[35] GOLOSOV, D. I., AND CHUBUKOV, A. V. Orientational transitions in Heisenberg antiferromagnets on triangular lattice. *JETP Letters 50*, 10 (NOV 25 1989), 451–454.

[36] GREEDAN, J. Geometrically frustrated magnetic materials. *Journal of Materials Chemistry 11*, 1 (2001), 37–53. 3rd Materials Discussion Meeting of the Royal-Society-of-Chemistry (MD3), Cambridge, England, SEP 26-29, 2000.

[37] HASENBUSCH, M., PELISSETTO, A., AND VICARI, E. Multicritical behaviour in the fully frustrated XY model and related systems. *journal of statistical mechanics-theory and experiment* (DEC 2005).

[38] HASTINGS, W. K. Monte Carlo sampling methods using Markov chains and their applications. *Biometrika 57*, 1 (April 1970), 97 – 109.

[39] ISHII, R., TANAKA, S., ONUMA, K., NAMBU, Y., TOKUNAGA, M., SAKAK-IBARA, T., KAWASHIMA, N., MAENO, YOSHITERU ANDBROHOLM, C., GAUTREAUX, D. P., CHAN, J. Y., AND NAKATSUJI, S. Successive phase transitions and phase diagrams of the quasi-two-dimensional triangular antiferromagnet Rb4Mn(MoO4)3. *ArXiv e-prints* (December 2009).

[40] JOSÉ, J. V., KADANOFF, L. P., KIRKPATRICK, S., AND NELSON, D. R. Renormalization, vortices, and symmetry-breaking perturbations in 2-dimensional planar model. *Physical Review B 16*, 3 (1977), 1217–1241.

[41] KADANOFF, L. P., GOTZE, W., HAMBLEN, D., HECHT, R., LEWIS, E. A. S., PALCIAUS, V. V., RAYL, M., SWIFT, J., ASPNES, D., AND KANE, J. Static phenomena near critical points - theory and experiment. *Reviews of Modern Physics 39*, 2 (1967), 395.

[42] KANKI, K., LOISON, D., AND SCHOTTE, K. Efficiency of the microcanonical over-relaxation algorithm for vector spins analyzing first and second order transitions. *European Physical Journal B 44*, 3 (APR 2005), 309–315.

[43] KANKI, K., LOISON, D., AND SCHOTTE, K. Microcanonical simulation on the first order phase transition of the XY antiferromagnet on the stacked triangular lattice. *Journal of the Physical Society of Japan 75*, 1 (JAN 2006).

[44] KANO, K., AND NAYA, S. Antiferromagnetism - the kagome Ising net. *Progress of Theoretical Physics 10*, 2 (1953), 158–172.

[45] KASTNER, M. Monte Carlo methods in statistical physics: Mathematical foundations and strategies. *Communications in Nonlinear Science and Numerical Simulation 15*, 6 (JUN 2010), 1589–1602.

[46] KAWAMURA, H. Spin-wave analysis of the antiferromagnetic plane rotator model on the triangular lattice - symmetry-breaking in a magnetic-field. *Journal of the Physical Society of Japan 53*, 8 (1984), 2452–2455.

[47] KAWAMURA, H. New critical-behavior .1. Heisenberg-antiferromagnet on the layered-triangular lattice. *Journal of the Physical Society of Japan 56*, 2 (FEB 1987), 474–491.

[48] KAWAMURA, H. Renormalization-group analysis of chiral transitions. *Physical Review B 38*, 7 (SEP 1 1988), 4916–4928.

[49] KAWAMURA, H. Universality of phase transitions of frustrated antiferromagnets. *Journal of Physics-Condensed Matter 10*, 22 (JUN 8 1998), 4707–4754.

[50] KAWAMURA, H., AND MIYASHITA, S. Phase-transition of the 2-dimensional Heisenberg-antiferromagnet on the triangular lattice. *Journal of the Physical Society of Japan 53*, 12 (1984), 4138–4154.

[51] KAWAMURA, H., AND MIYASHITA, S. Phase-transition of the two-dimensional Heisenberg-antiferromagnet on the triangular lattice. *Journal of the Physical Society of Japan 53*, 1 (1984), 9–12.

[52] KAWAMURA, H., AND MIYASHITA, S. Phase-transition of the Heisenberg-antiferromagnet on the triangular lattice in a magnetic-field. *Journal of the Physical Society of Japan 54*, 12 (DEC 1985), 4530–4538.

[53] KAWAMURA, H., YAMAMOTO, A., AND OKUBO, T. Z(2)-vortex ordering of the triangular-lattice Heisenberg antiferromagnet. *Journal of the Physical Society of Japan 79*, 2 (FEB 2010), 023701.

[54] KENZELMANN, M., LAWES, G., HARRIS, A. B., GASPAROVIC, G., BROHOLM, C., RAMIREZ, A. P., JORGE, G. A., JAIME, M., PARK, S., HUANG, Q., SHAPIRO, A. Y., AND DEMIANETS, L. A. Direct transition from a disordered to a multiferroic phase on a triangular lattice. *Phys. Rev. Lett. 98*, 26 (Jun 2007), 267205.

[55] KOGUT, J. B. Introduction to lattice gauge-theory and spin systems. *Reviews of Modern Physics 51*, 4 (1979), 659–713.

[56] KORSHUNOV, S. E. Phase-diagram of the antiferromagnetic XY model with a triangular lattice in an external magnetic-field. *Journal of Physics C-Solid State Physics 19*, 29 (OCT 20 1986), 5927–5935.

[57] KORSHUNOV, S. E. Phase-transitions in two-dimensional uniformly frustrated XY models .2. General scheme. *Journal of Statistical Physics 43*, 1-2 (APR 1986), 17–32.

[58] Korshunov, S. E. Kink pairs unbinding on domain walls and the sequence of phase transitions in fully frustrated XY models. *Physical Review Letters 88*, 16 (APR 22 2002).

[59] Korshunov, S. E. Phase transitions in two-dimensional systems with continuous degeneracy. *Physics-Uspekhi 49*, 3 (MAR 2006), 225–262.

[60] Korshunov, S. E., and Uimin, G. V. Phase-transitions in two-dimensional uniformly frustrated XY models .1. Antiferromagnetic model on a triangular lattice. *Journal of Statistical Physics 43*, 1-2 (APR 1986), 1–16.

[61] Kosterlitz, J., and Thouless, D. Ordering, metastability and phase-transitions in 2 dimensional systems. *Journal of Physics C-Solid State Physics 6*, 7 (1973), 1181–1203.

[62] Krupička, S., and Šternberk, J., Eds. *Elements of theoretical magnetism.* Iliffe books books ltd, 1968.

[63] Landau, D. P. Critical and multicritical behavior in a triangular-lattice-gas Ising model: Repulsive nearest-neighbor and attractive next-nearest-neighbor coupling. *Physical Review B 27*, 9 (1983), 5604.

[64] Landau, D. P., and Binder, K. Phase-diagrams and critical-behavior of a two-dimensional anisotropic Heisenberg anti-ferromagnet. *Physical Review B 24*, 3 (1981), 1391–1403.

[65] Lapilli, C., Pfeifer, P., and Wexler, C. Universality away from critical points in two-dimensional phase transitions. *Physical Review Letters 96*, 14 (2006), 140603.

[66] Lee, D., Joannopoulos, J., Negele, J., and Landau, D. Discrete-symmetry breaking and novel critical phenomena in an antiferromagnetic planar (XY) model in 2 dimensions. *Physical Review Letters 52*, 6 (1984), 433–436.

[67] Lee, D., Joannopoulos, J., Negele, J., and Landau, D. Symmetry analysis and monte-carlo study of a frustrated antiferromagnetic planar (XY) model in 2 dimensions. *Physical Review B 33*, 1 (JAN 1 1986), 450–475.

[68] Lee, J., Kosterlitz, J., and Granato, E. Monte-Carlo study of frustrated XY-models on a triangular and square lattice. *Physical Review B 43*, 13, Part B (MAY 1 1991), 11531–11534.

[69] Lee, S., and Lee, K. Phase transitions in the fully frustrated triangular XY model. *Physical Review B 57*, 14 (APR 1 1998), 8472–8477.

[70] LOISON, D. Binder's cumulant for the Kosterlitz-Thouless transition. *Journal of Physics-Condensed Matter 11*, 34 (AUG 30 1999), L401–L406.

[71] LOISON, D., QIN, C., SCHOTTE, K., AND JIN, X. Canonical local algorithms for spin systems: heat bath and Hasting's methods. *European Physical Journal B 41*, 3 (OCT 2004), 395–412.

[72] MARSAGLIA, G. Xorshift RNGs. *Journal of Statistical Software 8*, 14 (7 2003), 1–6.

[73] MELCHY, P.-É., AND ZHITOMIRSKY, M. E. Interplay of anisotropy and frustration: Triple transitions in a triangular-lattice antiferromagnet. *Phys. Rev. B 80*, 6 (Aug 2009), 064411.

[74] MELCHY, P.-É., AND ZHITOMIRSKY, M. E. Two-fold, three-fold and continuous symmetry breaking: the case of XY triangular antiferromagnet. To be soon published, Aug 2010.

[75] MERMIN, N. D. Topological theory of defects in ordered media. *Reviews of Modern Physics 51*, 3 (1979), 591–648.

[76] MERMIN, N. D., MINEYEV, V. P., AND VOLOVIK, G. E. Topological analysis of cores of singularities in He-3-a. *Journal of Low Temperature Physics 33*, 1-2 (1978), 117–126.

[77] MERMIN, N. D., AND WAGNER, H. Absence of ferromagnetism or antiferromagnetism in one- or 2-dimensional isotropic Heisenberg models. *Physical Review Letters 17*, 22 (1966), 1133.

[78] METROPOLIS, N., ROSENBLUTH, A. W., ROSENBLUTH, M. N., TELLER, A. H., AND TELLER, E. Equation of state calculations by fast computing machines. *Journal of Chemical Physics 21*, 6 (1953), 1087–1092.

[79] MICHEL, L. Symmetry defects and broken symmetry - configurations hidden symmetry. *Reviews of Modern Physics 52*, 3 (1980), 617–651.

[80] MILA, F. Quantum spin liquids. *European Journal of Physics 21*, 6 (2000), 499.

[81] MILA, F., POILBLANC, D., AND BRUDER, C. Spin dynamics in a frustrated magnet with short-range order. *Physical Review B 43* (1991), 7891–7898.

[82] MINEYEV, V., AND VOLOVIK, G. Planar and linear solitons in superfluid He-3. *Physical Review B 18*, 7 (1978), 3197–3203.

[83] MIYASHITA, S. Magnetic properties of Ising-like Heisenberg antiferromagnets on the triangular lattice. *Journal of the Physical Society of Japan 55*, 10 (1986), 3605.

[84] MIYASHITA, S., AND KAWAMURA, H. Phase-transitions of anisotropic Heisenberg antiferromagnets on the triangular lattice. *Journal of the Physical Society of Japan 54*, 9 (1985), 3385–3395.

[85] MIYASHITA, S., AND SHIBA, H. Nature of the phase-transition of the two-dimensional antiferromagnetic plane rotator model on the triangular lattice. *Journal of the Physical Society of Japan 53*, 3 (1984), 1145–1154.

[86] MOESSNER, R., AND CHALKER, J. Low-temperature properties of classical geometrically frustrated antiferromagnets. *Physical Review B 58*, 18 (NOV 1 1998), 12049–12062.

[87] NAKATSUJI, S., NAMBU, Y., AND ONODA, S. Novel Geometrical Frustration Effects in the Two-Dimensional Triangular-Lattice Antiferromagnet $NiGa_2S_4$ and Related Compounds. *Journal of the Physical Society of Japan 79*, 1 (JAN 2010).

[88] NGO, V. T., AND DIEP, H. T. Phase transition in Heisenberg stacked triangular antiferromagnets: End of a controversy. *Physical Review E 78*, 3, Part 1 (SEP 2008).

[89] NGO, V. T., AND DIEP, H. T. Stacked triangular XY antiferromagnets: End of a controversial issue on the phase transition. *Journal of Applied Physics 103*, 7 (APR 1 2008). 52nd Annual Conference on Magnetism and Magnetic Materials, Tampa, FL, NOV 05-09, 2007.

[90] NHO, K., AND LANDAU, D. Spin-dynamics simulations of the triangular antiferromagnetic XY model. *Physical Review B 66*, 17 (NOV 1 2002).

[91] NOH, J., RIEGER, H., ENDERLE, M., AND KNORR, K. Critical behavior of the frustrated antiferromagnetic six-state clock model on a triangular lattice. *Physical Review E 66*, 2, Part 2 (AUG 2002).

[92] OHTA, T., AND JASNOW, D. XY model and the superfluid density in 2 dimensions. *Physical Review B 20*, 1 (1979), 139–146.

[93] OLSSON, P. 2-phase-transitions in the fully-frustrated-XY model. *Physical Review Letters 75*, 14 (OCT 2 1995), 2758–2761.

[94] OLSSON, P., AND MINNHAGEN, P. On the helicity modulus, the critical-temperature and Monte-Carlo simulations for the 2-dimensional XY-model. *Physica Scripta 43*, 2 (FEB 1991), 203–209.

[95] OZEKI, Y., AND ITO, N. Nonequilibrium relaxation analysis of fully frustrated XY models in two dimensions. *Physical Review B 68*, 5 (AUG 1 2003).

[96] PAULING, L. The structure and entropy of ice and of other crystals with some randomness of atomic arrangement. *Journal of the American Chemical Society 57* (1935), 2680.

[97] PLUMER, M., CAILLÉ, A., AND HOOD, K. Multicritical points in the magnetic phase-diagrams of axial and planar antiferromagnets. *Physical Review B 39*, 7 (MAR 1 1989), 4489–4499.

[98] PLUMER, M., HOOD, K., AND CAILLÉ, A. Multicritical point in the magnetic phase-diagram of CsNiCl$_3$. *Physical Review Letters 60*, 1 (JAN 4 1988), 45–48.

[99] PLUMER, M. L., AND CAILLÉ, A. Magnetic phase diagrams of the antiferromagnetic planar model on a stacked triangular lattice. *Physical Review B 42*, 16 (1991), 10388.

[100] PLUMER, M. L., AND CAILLÉ, A. Finite-field chiral tetracritical behavior in a distorted triangular antiferromagnet. *Physical Review B 45*, 21 (JUN 1 1992), 12326–12329.

[101] PLUMER, M. L., AND CAILLÉ, A. Lagrangian spin-wave theory of frustrated antiferromagnets: Application to ABX_3 compounds. *Physical Review Letters 68*, 7 (1992), 1042.

[102] RASTELLI, E., TASSI, A., PIMPINELLI, A., AND SEDAZZARI, S. Triangular planar antiferromagnet in an external magnetic-field. *Physical Review B 45*, 14 (APR 1 1992), 7936–7944.

[103] SEN, A., WANG, F., DAMLE, K., AND MOESSNER, R. Triangular and kagome antiferromagnets with a strong easy-axis anisotropy. *Physical Review Letters 102*, 22 (JUN 5 2009).

[104] SENTHIL, T., BALENTS, L., SACHDEV, S., VISHWANATH, A., AND FISHER, M. P. A. Quantum criticality beyond the Landau-Ginzburg-Wilson paradigm. *Physical Review B 70* (2004), 144407.

[105] SENTHIL, T., VISHWANATH, A., BALENTS, L., SACHDEV, S., AND FISHER, M. P. A. Deconfined quantum critical points. *Science 303* (2004), 1490–1494.

[106] SHENG, Q., AND HENLEY, C. L. Ordering due to disorder in a triangular Heisenberg-antiferromagnet with exchange-anisotropy. *Journal of Physics-Condensed Matter 4*, 11 (MAR 16 1992), 2937–2959.

[107] SHIH, W., AND STROUD, D. Molecular-field approximation for Josephson-coupled superconducting arrays in a magnetic-field. *Physical Review B 28*, 11 (1983), 6575–6577.

[108] SHIH, W., AND STROUD, D. Superconducting arrays in a magnetic-field - effects of lattice structure and a possible double transition. *Physical Review B 30*, 11 (1984), 6774–6777.

[109] SOUTHERN, B., AND YOUNG, A. Spin stiffness in frustrated antiferromagnets. *Physical Review B 48*, 17 (NOV 1 1993), 13170–13173.

[110] STEPHAN, W., AND SOUTHERN, B. Monte Carlo study of the anisotropic Heisenberg antiferromagnet on the triangular lattice. *Physical Review B 61*, 17 (MAY 1 2000), 11514–11520.

[111] STEWART, J., EHLERS, G., WILLS, A., BRAMWELL, S., AND GARDNER, J. Phase transitions, partial disorder and multi-k structures in $Gd_2Ti_2O_7$. *Journal of Physics-Condensed Matter 16*, 28 (JUL 21 2004), L321–L326.

[112] SURUNGAN, T., OKABE, Y., AND TOMITA, Y. Study of the fully frustrated clock model using the Wang-Landau algorithm. *Journal of Physics A-Mathematical and General 37*, 14 (APR 9 2004), 4219–4230.

[113] SUZUKI, N. A microscopic theory of the phase-transition in $RbFeCl_3$-type hexagonal anti-ferromagnets - effects of the dipole-dipole interaction. *Journal of the Physical Society of Japan 52*, 9 (1983), 3199–3207.

[114] SYOZI, I. Statistics of kagome lattice. *Progress ofTheoretical Physics 6*, 3 (1951), 306–308.

[115] TEITEL, S., AND JAYAPRAKASH, C. Phase-transitions in frustrated two-dimensional XY models. *Physical Review B 27*, 1 (1983), 598–601.

[116] TISSIER, M., DELAMOTTE, B., AND MOUHANNA, D. Frustrated Heisenberg magnets: A nonperturbative approach. *Physical Review Letters 84*, 22 (MAY 29 2000), 5208–5211.

[117] TISSIER, M., DELAMOTTE, B., AND MOUHANNA, D. XY frustrated systems: Continuous exponents in discontinuous phase transitions. *Physical Review B 67*, 13 (APR 1 2003).

[118] TISSIER, M., MOUHANNA, D., AND DELAMOTTE, B. Nonperturbative approach of the principal chiral model between two and four dimensions. *Physical Review B 61*, 22 (JUN 1 2000), 15327–15330.

[119] TOLÉDANO, J.-C., AND TOLÉDANO, P. *The Landau theory of phase transitions.* Worlds scientific, 1987.

[120] TOMITA, Y., AND OKABE, Y. Finite-size scaling of correlation ratio and generalized scheme for the probability-changing cluster algorithm. *Physical Review B 66*, 18 (NOV 1 2002), 180401.

[121] TOULOUSE, G. Theory of frustration effect in spin-glasses .1. *Communications on Physics 2*, 4 (1977), 115–119.

[122] VILLAIN, J. Magnetic analog of stereoisomerism - application to helimagnetism in 2 dimensions. *Journal de Physique 38*, 4 (1977), 385–391.

[123] VILLAIN, J. spin glass with nonrandom interactions. *Journal of Physics C-Solid State Physics 10*, 10 (1977), 1717–1734.

[124] VILLAIN, J., BIDAUX, R., CARTON, J. P., AND CONTE, R. Order as an effect of disorder. *Journal de Physique 41*, 11 (1980), 1263–1272.

[125] WANNIER, G. Antiferromagnetism - the triangular Ising net. *Physical Review 79*, 2 (1950), 357–364.

[126] WANNIER, G. Errata. *Physical Review B 7*, 11 (1973), 5017.

[127] WEBER, H., AND MINNHAGEN, P. Monte-Carlo determination of the critical-temperature for the two-dimensional XY model. *Physical Review B 37*, 10, Part B (APR 1 1988), 5986–5989.

[128] WEISS, P. L'hypothèse du champ moléculaire et la propriété ferromagnétique. *Journal de Physique Théorique et Appliquée 6*, 1 (1907), 661 – 689.

[129] WILSON, K. G. Renormalization group and critical phenomena .1. Renormalization group and Kadanoff scaling picture. *Physical Review B 4*, 9 (1971), 3174–&.

[130] WILSON, K. G. Renormalization group and critical phenomena .2. Phase-space cell analysis of critical behavior. *Physical Review B 4*, 9 (1971), 3184–&.

[131] WILSON, K. G. Confinement of quarks. *Physical Review D 10*, 8 (1974), 2445–2459.

[132] WINTEL, M., EVERTS, H., AND APEL, W. Monte-Carlo simulation of the Heisenberg-antiferromagnet on a triangular lattice - topological excitations. *Physical Review B 52*, 18 (NOV 1 1995), 13480–13486.

[133] WINTEL, M., EVERTS, H. U., AND APEL, W. The Heisenberg-antiferromagnet on a triangular lattice - topological excitations. *Europhysics Letters 25*, 9 (MAR 20 1994), 711–716.

[134] XU, H., AND SOUTHERN, B. Phase transitions in the classical XY antiferromagnet on the triangular lattice. *Journal of Physics A-Mathematical and General 29*, 5 (MAR 7 1996), L133–L139.

[135] YAMAGUCHI, H., KIMURA, S., HAGIWARA, M., NAMBU, Y., NAKATSUJI, S., MAENO, Y., AND KINDO, K. High-field electron spin resonance in the two-dimensional triangular-lattice antiferromagnet $NiGa_2S_4$. *Physical Review B 78*, 18 (Nov 2008), 180404.

[136] YOSIDA, K. *Theory of Magnetism.* Springer, 1998.

Abstract

This doctoral dissertation presents a thorough determination of the phase diagrams of classical Heisenberg triangular antiferromagnet (HTAF) and its anisotropic variants based on theoretical and numerical analysis (Monte Carlo). At finite-field HTAF exhibits a non-trivial interplay of discrete $\mathbb{Z}_3$ symmetry and continuous S^1 symmetry. They are successively broken (discrete then continuous) with distinct features at low and high fields: in the latter case the ordering is along transverse direction; in the former case an intermediate collinear phase is stabilised before 120-degree structure is. Due to zero-field behaviour, transition lines close at $(T, h) = (0, 0)$.

Single-ion anisotropy is here considered. Easy-axis HTAF for moderate anisotropy strength $0 < d \leqslant 1.5$ possesses $\mathbb{Z}_6 \otimes S^1$ symmetry at zero-field which induces triple BKT-like transitions. At finite field the symmetry is the same as for HTAF: both thus share the same symmetry-breaking pattern. Yet specificities can be observed in the easy-axis system: splitting of zero-temperature transition at one-third magnetisation plateau, reduction of the saturation field.

Easy-plane HTAF belongs to the class of universality of XY triangular antiferromagnet: it thus interesting to start with this system. Zero-field behaviour results from the breaking of $\mathbb{Z}_2 \otimes S^1$ symmetry, where the discrete component is an emerging chiral symmetry. An intermediate magnetically chiral ordered phase exists which extends to finite-field where the symmetry is $\mathbb{Z}_2 \otimes \mathbb{Z}_3$. The upper limit of this intermediate phase along field axis is a multicritical point at which transition lines are inverted. Above, the intermediate phase is a collinear phase. At high field the compound symmetry is broken as a whole $\mathbb{Z}_6$.

Résumé

Cette thèse de doctorat présente la détermination théorique et numérique (Monte Carlo) du diagramme de phase du système classique antiferromagnétique de Heisenberg sur réseau triangulaire (HAFT) et de ses variantes anisotropes. Sous champ HAFT présente une intrication non triviale des symétries discrète Z3 et continue S1. Elles sont successivement brisées (discrète puis continue) selon des modalités différentes à champ fort et modéré : dans ce cas-là l'ordre a lieu selon la direction transverse ; dans ce cas-ci une phase colinéaire intermédiaire est stabilisée avant la phase à 120 degrés. Du fait du comportement à champ nul les lignes de transitions se terminent à $(T, h) = (0, 0)$.

L'anisotropie mono-ionique est ici considérée. HAFT avec anisotropie d'axe facile pour une anisotropie modérée, $0 < d \leqslant 1.5$, possède une symétrie $\mathbb{Z}_6 \otimes S^1$ à champ nul, qui induit une triple transition BKT. Sous champ, la symétrie est identique à HAFT : les deux partagent donc le même scénario de brisure de symétries. Le système anisotrope présente toutefois des spécificités ; séparation de la transition à température nulle au champ de tiers d'aimantation, réduction du champ de saturation.

HAFT avec anisotropie de plan facile appartient à la classe d'universalité de XY AFT il est donc intéressant de commencer par ce système-ci. Le comportement à champ nul résulte de la symétrie $\mathbb{Z}_2 \otimes S^1$ où la composante discrète est une symétrie chirale émergente. Une phase intermédiaire chirale magnétiquement désordonnée est stabilisée ; elle se prolonge sous champ, où la symétrie est réduite à $\mathbb{Z}_2 \otimes \mathbb{Z}_3$, jusqu'à un point multicritique auquel les transitions s'inversent. Au-dessus de celui-ci la phase intermédiaire est colinéaire. Sous champ fort la symétrie composite se brise comme une symétrie $\mathbb{Z}_6$ unique.